UCLouvain

AGRO LOUVAIN

Faculté des bioingénieurs

Investigating the contribution of Seychelles' seagrass meadows to marine carbon sequestration

Author: HANUISE Douchan
Supervisor: HANERT Emmanuel
Readers: HARLAY Jérôme ; OPFERGELT Sophie
Academic Year 2021-2022
Thesis presented in partial fulfillment of the requirements for the degree of Master in Bioengineering: Environmental Bioengineering

Abstract

The oceans are a key component of the climate system. They cover about 72% of the Earth's surface and have already absorbed about 40% of the carbon that was emitted by human activities since the 19^{th} century. Coastal ecosystems, such as seagrass meadows and mangroves, play a particular role in this blue carbon budget. They have the potential to capture carbon and to store it in deep reservoirs where it will remain for hundreds of years. This carbon sequestration potential remains however poorly understood and unquantified for most coastal ecosystems in the World. Here, we try to estimate the carbon sequestration potential of seagrass meadows on the Seychelles plateau. Seychelles has been developing extensively its blue economy and is keen to estimate the carbon offsetting capacity of its marine ecosystem. We develop a high-resolution ocean circulation model of Seychelles plateau and simulate ocean currents over 3-year period (2018-2020). These currents are then used to simulate the transport of virtual seagrass fragments from the different confirmed and potential meadows present on the plateau. Our results suggest that most of the seagrass meadows export a large fraction (>80%) of their fragments outside of the plateau, where the carbon contained in the fragments can settle to >1000m depth. We estimate that ∼6% of Seychelles seagrass meadows net primary production could be sequestrated in the deep ocean. This corresponds to ∼85 tC/yr for confirmed meadows and ∼7994 tC/yr for potential meadows. These estimates should help Seychelles quantify its global contribution toward net-zero emissions, as envisaged by the Paris Agreement on climate change.

Acknowledgements

This work is the result of a long year's work with the pleasure of seeing the same smiling people every week on Thursday at 2pm. Indeed, the first people who come to mind when I say thank you are those in the lab.

Foremost, I would like to thank my supervisor, Prof. Emmanuel Hanert, who proposed this incredible subject that I am very passionate about. I also thank him for his encouragement and his perpetual enthusiasm. His organisation allowed him to see us every week to support us in this work.

I would like to give also a great thanks to Thomas Dobbelaere to support my tons of mails when my SLIM simulations crashed. The support of Lauranne Alaerts also helped me a lot with her sound advice. Thanks also to the other members of the SLIM team that I have seen from near and far.

Thanks to Jérôme Harlay, who sent us some Seychellois sunshine during our Teams meetings by answering our questions and giving us relevant advice. I would also like to thank him and Sophie Opfergelt for agreeing to read and evaluate this work.

I would like to acknowledge Dr. Georges Pichot, who proofread my entire thesis.

A big thank you to my fellow students and especially Alex and Colin. I hope we'll meet again on the terrace after this. I wish them all the best for the future.

A last thanks to my friends, big up to the Mardicuriens and kot et danse, and family who supported me when I was stressed and boring.

List of acronyms

ADCP Acoustic Doppler Current Profiler
BC Blue Carbon
CMEMS Copernicus Marine Environment Monitoring Service
ECMWF European Center for Medium-Range Weather Forecast
GEBCO General Bathymetric Chart of the Oceans
GIS Geographic Information System
IPCC Intergovernmental Panel on Climate Change
LPT Lagrangian Particle Tracker
NOAA National Oceanic and Atmospheric Administration
OCC Organic Carbon Content
PIC Particulate Inorganic Carbon
POC Particulate Organic Carbon
SeyCCAT Seychelles Conservation and Climate Adaptation Trust
SLIM Second-generation Louvain-la-Neuve Ice-ocean Model
UNEP United Nations Environment Program

Table of contents

1 Introduction

1.1 Context

Currently many phenomena, often interpreted as negative, occur under the same name: global warming. Technological progress and science have improved enormously over the last century, which has brought various phenomena to the fore. The changes thus assessed are changing the properties of the entire Earth system and all its components: biosphere, hydrosphere, cryosphere and atmosphere.

Following this, in 2007, work was carried out to promote a new concept: the Anthropocene [1]. Climatologists Will Steffen and Paul Cruzen, together with historian John McNeill, believed that this was the beginning of a new era, bringing the current era to an end: the Holocene. Indeed, human activities have increased so much that in 2016, a first scientific work confirmed the trend by confirming the concept of Great Acceleration [2]. This trend could be described by a very marked acceleration from 1950 onwards of various human activities such as demography, global primary energy consumption, international tourism or water use. The transition from the Holocene to the Anthropocene is marked by many changes such as the atmospheric concentrations of CO_2, NO_x and CH_4 accompanied by a sharp drop in δ^{13}C captured by trees, an increase in the average global temperature of 0.6 to 0.9°C since 1900 and, by analogy, an increase in δ^{18}O in the Greenland ice and a rise in sea level [2].

Fig. 1 shows the main Earth system trends occurring during the transition phase between Holocene and Anthropocene. It's based on 12 indicators, representing the global state of the planet. The four first indicators show the state of the atmosphere. Atmospheric CO_2, NO_2 and CH_4 had increased over the 1750-2010 period ranging from 100 to 1000 ppm in function of the gas considered. These 3 GHGs (GreenHouse Gases) have the higher relative global warming potentials. Indeed, CH_4 and NO_2 warming potentials are evaluated to 25 times that of CO_2 and 298 times that of CO_2 respectively [3]. The sources of these gases are natural wetlands, anthropogenic activities, and biomass burning for CH_4 [4] and nitrogen fertilisation, cropland expansion, processes due to fossil-fuel combustion [3] for NO_2 emissions. While GHGs increased, stratospheric ozone had decreased by $\sim$60% , mainly due to chlorofluorocarbons emissions of human activities [5]. These four indicators are directly related to the rise of surface temperature, less ozone contribute to less UV reflexion [6] and more GHGs increase the infrared absorption of the Earth surface.

Another face of the Earth trends is the ocean. Again human activities are the main cause of these process. Indeed, rises of ocean acidification and nitrogen coastal euthrophication are respectively linked to atmospheric carbon dioxide increase [7] and increase in nitrogen flux by rivers to coasts [8]. Unfortunately the consequences of these are numerous and impact biodiversity and ocean chemistry [7]. Others indicators could be used to assess the ocean health such as marine fish capture or the shrimp aquaculture. Their evolution during the 1750-2010 period is dramatic with a major effect on biodiversity loss. However, increasing aquaculture production might have been a good idea but these farms require far too much fish to be sustainable (e.g. to feed carnivorous fish) [9].

Finally last indicators are related to land change. The increase in domestic land has increased by $\sim$25% during the period 1750-2010 while tropical forests have lost almost $\sim$25% of their territory. All this results in a loss of biodiversity.

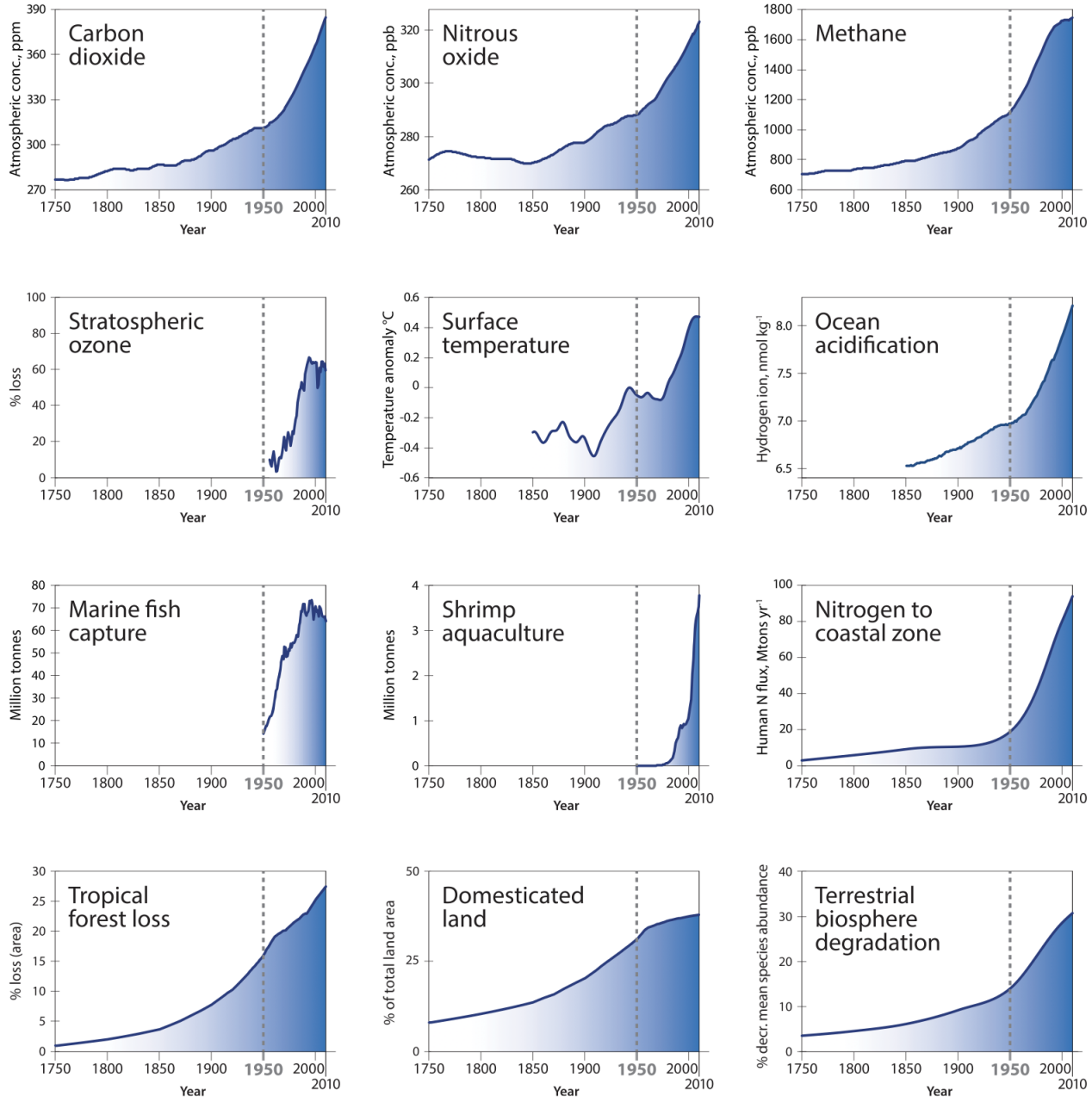

Figure 1: Earth system trends during the period 1750-2010 [10]

These changes lead directly to current issues that are taken up in political debates: loss of biodiversity, pollution, air quality, etc. It is not easy to discern the causes from the consequences, however, Steffen et al. [11] has attempted to define thresholds beyond which new states of equilibrium could appear, thus changing the entire earth system and potentially generating catastrophic consequences for human life: planetary boundaries (Fig. 2). These boundaries are established according to their current status and their status during the pre-industrial era, according to these two values a limit is established. The inner green shading represents the proposed safe operating space for the 9 different process, while the red wedges show the current estimate of them.

For certain processes such as climate change, several indicators are taken into account to draw the planetary boundaries shown in Fig. 2: change in radiative forcing and atmospheric carbon dioxide concentration. This representation remains very vague, although it is based on scientific measurements, but it makes it possible to establish the critical processes driving the Earth system changes. Currently three boundaries are exceeded: biodiversity loss, climate change and nitrogen

cycle. Biodiversity loss is the most dramatic situation, its boundary is expressed by the rate of extinction (number of species per million species per year). The proposed boundary is estimated to 10 but the current status is set to >100 [11]. The second critical process is related to nitrogen cycle, expressed in amount of N_2 remove from the atmosphere for human use (in millions of tonnes per year). The boundary is set to 35 but currently it's estimated to 121 [11]. The other subsystems are still within the limits of acceptability (ocean acidification, phosphorus cycle, global freshwater use, change in land use, stratospheric ozone depletion) or exceed them slightly and can still be modulated through action (climate change). It should be noted that two subsystems have not yet been quantified (chemical pollution, atmopsheric aerosol loading) and could perhaps prove dramatic.

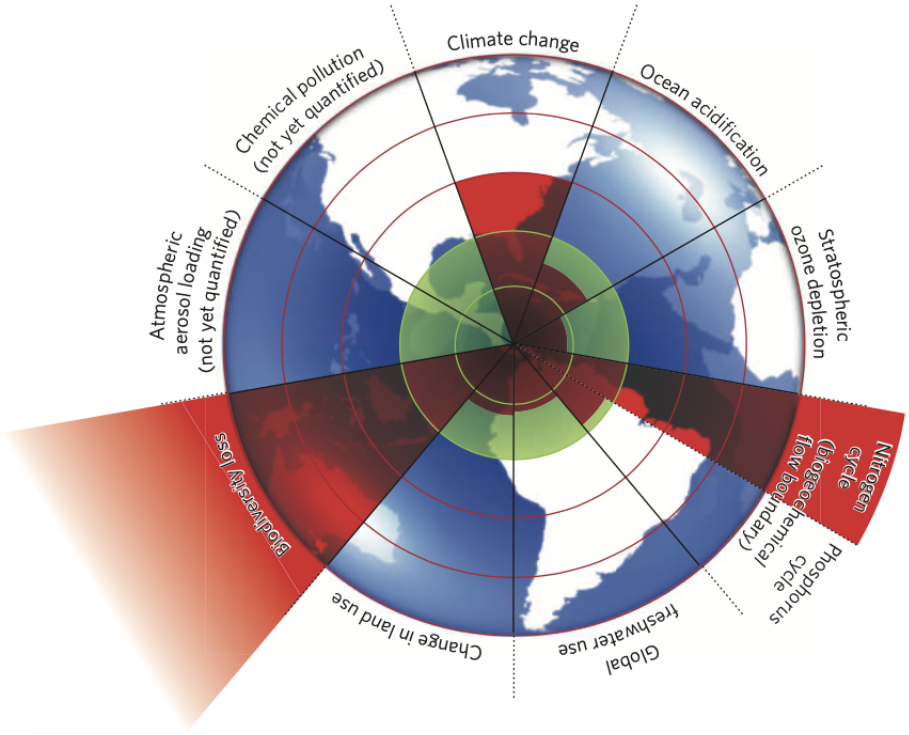

Figure 2: Visualisation of planetary boundaries for 9 processes of the Earth system [11]

All the processes described in Fig. 1 are interdependent and have sometimes disastrous consequences for life on Earth. For example, the atmospheric concentration of carbon dioxide directly induces the acidification of the oceans. This last phenomenon is dramatic for the marine environment, as it unbalances the carbon cycle by reducing the pH, the concentration of carbonate ions and thus the formation of limestone [12]. Many marine ecosystems and animals are affected by this process, such as corals and other marine living organisms that need to build their skeletons with these elements. The case of coral extinction is widespread, with around 32.8% of species with conservation status being critically endangered [13]. The causes of this extinction, in addition to acidification, are also the increase in ocean temperature, the destruction of its habitat and overfishing [14] (Fig. 1). A scientific study estimates that between 30 and 60% of the loss in genetic diversity of reefs is linked to human activities [14]. The example of coral is a specific case, but there are many other cases where the same causes are at play, there is never just one independent cause, just as there is no isolated case.

To mitigate all these changes and to avoid too much damage on a global scale, it is necessary to act and to find levers for action. The first direct point of action is the regulation of human activities. Indeed, according to the last IPCC[1] report [15], mankind, despite the consequences for human life,

[1]Intergovernmental Panel on Climate Change

is considerably influencing these changes (Fig. 3). Therefore, various conferences and organisations have emerged to regulate human activities and especially their impacts on the environment, the most popular being the United Nations (UN). Among these, the first one took place in 1972 in Stockholm, the first time that the environment was integrated into political debates. This was a precursor conference to which we owe the United Nations Environment Programme (UNEP) [16]. The programme includes various reports and targets, such as the global goal of zero net emissions by mid-century and keeping the 1.5°C temperature within reach. Currently 49 countries have committed to this goal as mentioned in the latest emissions gap report of 2021 [17].

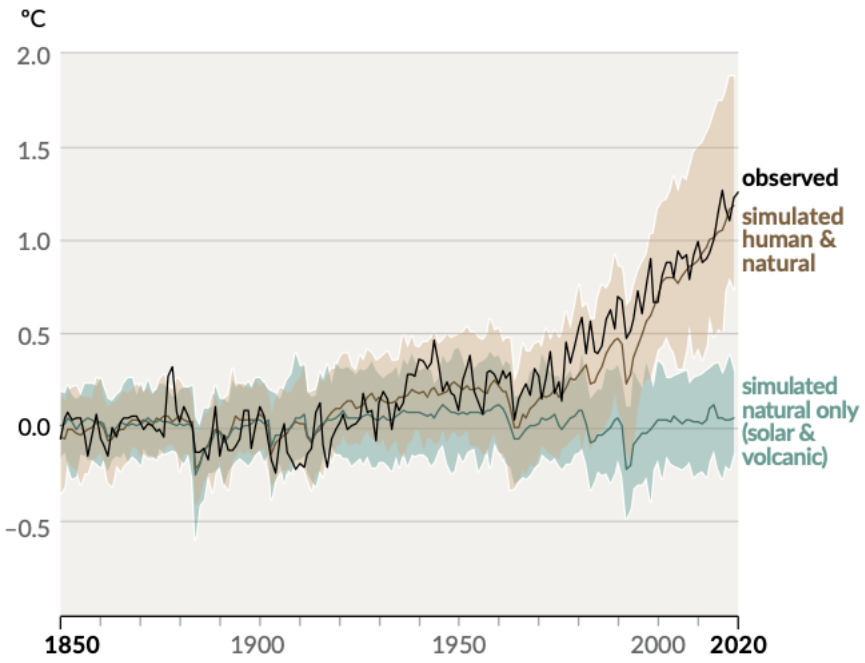

Figure 3: Change in global surface temperature (annual average) as observed and simulated using human & natural and only natural factors (both 1850–2020) [15]

In addition to measures taken on human activities, other measures can be taken on the environment directly where there are several levers of action. Indeed, the various sub-systems (biosphere, hydrosphere, atmosphere, etc.) of the Earth system all have a carbon storage capacity (Fig. 4). Depending on the emission scenario to be followed, this potential will change in each sub-system. In Fig. 4, the scenarios on the left represent low emission scenarios while the scenarios on the right are the worst case scenarios. The worst-case scenarios (SSP3-7.0 and SSP5-8.5) are based on GHGs emissions doubling from current levels by 2100 and 2050 respectively. In this case, only 38 to 44% of total emissions will be taken up by land and ocean carbon sinks. In contrast, the best-case scenarios (SSP1-1.9 and SSP1-2.6), considering emissions decreasing to net zero by 2050 followed by negative emissions, estimate that ocean and land carbon sinks could store between 65 and 70% of these atmospheric emissions. The role of oceans and soils is therefore important in managing climate change. The carbon cycle is therefore a key element to be taken into account in environmental measures.

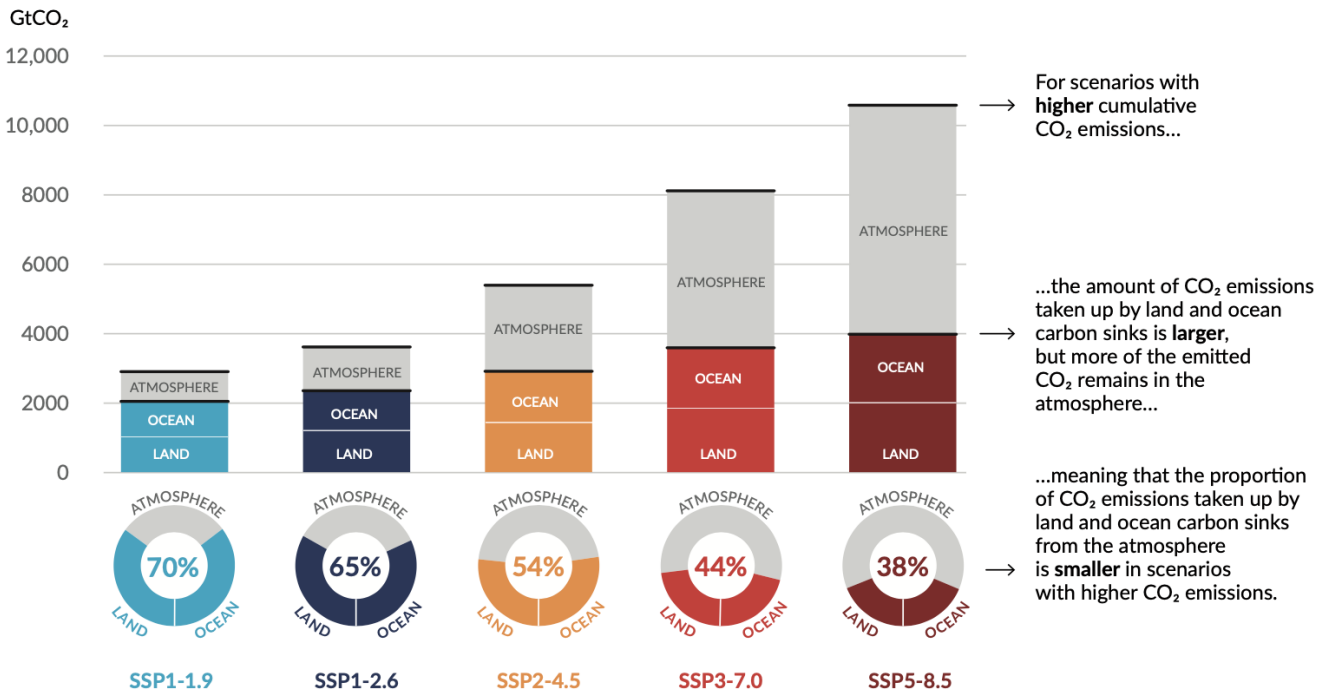

Figure 4: Total cumulative CO_2 emissions taken up by land and ocean (colours) and remaining in the atmosphere (grey) under five illustrative scenarios from 1850 to 2100 [15]

1.2 Carbon cycle

Biogeochemical cycles are of great importance in regulating climate processes, in particular, the carbon cycle has an impact on these changes with two very powerful greenhouse gases: carbon dioxide (CO_2) and methane (CH_4). Although the atmospheric reservoir is important, the below-ground processes are even more important. The contribution of these processes to greenhouse gas (GHGs) fluxes is quantified at 30% for CO_2, 70% for CH_4 and 90% for N_2O [18]. This makes the Earth's crust the largest reservoir of carbon with a storage capacity of 50.10^6 GtC (i.e. 5.10^{16} tC), which is 1.000 times the capacity of the oceans, 20.000 times the capacity of the soil and 50.000 times the carbon stock in the atmosphere [19] (Fig. 5). However, the stocks mentioned above and the fluxes represented in Fig. 5 are not fixed, they can vary enormously depending on various factors such as anthropogenic emissions. Indeed, the absorption capacity of soils or oceans depends on the atmospheric CO_2 concentration, which is called the positive feedback between future climate change and the carbon cycle. If we quadruple the atmospheric CO_2 concentration, it is estimated that the capacity of soils and oceans to absorb carbon will decrease by 54% and 38% respectively [20].

On all these carbon flows, 93% of terrestrial CO_2 is stored or recycled in the oceans and seas, a total of about 4.10^{13} t/yr [21]. To recycle all this carbon, several mechanisms come into play. In fact, there are three major carbon pumps in oceans: the soft tissue, carbonate and solubility pumps [22]. Thanks to these mechanisms, the oceans have a role in regulating the concentration of CO_2. This regulation combines two opposite phenomena, the uptake of CO_2 by the ocean (1) and the release of CO_2 to the atmosphere (2) [23], which can be expressed by the two simple reactions below:

$$CO_2 + H_2O \rightarrow CH_2O + O_2 \quad (1)$$

$$Ca^{2+} + 2HCO_3^- \rightarrow CaCO_3 + CO_2 \quad (2)$$

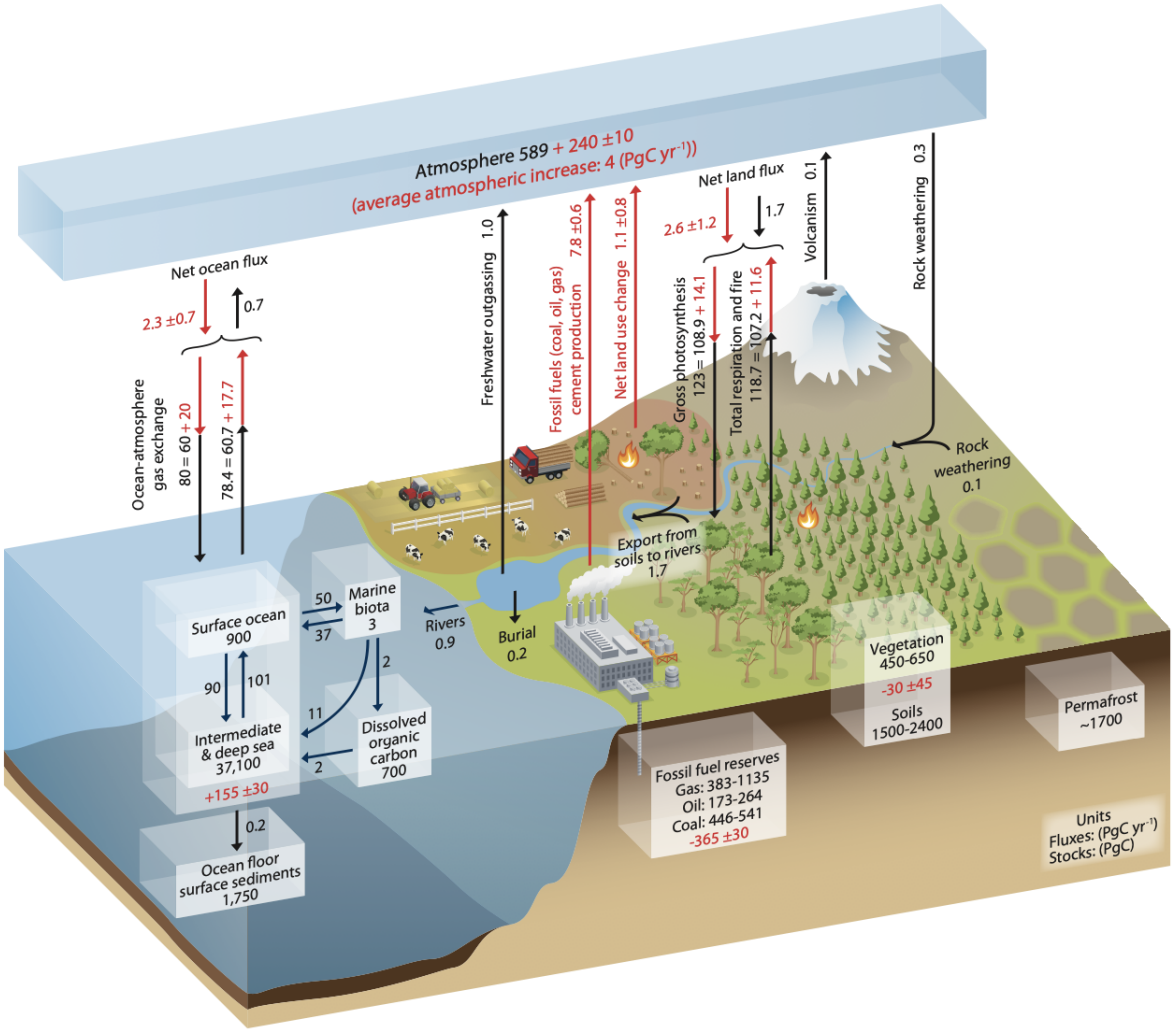

Figure 5: The global carbon cycle showing the main annual fluxes and mass stocks where the pre-industrial fluxes (estimated for the time prior to the Industrial Era, about 1750) are shown in black and anthropogenic fluxes averaged over the 2000-2009 time period in red [24]

The three pumps mentioned above play on these two opposing phenomena. The solubility pump is regulated by the solubility of CO_2, whose main driver is temperature, with better absorption at low temperatures [25]. Carbon dioxide present in the atmosphere will be assimilated by the ocean through a relationship between the concentration of CO_2 in the atmosphere and in the ocean. This happens at the water-air interface and it is a dynamic process. The biological pump includes the phenomena of carbon absorption towards the deep ocean, which are carried out by biological processes such as photosynthesis made by marine organisms for their growth and lead to the formation of organic matter as well as the precipitation of $CaCO_3$, which releases CO_2 [26]. Microorganisms represent 90% of the biomass of the oceans and play a considerable role in the storage of carbon, they participate in more than 95% of the primary production of marine environments [21]. This biological pump is sometimes expressed as two pumps: the soft tissue pump, which includes biological phenomena such as photosynthesis and thus the flow of carbon to the ocean floor, and the carbonate pump, which includes the mineral flows of sediment formation [23].

All the mechanisms described above are not yet well understood. Indeed, the latest models used to predict CO_2 fluxes between the atmosphere and the ocean underestimate carbon uptake by the oceans [27]. Currently the oceans can absorb about 25% of anthropogenic emissions, i.e. a total of 2 PgC per year [27]. The oceans are therefore an important action point for future climate change.

1.3 Ocean-based solutions and blue carbon

The oceans cover no less than 70% of the Earth's surface, and although more and more is being studied, there is still a lot of uncertainties about it [28]. However, the potential of the oceans is now well documented, indeed, by 2030 marine-based solutions could absorb up to 4.10^6t of CO_2e from the atmosphere, and by 2050, if measures are taken, oceans could absorb 11.10^6t of CO_2e. This would contribute to 21% of the 2050 emission reduction targets under the 1.5°C scenario and 25% of emissions under the 2°C scenario [29]. This potential to store carbon can be exploited through various ocean-based solutions such as replacing energy produced by coal-fired power plants with renewable energy sources from the ocean (marine wind turbines, energy extracted from tides and waves), reducing international marine transport, reducing fishing by changing diets or increasing the conservation of marine ecosystems important in the carbon cycle and recycling (Fig. 6) [28]. This list is obviously not exhaustive, there are many more ocean-based solutions to climate change.

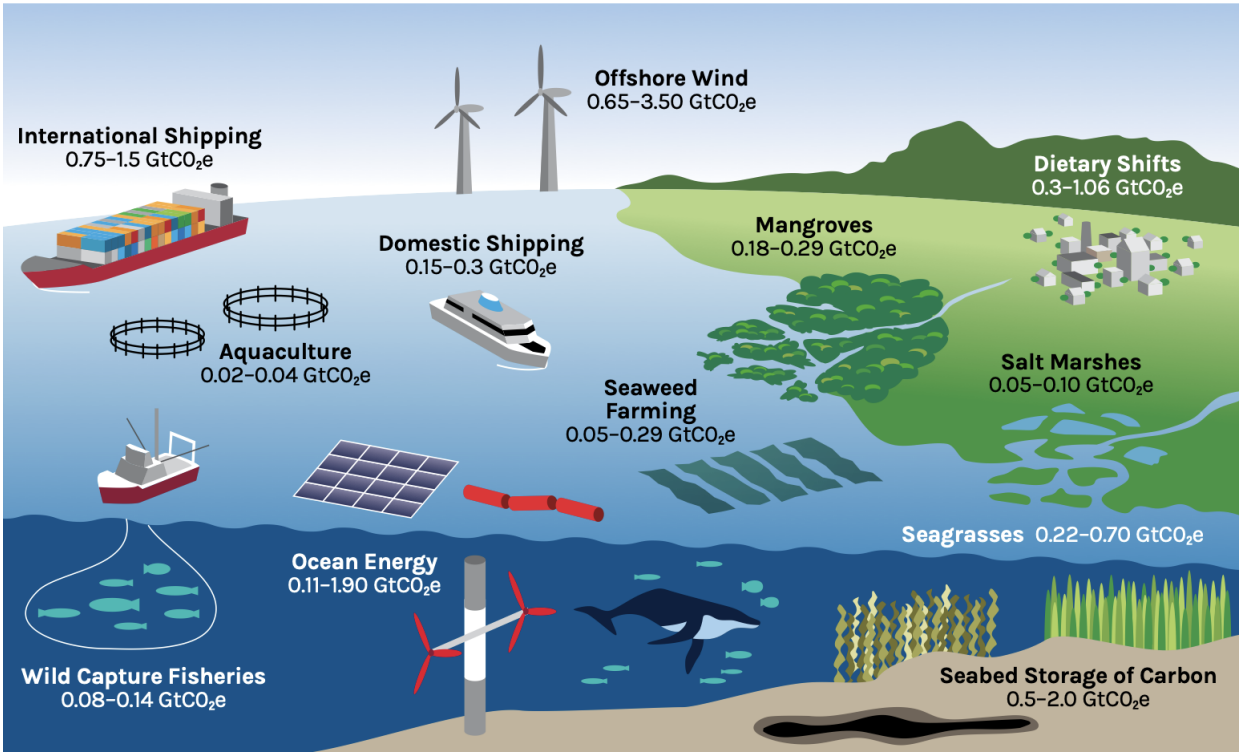

Figure 6: Potential ocean based-solutions that could be explored and their annual mitigation potential for the horizon 2050 [28]

Focusing on the seagrass meadows, subject of this work, Fig. 6 shows a carbon storage potential ranging from $2{,}2.10^8$ up to 7.10^8t of CO_2e for the horizon 2050. Currently worldwide seagrasses represent a carbon stock ranging from $4{,}8.10^7$ to $11{,}2.10^7$tC year^{-1} [30]. This stock is difficult to assess because, depending on the study, the area covered by seagrass varies between 177.000 and 600.000 km^2 [31]. On the contrary the surface area covered by forests is more precisely defined and its net global carbon sink is evaluate to $1{,}1.10^9 \pm 0{,}8.10^9$t C year^{-1} [32]. But in order to have a better comparison between the potential of theses ecosystems, Fig. 7 shows the C_{org} storage for different ecosystems. Seagrass meadows are in the same order of magnitude as forests in terms of carbon storage. Mangrove ecosystems outperform all others.

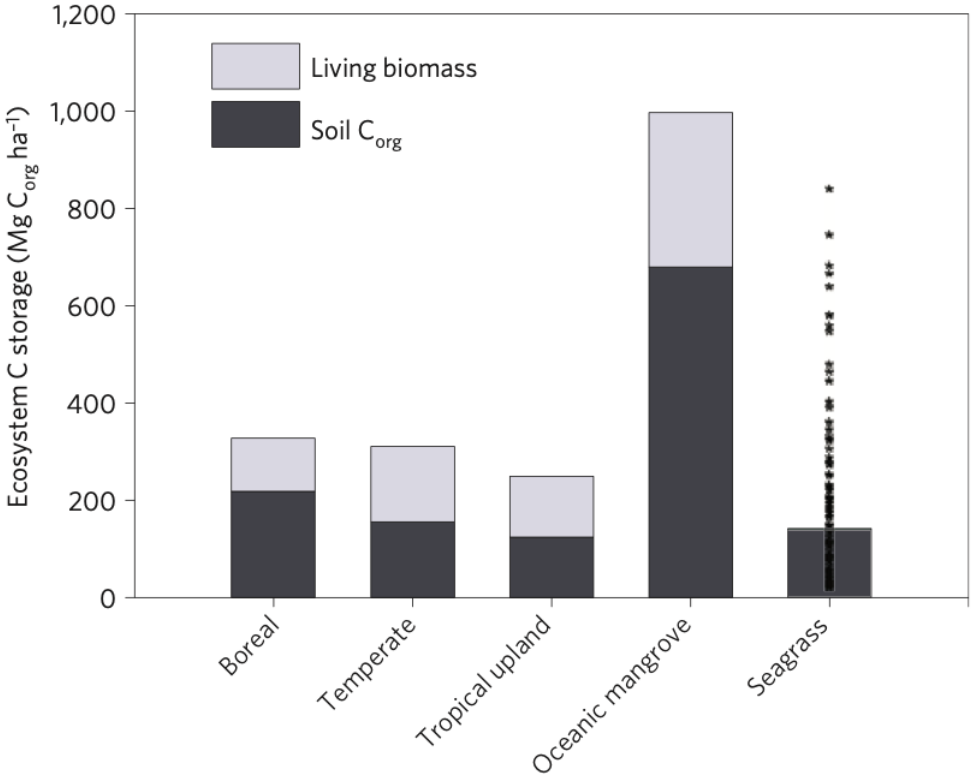

Figure 7: A comparison of seagrass soil C_{org} storage in the top meters of the soil with total ecosystems C_{org} storage for major forest types [33]

The ocean-based solutions cited above and shown in Fig. 6 express the potential of the oceans as a carbon sink. However, this carbon potential is changing over time. Climate change is already underway and some consequences are already being felt such as sea level rise (10-25cm over the last 100 years) [34], ocean acidification and ocean temperature increases. Indeed the ocean heat content (OHC) increased in mean by up to $5{,}7.10^{21}$ J.yr^{-1} during the last 63 years (1958-2021)[35]. This is harmful for ecosystems with a large role in carbon storage such as mangroves and salt marshes which are very sensitive to sea level rise or seagrass ecosystems which are affected by sea temperature rise [36]. The solution requiring the protection of these ecosystems should be implemented quickly so as to avoid reducing our possibilities. A new concept has been created in 2009 to raise awareness and even turn it into a branch of science: Blue Carbon (BC) science [21]. It is a generic term that refers to all marine ecosystems where the carbon stock is still significant and which therefore have a potential to play a role in managing global warming. To complete this description of the concept, *Nelleman et al.* [21] gives us another definition: *"Out of all the biological carbon (or green carbon) captured in the world, over half (55%) is captured by marine living organisms —not on land— hence it is called Blue Carbon"*. In addition to these definitions, criteria have been defined to determine whether an ecosystem is considered as a "blue carbon ecosystem" [37].

The main blue carbon ecosystems are salt marshes, mangroves and seagrass meadows. Between them, they account for 71% of the carbon recycling and storage in the oceans [21], in other words, these three ecosystems store $1{,}3.10^{8}$ - $4{,}9.10^{8}$t C.y^{-1}, i.e. roughly the same amount of carbon as terrestrial forests annually ($1{,}1.10^{9} \pm 0{,}8.10^{9}$t C.$y^{-1}$ [32]) but cover only 0.2% of the world's sea floor, or 3% of the surface area of these terrestrial forests [30]. In terms of storage, these three ecosystems can respectively store 467.5 tC ha^{-1} (1714 tCO_{2e} ha^{-1}) for mangroves, 393 tC ha^{-1} for salt marshes and 72 tC ha^{-1} for seagrass meadows [38]. In other words, 1 ha of mangroves could store the equivalent of CO_2 emitted by 330 passengers vehicles on average in the USA per year. Mangroves are the best-known among the three ecosystems, but are also the ecosystems with the

highest storage potential for a lower habitat area (Fig. 8). In order to address the uncertainties still present in establishing the carbon balance of these ecosystems [39], and particularly for seagrass meadows and salt marshes, it is important to focus on these ecosystems. In this master thesis, the focus will be on seagrass meadows.

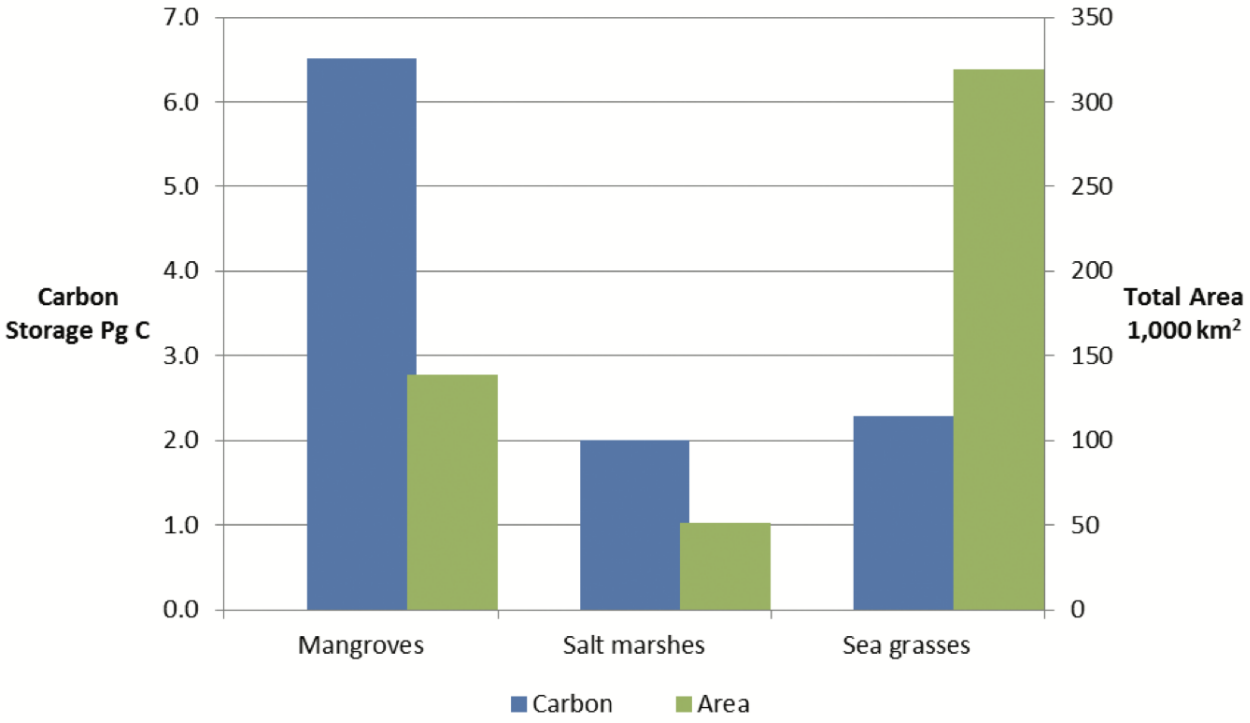

Figure 8: Global carbon storage (PgC = 10^9tC) and habitat area of mangroves, salt marshes and seagrasses [38]

1.4 Storage by seagrass meadows

Seagrasses are habitats made up of plant species adapted to marine life. These ecosystems are found all over the world except in Antarctica, covering about 600.000 km^2 of the seabed. They are made up of several species that differ from region to region, with a total of 72 species identified as part of these seagrass meadows ecosystems [40]. These habitats are very different from other BC ecosystems because of their carbon recycling mechanisms. They first capture CO_2 in order to carry out photosynthesis. In case of strong currents, these algae can detach from the seabed and be transported over long distances [41]. If algal detritus arrive on the seabed then sedimentation can occur and the carbon will be stored, it can remain there for decades to centuries before being remineralised and return to the atmosphere [21].

The residence time of this detritus depends mainly on the oxygen content of the seabed and the particulate organic carbon (POC) fluxes. Residence time estimates are short when based on POC fluxes (few years), while they tend to be longer when based on oxygen demand (until 100 years) [42]. Before being sequestrated, the detritus spend can vary greatly (Fig. 9) and depends on the species. This time can range from weeks for *Halophila* to roughly a year for *Posidonia* [43]. The export of this detritus over varying distances makes seagrass meadows indispensable for certain species and ecosystems that are sometimes far from the seagrass meadows. For example, debris can reach areas with lower primary productivity or nutrient deficits such as in deep areas like canyons. Exports then have a major role in balancing the nutrients in the ocean [41]. In addition seagrass detritus latter have a great potential in shelter numerous finfish and some crustacean larvae. Many

other animals depend on these algae for food, such as turtles, sea urchins, dugongs and manatees [41]. The sequestration process has been shown to be important by analyzing the contribution of this carbon via isotopic carbon ratio (C:N and δC^{13} : C^{12}). It was deduced that some species are highly dependent on this carbon export such as sea urchins and sea cucumbers [44].

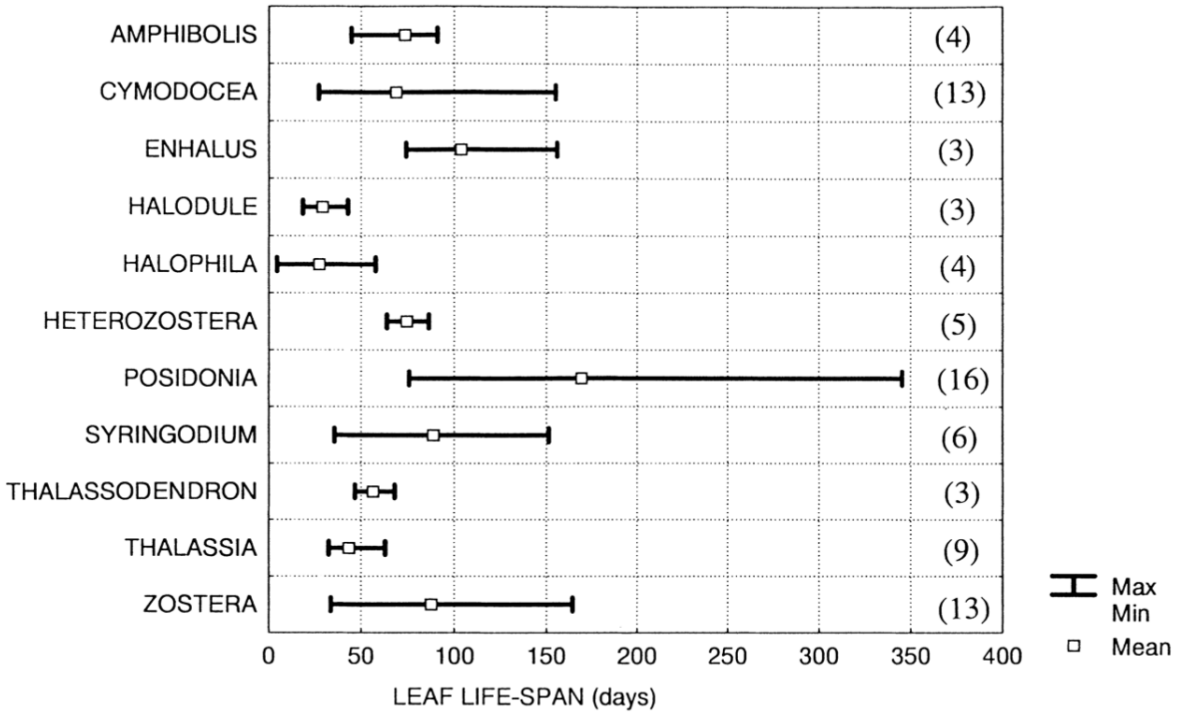

Figure 9: Leaf longevity (days) in seagrasses, in brackets the number of observations [43]

Another feature of these habitats is a mitigation potential of ocean acidification. Indeed, seagrass meadows have the capacity to absorb dissolved CO_2 and not only CO_2 from the atmosphere like salt marshes and mangroves. This has a positive effect on the pH, which increases in the vicinity of seagrass meadows [45]. These ecosystems therefore have a huge impact both locally and globally. The carbon sequestration rate by seagrass meadows varies by region. Latitude, but also the species present, influence the sequestration dynamics [46]. Recycled or sequestered carbon can be organic (POC) or inorganic (PIC), seagrass meadows store 5 times more PIC than POC. PIC stocks are therefore very high near these habitats. The geographical contribution to this stock is variable but the Indian Ocean is one of the most productive regions for the contribution to the PIC stock, with an estimated $7{,}14.10^2$t PIC ha^{-1}[46]. The Seychelles therefore appears to be a suitable location for the study of these ecosystems.

1.5 Blue carbon potential in Seychelles

Seychelles is an archipelago of 115 islands, of which Mahé is the largest, in the center of the Indian Ocean (Fig. 10) [47]. Seychelles exclusive economic zone (EEZ) is very impressive with $1{,}3.10^6$ km^2 [48], but in this study the focus will be on the Mahé plateau, with a surface area of roughly 40.000 km^2 [49]. Isolated from the rest of the world, these granite and coral islands allow a beautiful biodiversity to proliferate on land and in the sea. Among the marine species, there are 330 species of algae, 165 species of crustaceans, 500 species of molluscs and more than 27 species of cetaceans, this list is obviously non-exhaustive [50]. This biodiversity has led the country to develop its strong tourism sector [51], thus leading them to protect coastal waters. In 2018, the Seychelles government

became the first to invest in blue bonds [52]. These are defined by the World Bank [53] as *"a debt instrument issued by governments, development banks or others to raise capital from impact investors to finance marine and ocean-based projects that have positive environmental, economic and climate benefits"*.

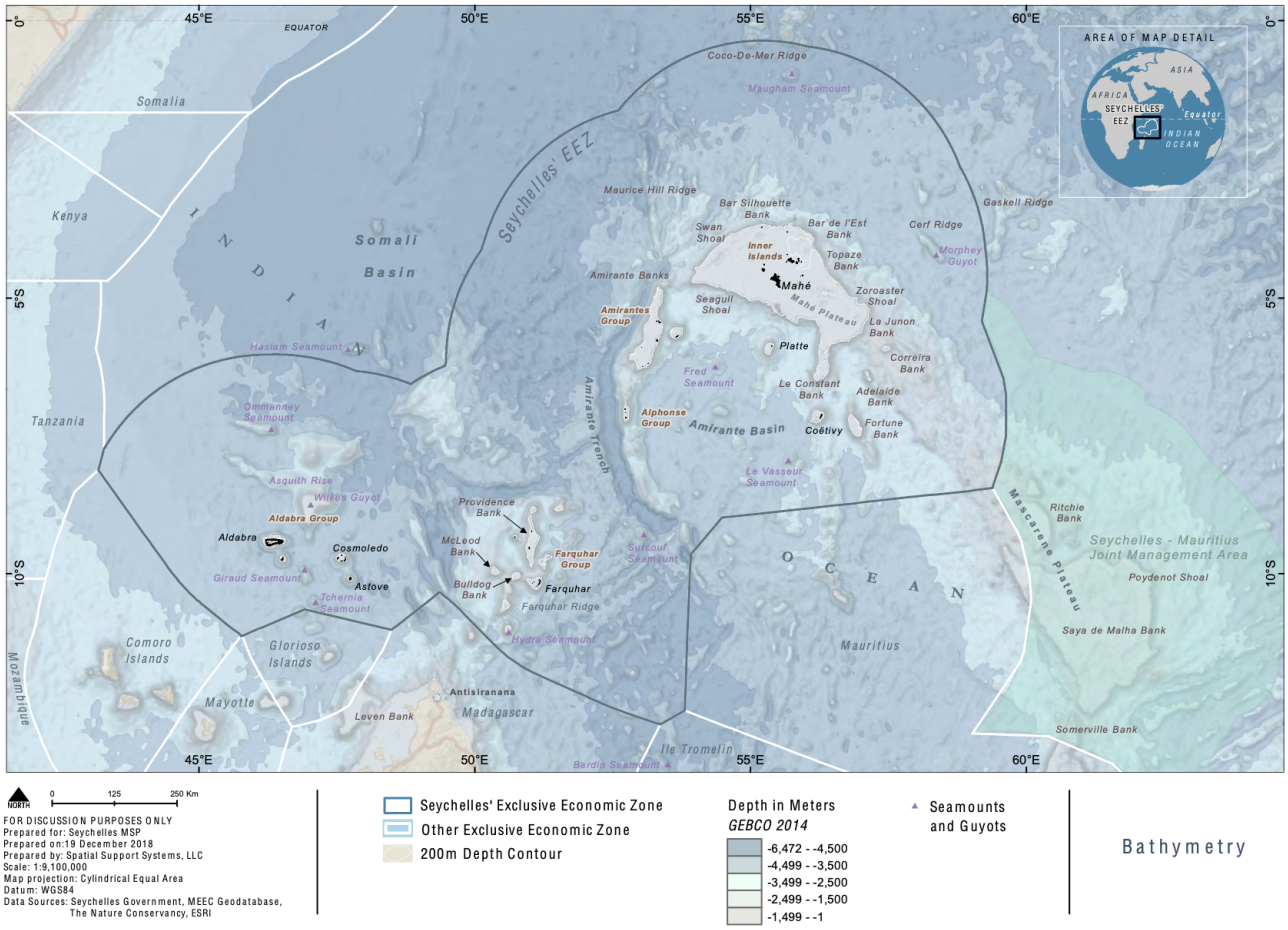

Figure 10: Seychelles islands, Economic Exclusive Zone (EEZ) and bathymetry established by the Marine Spatial Plan [54]

This strategy based on the protection of the ocean has led Seychelles to develop research on Blue Carbon and especially on seagrass meadows. In 2015, the Seychelles Conservation and Climate Adaptation Trust (SeyCCAT) was created and will lead to different policies in the protection of the oceans [55]. In 2019, the government of Seychelles placed blue carbon in its nationally determined contribution (NDC), including the protection of mangroves and seagrass meadows [56]. To continue, by 2030, Seychelles would like to protect 100% of its coastal wetlands. A survey to estimate the carbon storage capacity of the Seychelles has recently been set up, aiming in particular to map the seagrass meadows in the Seychelles [57], in response to a lack of data. Comparing the blue carbon potentials of Seychelles' neighbours, the potential of Seychelles can be estimated between 0,15 and 3.10^6 tC.y^{-1} [58]. In order to face this potential with the potential of a forested country like Brazil, the latter has an estimated potential of $2.7.10^6$ tC.y^{-1} [59]. This attests to the power of the oceans for carbon sequestration. However, there is still too little data on marine ecosystems especially in the Seychelles. Currently, only four works contain data on blue carbon in the Seychelles, most of them dating from the end of the 20^{th} century [60]. However, UNEP has a recent database of some seagrass meadows sightings in the Seychelles [61]. In addition, as part of the Marine Spatial Plan, a study was carried out to estimate the probability of seagrass occurrence in the Seychelles (Fig. 11) [54].

These maps were based on satellite images and were not verified by field measurements. A more comprehensive renewal of databases is welcome in the face of current environmental problems.

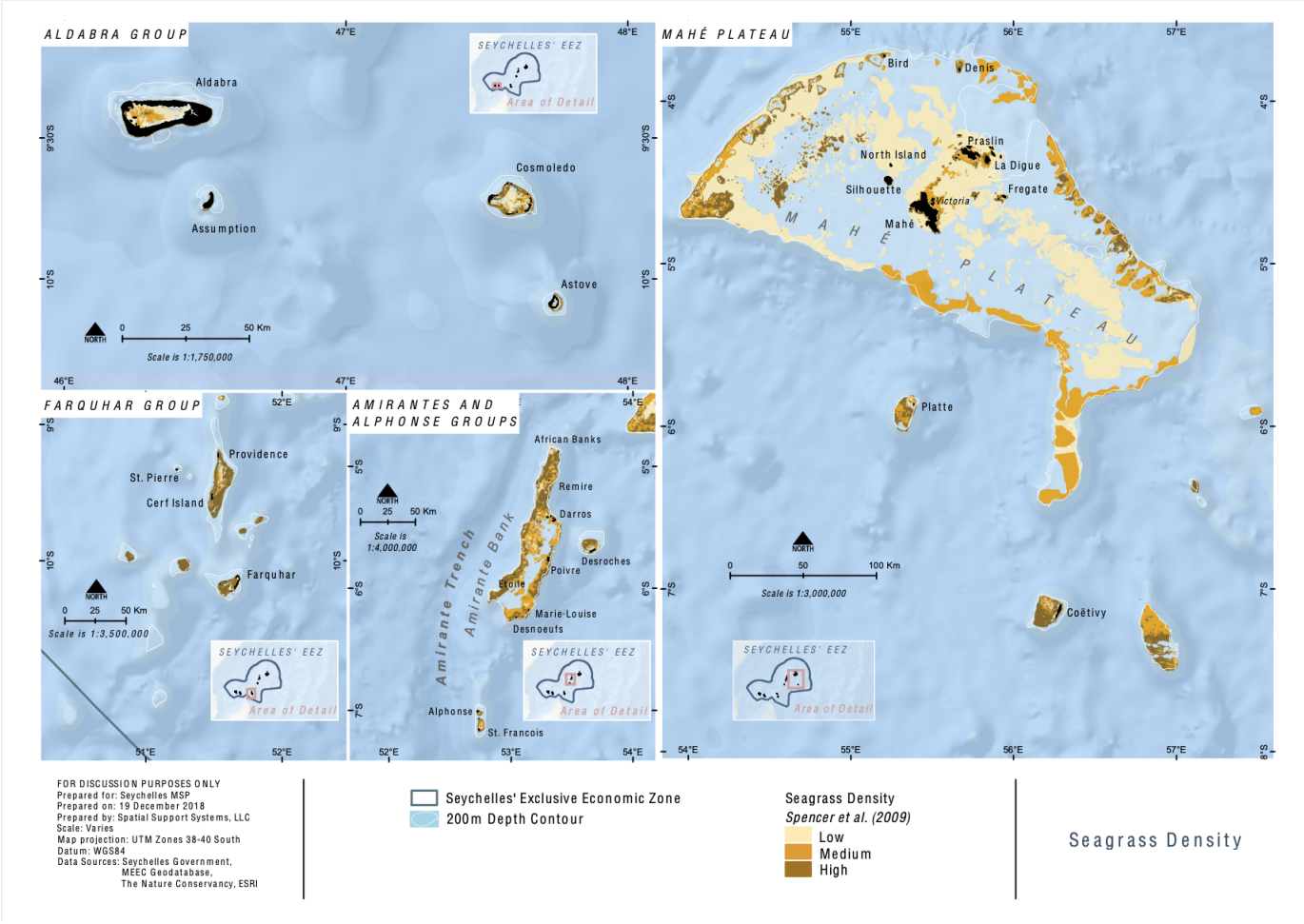

Figure 11: Seychelles seagrass density maps established by the Marine Spatial Plan [54]

1.6 Objectives

Blue carbon will play an important role to mitigate future global warming. It is therefore important to quantify the carbon storage potential of marine ecosystems and particularly those found in small island developing states such as Seychelles. With $1{,}3.10^6$ km^2 exclusive economic zone (EEZ) [48], Seychelles has a significant carbon storage capacity that needs to be quantified. This study will try to estimate a little part of this huge area, by quantifying the seagrass carbon exports of the Mahé plateau. The driving question will be, how much do seagrass meadows could contribute to marine carbon sequestration in the Seychelles?

In order to answer this question, the SLIM model will be used to simulate the currents and the dispersion of the exports. An estimate of the current potential based on data confirmed by Dr. Jérôme Harlay (Univerity of Seychelles) and an estimate of the possible potential will be made. Particular interest will be given to exports reaching the outer shelf. The latter have a greater impact on marine carbon sequestration.

2 Material and methods

This work is divided into two main parts: the hydrodynamic modelling of the area of interest and the simulation of propagules exports from seagrass meadows. These two steps are carried out using the finite-element Second-generation Louvain-la-Neuve Ice-ocean Model (SLIM).

2.1 Hydrodynamic modelling

2.1.1 SLIM model

SLIM[2] is a hydrodynamic model based on the Discontinuous Galerkin finite element method. It solves the ocean circulation governing equations on an unstructured mesh, which allows users to adapt the simulation resolution to several factors such as the distance to features of interest and the bathymetry. The mesh can then have a finer resolution in specific areas and a coarser resolution elsewhere. SLIM includes 3 different types of models: a 1D model river flows; a 2D barotropic model for rather shallow areas (used in this work) and a 3D baroclinic model for the deep ocean. This model can be adapted to a wide variety of areas and cover many hydrological ecosystems. After the hydrodynamic modelling, it is possible to couple result with an Eulerian and Lagrangian model in order to add a transport model or a particle tracker to simulate the transport and fate of sediments, pollutants or seagrass fragments.

2.1.2 Definition of the studied area

The study area established for this work was defined such that open-ocean boundary corresponds to the 400m isobath. The minimum bathymetry level was set to 3m to ensure having dry mesh at low tide. The bathymetry that was used for the simulations (Fig. 12) is based on two different data sources.

Bathymetric data from GEBCO[3] [62] were the first to be used. However, this bathymetry includes a 700m deep area North of La Digue, which appears rather surprising on such a shallow plateau. Bathymetry from ETOPO [63] was used for comparison (Fig. 13). In the absence of field data confirming the existence or otherwise of this oceanic trench, bathymetric single beam data, from NOAA[4] [64], was used to establish the most reliable bathymetry.

[2] `https://www.slim-ocean.be`

[3] General Bathymetric Chart of the Oceans.

[4] National Oceanic and Atmospheric Administration.

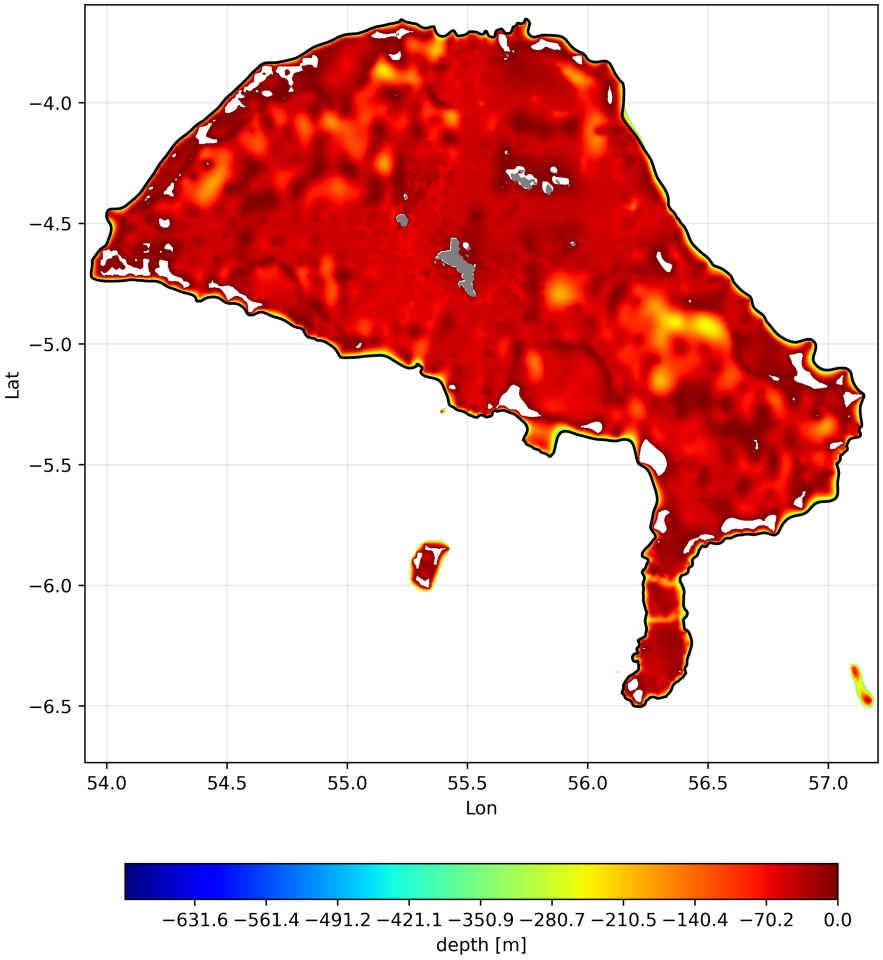

Figure 12: Bathymetry used for the simulations and the mesh generation

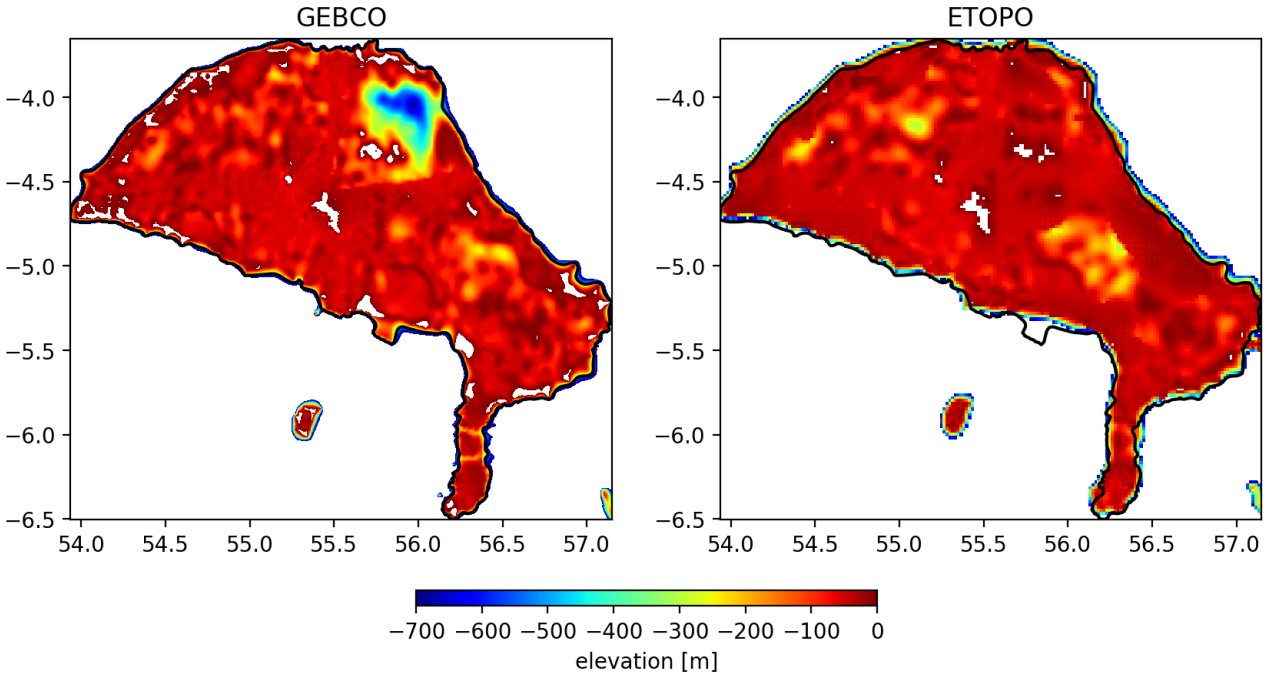

Figure 13: Comparison between GEBCO and ETOPO bathymetry

Looking at the RMSE[5] and MAE[6] (Tab. 1), the GEBCO bathymetry seems to be slightly more suitable based on the single beam data. However, it is necessary to be critical of these statistics as it is impossible to know the reliability of the observations. For the following, the bathymetry used (Fig. 12) is a mix between GEBCO for most of the area and ETOPO in the area north of Praslin and La Digue.

Bathymetry	RMSE	MAE
GEBCO	1092.34 m	389.41 m
ETOPO	1097.54 m	398.25 m

Table 1: Statistics of the two data sources (GEBCO and ETOPO) compared to the NOAA observations dataset

It might seem odd to get an RMSE value of 1000m when the plateau is only about 100m deep on average. This can be explained by a very steep gradient at the exit of the domain. The average error values on the plateau are of the order of 20m while some values at the edge of the domain, close to 3500m, are high and deviate from the average (Fig. 14).

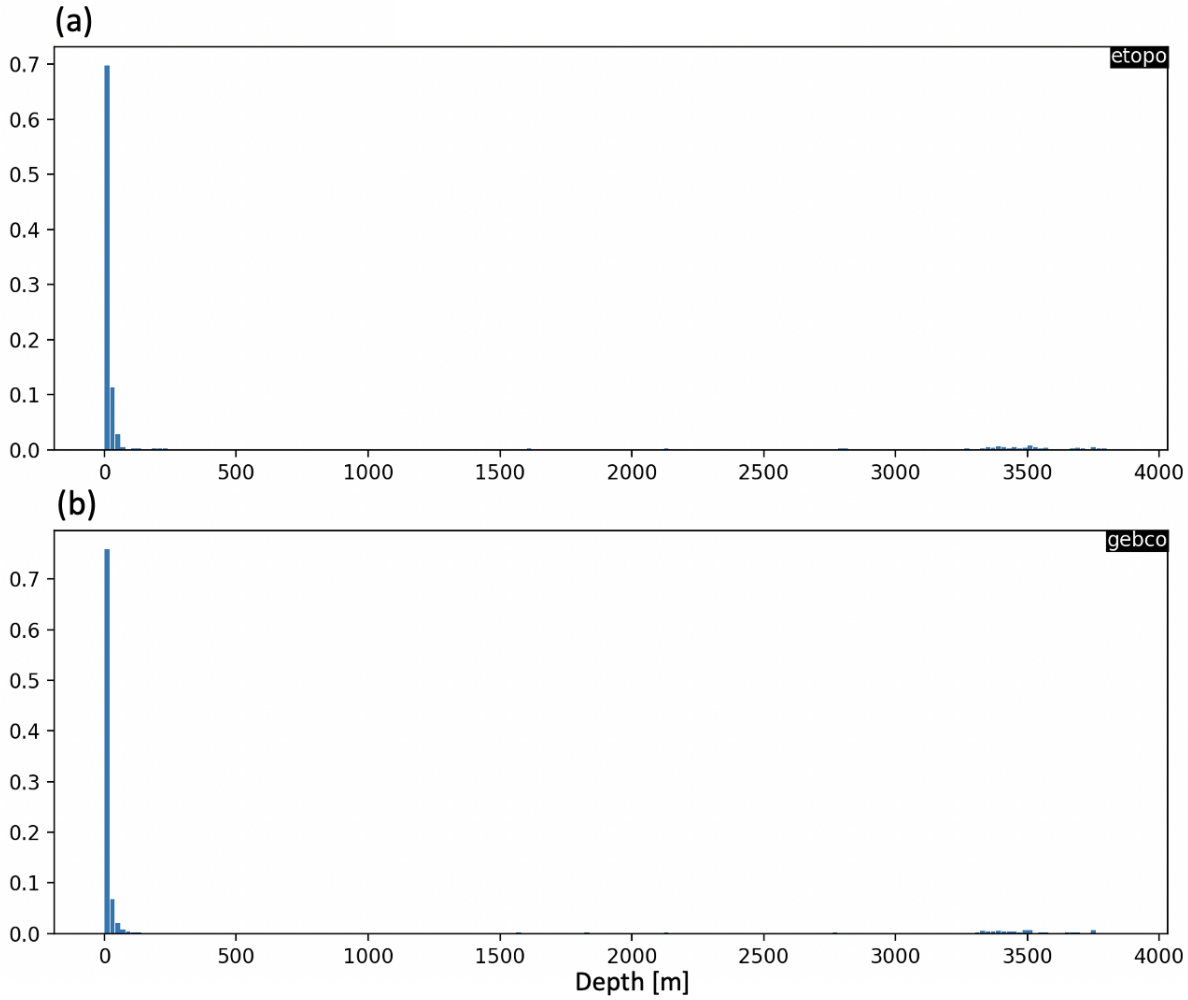

Figure 14: Distribution of the mean absolute error for (a) ETOPO and (b) GEBCO

[5]Root Mean Squared Error.
[6]Mean Absolute Error.

2.1.3 Generate a mesh

The mesh resolution depends only on the distance from the coast. Along the coast (< 5km), the minimum resolution is set to 140m and it increases to 4643m further away (Fig. 15).

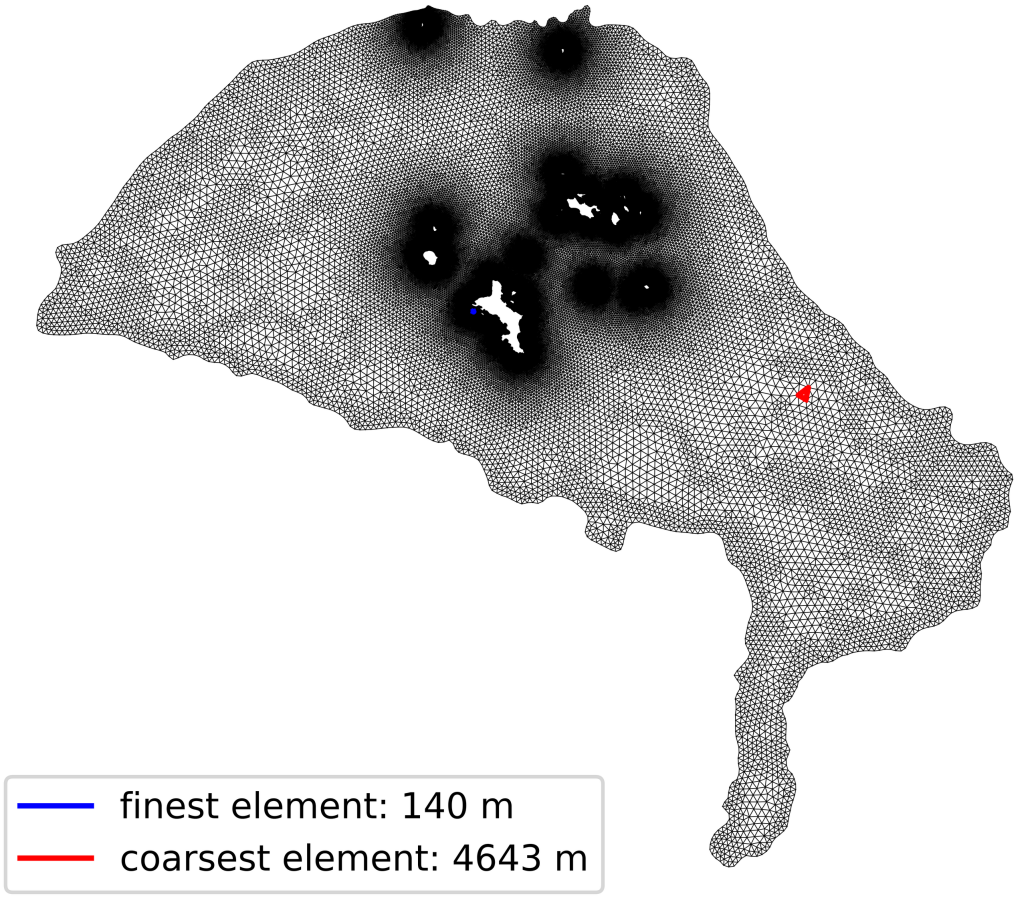

Figure 15: Mesh used for the simulations

2.1.4 Model equations

Here the two-dimensional version of SLIM is used. SLIM2D solves the depth-averaged Navier-Stokes equations (shallow water equations) for the surface elevation η and the horizontal velocity $\boldsymbol{u}$. These equations assume that the water density is constant everywhere. The corresponding non-linear equations are as follows:

$$\frac{\partial \eta}{\partial t} + \boldsymbol{\nabla} \cdot (H\mathbf{u}) = 0 \tag{3}$$

$$\frac{\partial \mathbf{u}}{\partial t} + \mathbf{u} \cdot \boldsymbol{\nabla}\mathbf{u} = -f\mathbf{e}_z \times \mathbf{u} - g\boldsymbol{\nabla}\eta - \frac{g||\mathbf{u}||\mathbf{u}}{C^2 H} - C_S \frac{|\mathbf{u} \cdot \boldsymbol{\nabla} H|}{H} \cdot \mathbf{u} + \frac{\boldsymbol{\tau}}{\rho H} + \frac{1}{H}\boldsymbol{\nabla} \cdot [H\nu(\boldsymbol{\nabla}\mathbf{u})] \tag{4}$$

Where $H = h + \eta$ is the depth of the water column; h is a reference depth level; f is the Coriolis factor; $\boldsymbol{e_z}$ is a unit vector pointing vertically upwards; $\boldsymbol{\tau}$ is the surface wind stress; g is the gravitational acceleration; ρ is the water density; ν is the horizontal viscosity; C is the Chezy bottom-stress coefficient and C_S is the numerical slope stress coefficient (here, it has been set at 5). In this study Δt = 900s. The results of SLIM are exported every hour.

The Chezy bottom-stress coefficient is defined as the ratio between the depth of the water column H and the Manning coefficient n which depends on the characteristics of the fluid:

$$C = \frac{H^{1/6}}{n} \tag{5}$$

For this work, the Manning coefficient has been set up to 0.025 $m^{-1/3}s$, which corresponds to a sandy seabed [65].

The surface wind stress is defined as function of the air density (ρ_{air}), a drag coefficient (C_D) and the wind speed ($\boldsymbol{u_{10}}$). It follows the theoretical formula found in Cushman-Roisin and Beckers (2006) [66]:

$$\boldsymbol{\tau} = \rho_{air} C_D ||\boldsymbol{u_{10}}|| \boldsymbol{u_{10}} \tag{6}$$

The wind speed data are from the ERA5 (ECMWF Reanalysis 5^{th} Generation) dataset released by the ECMWF[7] and express the wind speed of the first 10 metres water column. The drag coefficient C_D expresses the fact that stronger winds cause a rougher sea surface, and hence more drag (Smith & Banke parametrization (1975) [67]):

$$C_D = 0.001(\alpha + \beta||\boldsymbol{u_{10}}||), \tag{7}$$

where α and β are equal to 0.63 and 0.066 $m^{-1}s$ based on Geernaert, 1987 [68]. These parameters are valid for wind speeds between 3 and 21 ms^{-1}.
Finally, the last parameter to estimate is the viscosity ν. For this parametrization, the Smagorinsky equation was used [69]:

$$\nu = (\tilde{C}_s \Delta)^2 \sqrt{2(\frac{\partial \boldsymbol{u}}{\partial x})^2 + 2(\frac{\partial \boldsymbol{v}}{\partial y})^2 + (\frac{\partial \boldsymbol{u}}{\partial x} + \frac{\partial \boldsymbol{v}}{\partial y})^2} \tag{8}$$

Where Δ is the local mesh element size; (x, y) are the Cartesian horizontal coordinates; (u, v) represent the depth-integrated velocity of the vector $\boldsymbol{u}$; and $\tilde{C}_s$ is the Smagorinsky coefficient, here estimated to 0.1 according to Lambrechts et al. (2008) [70].

2.1.5 Model forcings

Three forcings are taken into account in addition to the above parameterisation to make the simulation as realistic as possible. These are the tides, the wind and the large-scale currents. Variables such as η and 3D velocity[8] come from the Copernicus Marine Environment Monitoring Service (CMEMS) which provides these data with a 0.83° grid resolution. Surface data, wind and pressure data[9] are from the ERA5 (ECMWF Reanalysis 5^{th} Generation) dataset released by the ECMWF (cfr. section 2.1.4). This last one has a spatial resolution of 30km. Finally, the tides data (tidal velocity and elevation) are provided by the global tidal model TPXO9[10], a baroclinic model with a spatial resolution of about 1/30°.

At the begining of the simulations, the velocity and sea surface elevation are set to 0. After a spin-up of a few days, currents and elevation converge towards a dynamically-balanced solution. Here, the spin up time was set to 2 weeks, so the hydrodynamics simulation starts on the 15^{th} of December 2017, but the selected simulation starts on the 1^{st} of January 2018.

[7] European Center for Medium-Range Weather Forecast

[8] https://resources.marine.copernicus.eu/product-detail/GLOBAL_ANALYSIS_FORECAST_PHY_001_024/INFORMATION

[9] https://www.ecmwf.int/en/forecasts/datasets/reanalysis-datasets/era5

[10] https://www.tpxo.net/global/tpxo9-atlas

2.2 Seagrass detritus dispersal

The hydrodynamic simulation performed in the previous section can now be coupled with another model for seagrass fragments dispersal. This step will be decisive in answering the research question, i.e. estimate the fraction of seagrass propagules that leaves the shelf for long-term sequestration in the deep ocean.

2.2.1 Seagrass data

As part of this work, data on seagrass occurrence areas in the Seychelles were provided by Dr. Jérôme Harlay (University of Seychelles). The simulations that will be carried out later will take these areas as a starting point for the virtual particles. In order to verify these data, data from UNEP [71] were used for comparison. In addition to these data, the focus of this work was also on potential areas where seagrass meadows could grow. Seagrass meadows tend to develop in shallow areas, of depth less than ∼20m. In order to assess the maximum blue carbon potential of the Seychelles shelf these areas were also considered by the particle tracker. They were defined on the basis of the bathymetry used for the hydrodynamic simulation (cfr. 2.1.2). Fig. 16 shows all these data.

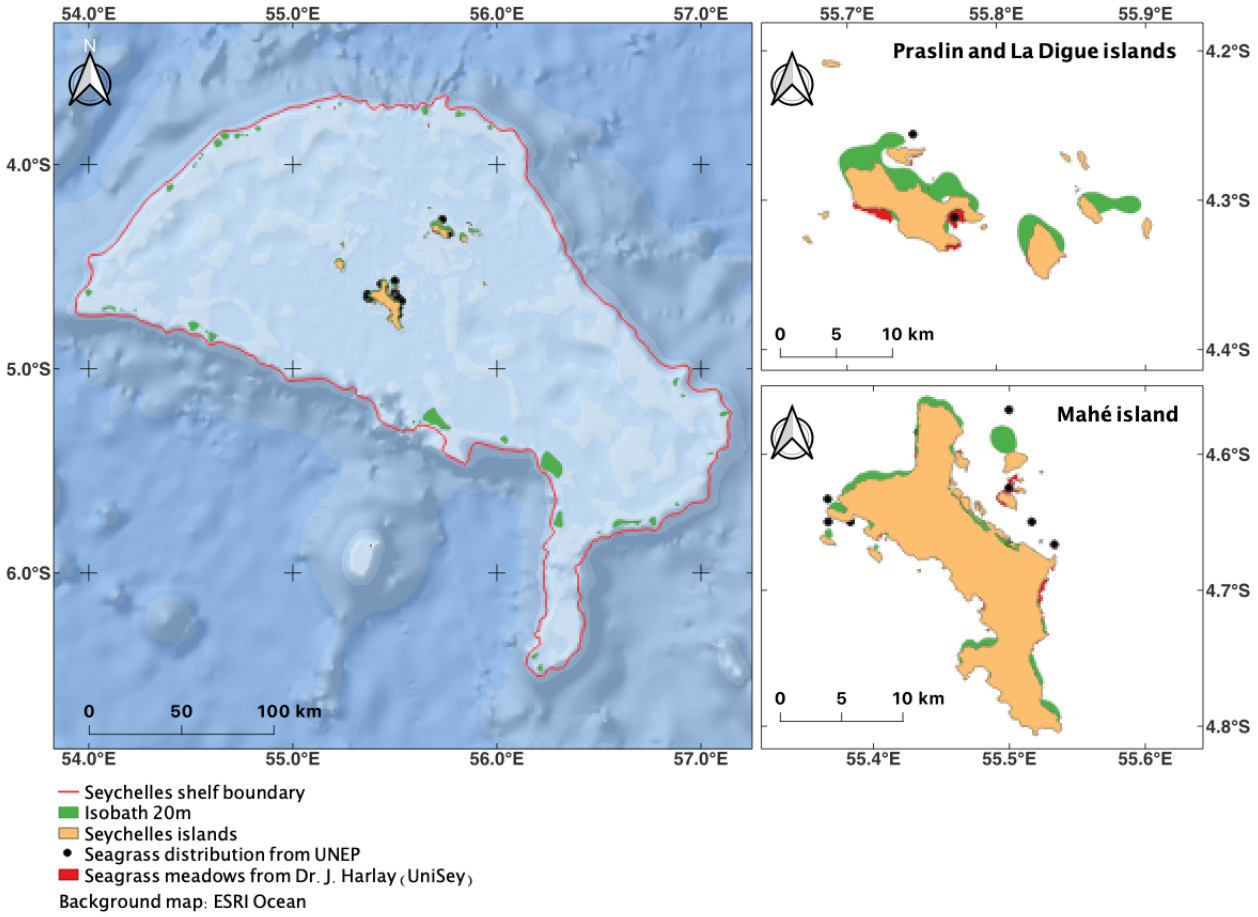

Figure 16: Seagrass occurrence areas from the University of Seychelles and UNEP [71] and seagrass potential areas related to the isobath 20m

The areas where seagrass beds are found are mainly around the islands of Mahé, Praslin and La Digue. These areas seem to be validated by UNEP observations [71]. The zones of hypothetical seagrass presence of are much more scattered on the plateau, there are some along the coasts but also on the whole perimeter of the plateau. As these areas are hypothetical, there is no real way

of verifying them. However, taking Fig. 11 of this report (cfr. section 1.5), the 20m isobath zones shown in the figure above appears to be represented by a medium probability according to the Marine Spatial Plan satellite data [54]. From a quantitative point of view, the UNEP data consists of 14 areas of seagrass meadows on the Seychelles plateau; the data from Dr. Jérôme Harlay refers to 41 areas and finally the areas represented by the 20m isobath have 59 areas in total. This represented surface areas of 4.92 km^2 for the observed patches and 466 km^2 for the hypothetical patches, i.e. a total surface area of $\sim$470 km^2 in the whole plateau.

2.2.2 Lagrangian particles tracker (LPT)

The passive transport of virtual particles over the plateau was modelled using a random walk formulation of the 2D advection-diffusion equation. This was implemented following the works of Dimou and Adams [72] and Thomas [73]. This methodology is discussed by Spagnol et al. [74]. The random-walk particle-tracking scheme implemented in the LPT is defined as:

$$\boldsymbol{x}_{n+1} = \boldsymbol{x}_n + \boldsymbol{v}_n \Delta t + \frac{\boldsymbol{R}_n}{\sqrt{r}} \sqrt{2K\Delta t} \tag{9}$$

With

$$\boldsymbol{v}_n = (\boldsymbol{u} + \frac{K}{H}\boldsymbol{\nabla} H + \boldsymbol{\nabla} K)|\boldsymbol{x}_n \tag{10}$$

where $\boldsymbol{x}_n$ and $\boldsymbol{x}_{n+1}$ are the particles positions at time iterations n and $n+1$ respectively; Δt is the time difference between iterations; K is the horizontal diffusivity coefficient; $\boldsymbol{u} = \boldsymbol{u}(x,t)$ is the instantaneous depth-averaged horizontal water velocity modeled with SLIM; H is the water column depth and $\boldsymbol{R}_n$ is a two-dimensional vector of random numbers with a mean of zero and a variance of $r \equiv < R^2 >$ ($\frac{\boldsymbol{R}_n}{\sqrt{r}}$ is a vector of random r numbers with unit variance).

Equation 9 can be broken down into two parts. On the one hand, a deterministic term: $\boldsymbol{x}_{n+1} = \boldsymbol{x}_n + \boldsymbol{v}_n \Delta t$ with $\boldsymbol{v}_n$ expressed in 10. The parameters H and $\boldsymbol{u}$ are directly taken from the hydrodynamic simulation performed in the section 2.1. On the other hand, the last term of the equation 9 is a stochastic term as this equation is called a random walk formulation. This represents the random displacement due to subgrid scale turbulent process.

For this, the definition of the diffusivity coefficient K was made such as the de Brye et al. [75], inspired by Okubo [76].

$$K = \alpha \Delta^{1.15} [m^2/s], \tag{11}$$

where Δ is the local element size of the mesh and the α coefficient is calibrated for coastal waters in the Great Barrier Reef by Andutta et al. [77]. For this work, the value taken for α will be the same, i.e. 0.041 m$^{0.85}$s^{-1}. There are other possible parameterisations for the diffusivity coefficient, but this one stands out from the others because of its dependence on the mesh size.

2.2.3 Biological behavior

During the LPT simulations, seagrass particles are launched from each area defined in the section 2.2.1. The seagrass virtual propagule is transported passively by the currents and a fraction of the wind speed. Here this fraction was set to 1.5%, with wind drag coefficient that has been set up. The position at any time of these particles can then be calculated and the model shows the number of particles that have left the shelf after the simulation. Particles are released every 3 hours with a density of 50 particles per km^2.

Seagrass exports are therefore mainly regulated by current and wind speed. Once the virtual propagule is exposed to the currents, its transport is primarily regulated by its lifespan and wind drag coefficient. The latter defined as:

$$C_d = \frac{t_{ls} - t}{t_{ls}}, \tag{12}$$

where t_{ls} is the lifespan for the seagrass fragment; t is the simulation time and $\boldsymbol{u}_w$ is the wind speed for which only 1.5% are taken into account for the particle speed. This parameter has the effect of decreasing the effect of the wind on the particle as time passes, implying that the particle decomposes slowly and is less and less affected by the wind.

The lifespan coefficient is defined by a constant based on Hemminga et al. [43] (cfr. 1.4). The seagrass leaf longevity is on average 88.4 days, but it varies according to the species. During this study, the lifespan coefficient was set to 70 days. This number represents 10 weeks of transport for a particle, which is close to the average lifetime of Hemminga et al [43]. However, it was set this way according to Stafford-Bell et al. [78] study that measured many characteristics of *Z. muellieri* including its buyoncy and its evolution.

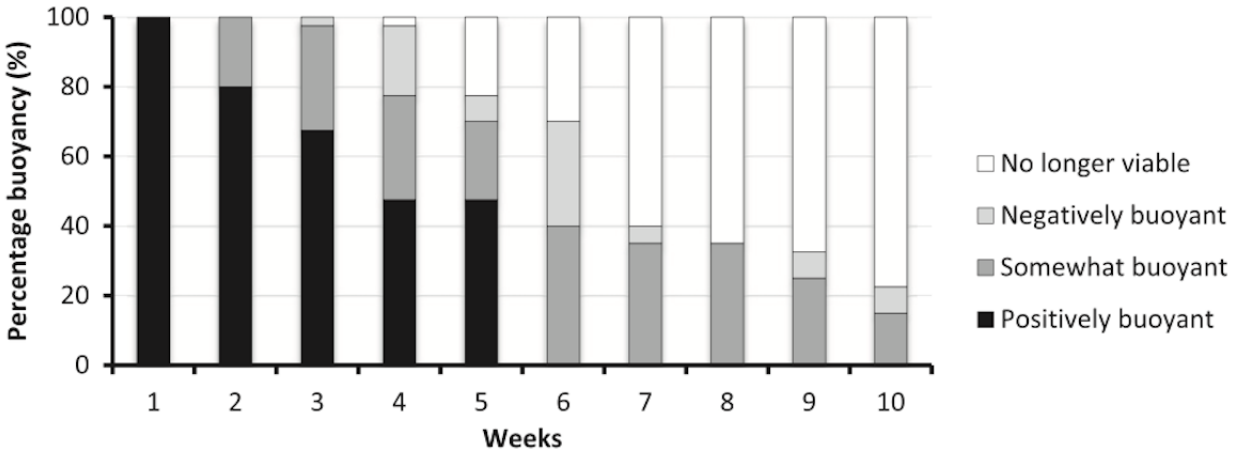

Figure 17: Buyoncy of *Zostera muelleri* vegetative fragments over a ten-week period [78]

Fig. 17 shows the observations of this study. Initially all detritus floats at the surface until they start to settle down. The leaves go through several stages during their transport. Based on these observations, the LPT model takes into account 3 different transport stages for seagrass defined such as:

1. **Positively buoyant**
   This is the first stage for all particles, they are carried away by the currents and float on the surface because they have not yet broken down. During this stage, the particles are transported under the combined effect of currents and 1.5% of the wind velocity.

2. **Negatively buoyant**
   The second stage appears as early as the second week of transport for 20% of the particles. It represents the beginning of decomposition, the particles do not float very well anymore. They are no longer on the surface and this is represented in the model by a transport only due to currents. The wind has no effect as they are deeper in the water column.

3. **No longer viable**
   The final stage for particles is a sedimentation stage. The seagrass propagule is so deep that at some point it settles on the seabed and stops moving. At this point, the particles are not subject to any force and stop moving.

These three states through which seagrass exports pass as implemented in the model are shown in Fig. 18. The transition from one state to another has been copied from Fig. 17 and is represented as a percentage. This means that after each week, a fraction of the particles from the "positively buoyant" stage will change to the "negatively buoyant" stage and so on until they reach the "no longer viable" stage.

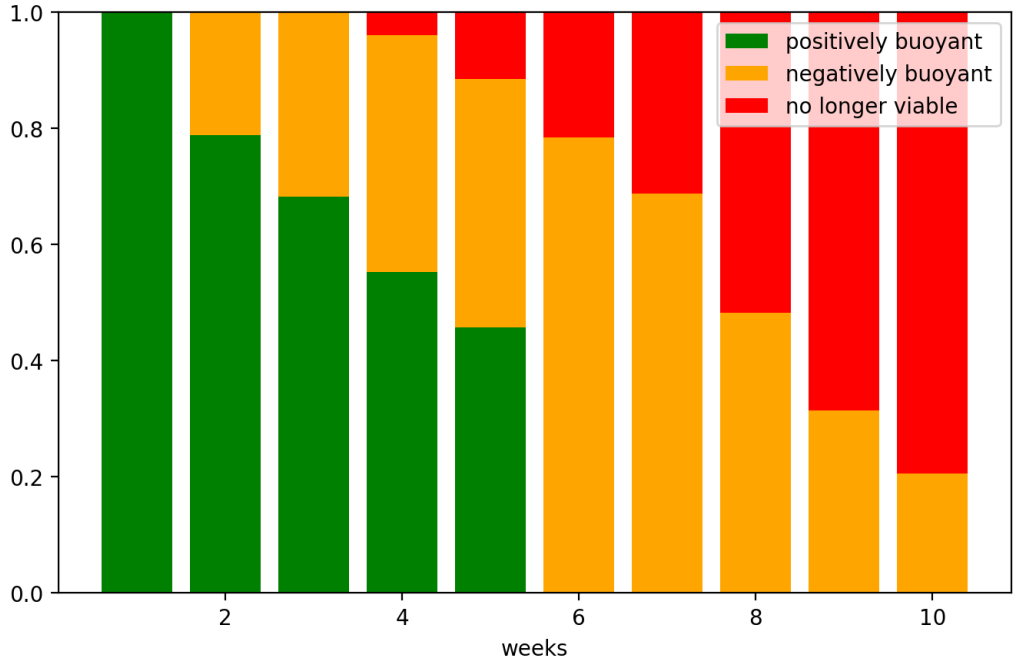

Figure 18: Buyoncy state evolution of seagrass detritus as implemented in the LPT model

2.3 Indicators

In this section, the indicators used to estimate the fraction of exports that leave the plateau will be detailed.

2.3.1 Model outputs

The LPT model used for the simulations returns the results as a CSV file and a shapefile. The latter allows the calculation of the number of particles that left the plateau for each month of the year and each meadow. From then on, using the QGIS program (a GIS[11] program), it is possible to produce a colour map representing the rates exported by each seagrass meadow. It will be the first indicator used for this study.

2.3.2 Duarte conversion factor

In order to quantify the blue carbon impact of Seychelles, it is necessary to convert the fraction of virtual propagules exported from each meadow into an actual mass of carbon. This conversion is based on the Duarte conversion factor [79], which calculates the organic carbon content (OCC) present in seagrass on a dry weight basis. The amount of carbon is then calculated such as:

$$OCC \sim 0.336DW, \tag{13}$$

[11] Geographic Information System.

where DW is the dry weight of seagrass. This coefficient was calculated on the basis of several studies [79] that analysed seagrass species in different regions of the world. This coefficient has recently been validated for seagrass from Indonesia [80]. It will be used to multiply the dry weight of each of the simulated virtual propagules.

2.3.3 Theoretical estimations for the conversion

In order to calculate exported carbon flux, it is necessary to define some parameters and assumptions. First, seagrass dry weight will be estimated in order to obtain the initial propagules carbon content by using eq. 13. Second, the frequency and rate of exports will be estimated and compared with an estimated net primary productivity (NPP), which can be estimated on the basis of the meadows surface area. These estimations will be used to identify the carbon weight of seagrass virtual particles exports.

1. **Dry weight**
   The dry weight of seagrass leaves is subject to strong seasonal variations. During the off-season the leaves are smaller and have a DW of about 37 mg, whereas during the good season the growth of the seagrass contributes to an increase in leaf weight (Fig. 19). Olesen et al. [81] have estimate these biomass-density relationships for the seagrass species *Zostera marina* on 29 populations distributed between 30° and 56°N in different regions.

	Winter	n	Summer	n
Leaf biomass ($g\ DW\ m^{-2}$)	31 (5–82)	32	245 (111–391)	40
Total plant biomass ($g\ DW\ m^{-2}$)	98 (19–170)	24	354 (150–538)	25
Shoot density ($shoots\ m^{-2}$)	604 (143–2069)	24	905 (257–2193)	32
Mean shoot weight ($mg\ DW\ shoot^{-1}$)	37 (16–188)	24	273 (76–924)	32

Figure 19: Eelgrass leaf and total plant biomass, leaf shoot density and mean shoot weight of *Zostera marina* at the winter minimum and the summer maximum. Value are given as the median and 10-90% fractiles (in parentheses) of all populations examined [81]

Seasonal variations are strong and are very different between species [82]. Here, the species *Zostera marina* was considered as a reference. The growth period for southern hemisphere seagrass starts in September, with the production of new stems and flowers, and ends in early autumn (March) with a peak in production during December/January [83]. A confirmation of this seasonal productivity has been made in New Zealand by Turner [84] for the species *Zostera capricorni*.

For the conversion in terms of carbon, a linear regression was performed based on the dry weight presented in Fig. 19. As the peak biomass value (273 mg DW) refers to a leaf from January while the lowest dry weight value (37 mg DW) refers to a leaf from July, the values for the intermediate months are interpolated between these two extremes (cfr. table 2). For each

month, the leaves will have a different dry weight and will contribute more or less to carbon sequestration. The amount of virtual particles can then be expressed in terms of carbon while taking into account seasonal variability.

2. **Exports rate**
   As the dry weight varies between seasons, the exports rate will vary proportionally. Fry et al. [85] have quantified the export rate of the species *Syringodium* in Florida during May-August (Fig. 20). These values tend to confirm the summer trend expressed in Fig. 19, with export rates in the range of 0.15-0.38 g DW.m^{-2}. May-August period corresponds to summer in Florida [86]. Based on this data, the export rate will be set at 1 shoot.m^{-2}.d^{-1}, assuming that the mass of exports per m^2 expressed in Fig. 20 is equal to the DW of one seagrass shoot expressed in Fig. 19. This assumption makes it possible to add a notion of surface area to the previously stated dry weight values. This is presented in Tab. 2.

	Site 1	Site 2a	Site 2b	Site 2c	Site 2d
Dates sampled	May–June	May–June	May–June	May–June	July–August
Area enclosed (m^2)	3.77	0.93	0.83	0.96	4.23
A. Leaf growth per shoot (cm day^{-1})	1.76 ±0.07 (80)	1.88 ±0.11 (80)	1.88	1.88	1.77 ±0.03 (62)
B. Leaf length per shoot (cm)	42.6 ±3.5 (116)	71.3 ±1.8 (99)	71.3	71.3	77.4 ±1.0 (150)
C. Turnover (% day^{-1} = A/B)	4.1	2.6	2.6	2.6	2.3
D. Leaf standing stock (g dry wt. m^{-2})	43.8	67.8	70.1	69.3	80.8 ±7.6 (6)
E. Leaf production = C×D (g dry wt. m^{-2} day^{-1})	1.80	1.76	1.82	1.80	1.86
F. Leaf export (g dry wt. m^{-2} day^{-1})					
Fresh green leaves	0.27 ±0.02 (15)	0.38 ±0.06 (15)	0.15 ±0.03 (15)	0.14 ±0.02 (15)	0.23 ±0.06 (7)
Total	0.48 ±0.03 (15)	1.39 ±0.22 (15)	0.79 ±0.07 (15)	0.95 ±0.09 (15)	0.65 ±0.12 (7)
G. % Export (F/E)					
Fresh green leaves	15	22	8	8	12
Total	27	79	43	53	35

Figure 20: Calculation of leaf production (± s.e.; n in parentheses) and percent export in *Syringodium* meadows of Indian River Lagoon, Florida, May-August 1982 [85]

3. **Net Primary Production**
   NPP values will be used to validate the carbon flux estimation. Indeed, quantification of seagrass fragments exports is often expressed in percentage of NPP. Duarte et al. [87] shows that seagrass exports represents in average 20% of its NPP, but this quantity of exports can vary ranging from 10% to 50%.

   It's estimated that seagrasses cover 6.10^5 km^2 of the global seafloor with an associated NPP equivalent to 5.10^8 tC.y^{-1} [88]. In the Seychelles shelf, observed patches cover 4.92 km^2 and hypothetical areas cover 466 km^2, i.e. a total surface area of ∼470 km^2. Making the conversion, Seychelles seagrasses NPP should be in the range of ∼3,93.10^5 tC.y^{-1}.

   However, as shoot dry weight, seagrass productivity is subject to seasonal variations [89]. Fry et al. [85] observed that productivity was ranging from 0.5 in winter to 4 g DW.m^{-2}.d^{-1} in summer. In the same way as for dry weight estimation, a linear interpolation was performed between the two seasonal peaks to represent this annual variability. It's presented in the Tab. 2.

4. **Final calculation**
   Finally, the calculation made to convert the simulations into carbon flows is detailed below:

$$OCC = N * E * 0.336 * \frac{1}{R_s} \tag{14}$$

where OCC is the Organic Carbon Content in [gC]; N is the number of virtual seagrass propagules; E is the export rate expressed in [g DW.m^{-2}.d^{-1}] and showed in the Tab. 2; 0.336 is the Duarte conversion factor explained in 2.3.2 and expressed in [g C.g DW^{-1}] and finally R_s is the seeding rate [particles.m^{-2}.d^{-1}]. As said in the section 2.2.3, the LPT model releases 50 particles/km^2 every 3h. R_s is therefore defined to convert spawning rate of the model into carbon mass units:

$$R_s = 4.10^{-4}[particles.m^{-2}.d^{-1}] \tag{15}$$

Here the number of days and surface area are not taken into account as the simulations were carried out for each month of the year and each area, so the number of days and meadows surface areas are indirectly included in the number of particles N.

Month	DW	E	NPP
January	273	0,273	4
February	233	0,233	3,42
March	194	0,194	2,83
April	155	0,155	2,25
May	115	0,115	1,67
June	76	0,076	1,08
July	37	0,037	0,5
August	76	0,076	1,08
September	115	0,115	1,67
October	155	0,155	2,25
November	194	0,194	2,83
December	233	0,233	3,42

Table 2: Theoretical parameters used for the carbon conversion for each month calculated by linear interpolation (DW = Dry Weight of one shoot [mg.shoot^{-1}]; E = Estimated exports [g DW.m^{-2}.d^{-1}]; NPP = Net Primary Production [g DW.m^{-2}.d^{-1}])

3 Results

This section will present the results obtained. First, the hydrodynamics results will be presented. The quantification of seagrass exports will take place secondly.

3.1 Model validation

3.1.1 SLIM

In this work, the hydrodynamic simulation was carried out for a three year period (2018-20). A validation of the simulations for currents and sea surface elevation was carried out with the help of observations. Sea elevation observations come from the Space, Security and Migration Directorate - JRC Ispra Site[12] and ADCP[13] current observations are from Seychelles Local Ocean Modeling and Observations (SLOMO). Fig. 21 shows the geographical positions of these observation points.

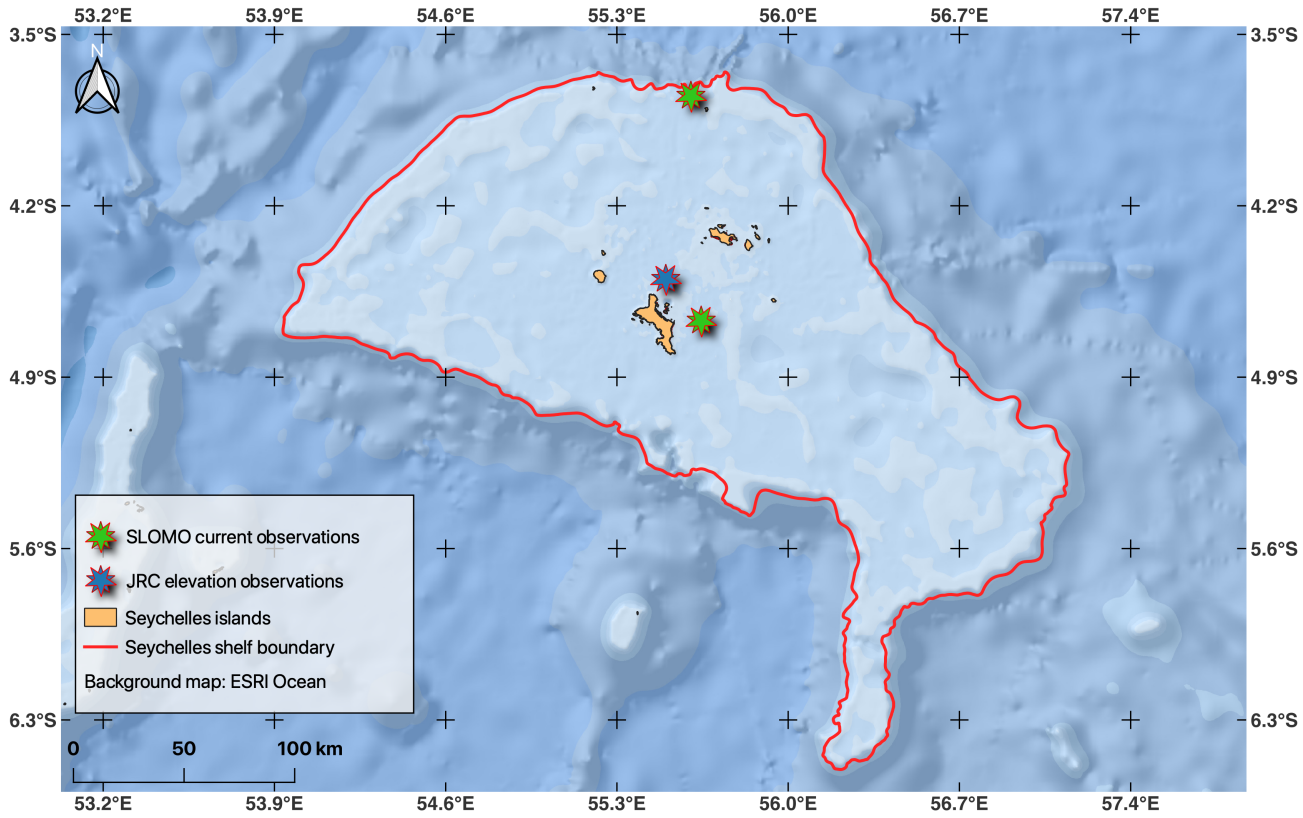

Figure 21: Validation data points: SLOMO data are used for currents validation and JRC data for sea elevation validation

The validation for sea surface elevation is shown in Fig. 22. The simulated values are quite close to the observed values, even in places where there may be a slight over- or underestimation. This figure has been represented for 4 months for the sake of clarity. The validation for sea level maintains the same trend for the following months, expressed by the mean RMSE for the year 2018:

$$\text{RMSE}_{4months} = 0.077 \text{ m} \quad | \quad \text{RMSE}_{2018mean} = 0.0758 \text{ m}$$

[12] https://webcritech.jrc.ec.europa.eu/SeaLevelsDb/Tools/Chart/?deviceId=925

[13] Acoustic Doppler Current Profiler.

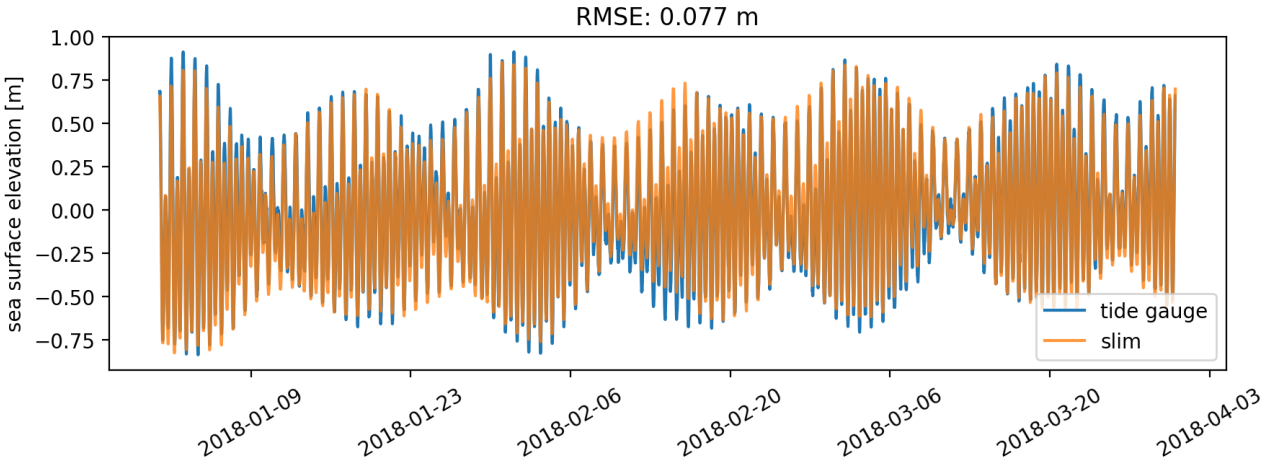

Figure 22: Validation of the sea surface elevation simulated with observations from tide gauge WSL-925-Seychelles-Pt. La Rue for a 4 months duration

On the other side, the validation plot for the currents velocity data is shown in Fig. 23. As presented, there are two points with observations for currents in the Seychelles shelf but only the point East of Mahé has recorded continuous data for the year 2018. Here, the validation shows the two data point but afterwards, only the East of Mahe data point will be considered due to this lack of observations (cfr. appendix A for validation of the North point).

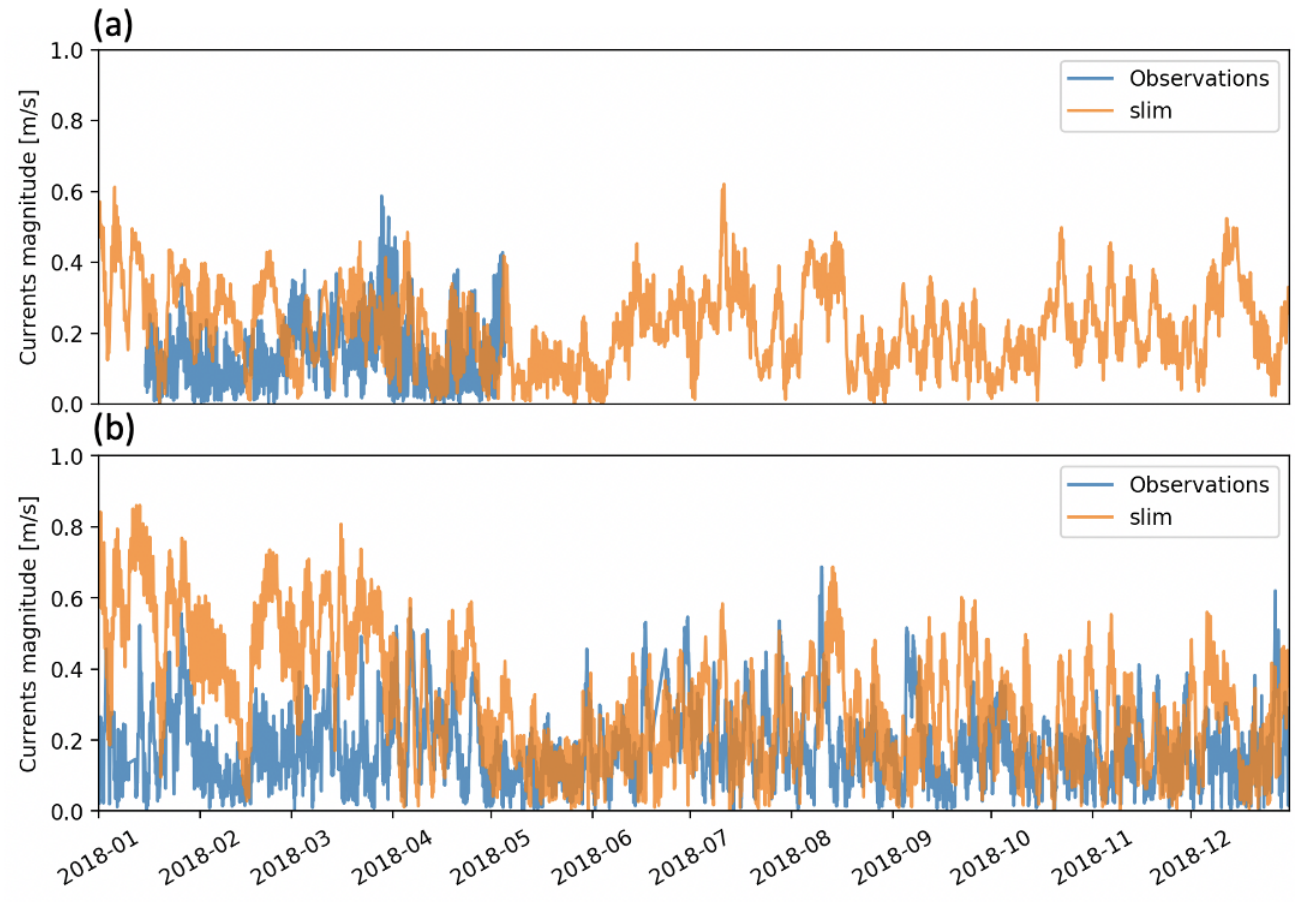

Figure 23: Currents magnitude validation with ADCP data from (a) the North data point (3°44'59.95"S 55°36'6.78E) (b) the East Mahe data point (4°40'8.39"S 55°38'45.63"E)

The simulated currents often overestimate the observed values, especially during the first four months of the year (Fig. 23). The value of the RMSE highlights these differences:

$$\text{RMSE}_{2018mean} = 0.24 \text{ m/s} \quad | \quad \text{RMSE}_u = 0.16 \text{ m/s} \quad | \quad \text{RMSE}_v = 0.36 \text{ m/s}$$

Where $\text{RMSE}_{2018mean}$ is related to the mean current magnitude over the whole year while RMSE_u and RMSE_v are referring to directional current magnitudes, longitude and latitude respectively. Fig. 24 illustrates these differences between SLIM and observations for the East point of Mahé. The hydrodynamic simulation over-estimates current amplitudes and this over-estimation is mostly present in the North direction. Current directions are mainly oriented on the North-South axis. This trend is also showed in the Fig. 25.

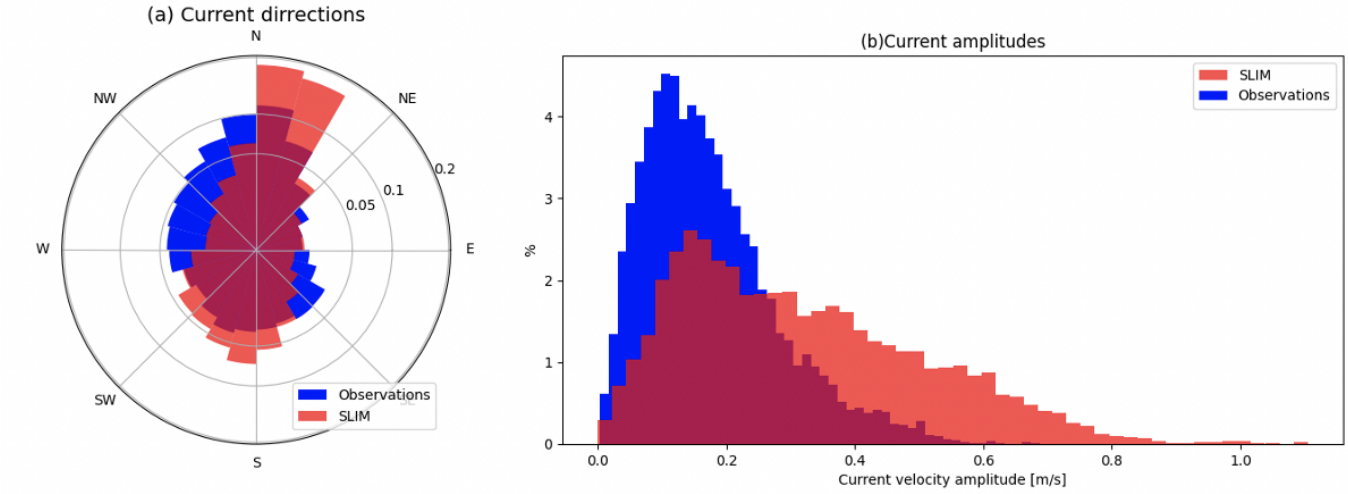

Figure 24: Histograms of (a) the direction and (b) amplitudes of the currents comparing SLIM with SLOMO observations for the year 2018 (East point of Mahé)

Fig. 25 shows different forcings related to currents velocities as quiver plots that indicate velocity directions, wind forcings in the 10 first meters of the water column and the Mercator currents evolution.

The Mercator data come from the NEMO model [90] and are used in this case as boundary conditions. They were also used to perform nudging, i.e. to force SLIM towards the Mercator currents in deeper areas where the dynamic becomes baroclinic.

In view of this validation, the simulation for the sea surface elevation seems to be close to the observations, while the speed and direction of the currents seem much less reliable: the directions of the currents are very different as well as the speed norms which differ greatly between observations and Mercator data. These currents data will greatly influence the particle tracker model for seagrass meadows. It will be important to take this aspect into account during the discussion.

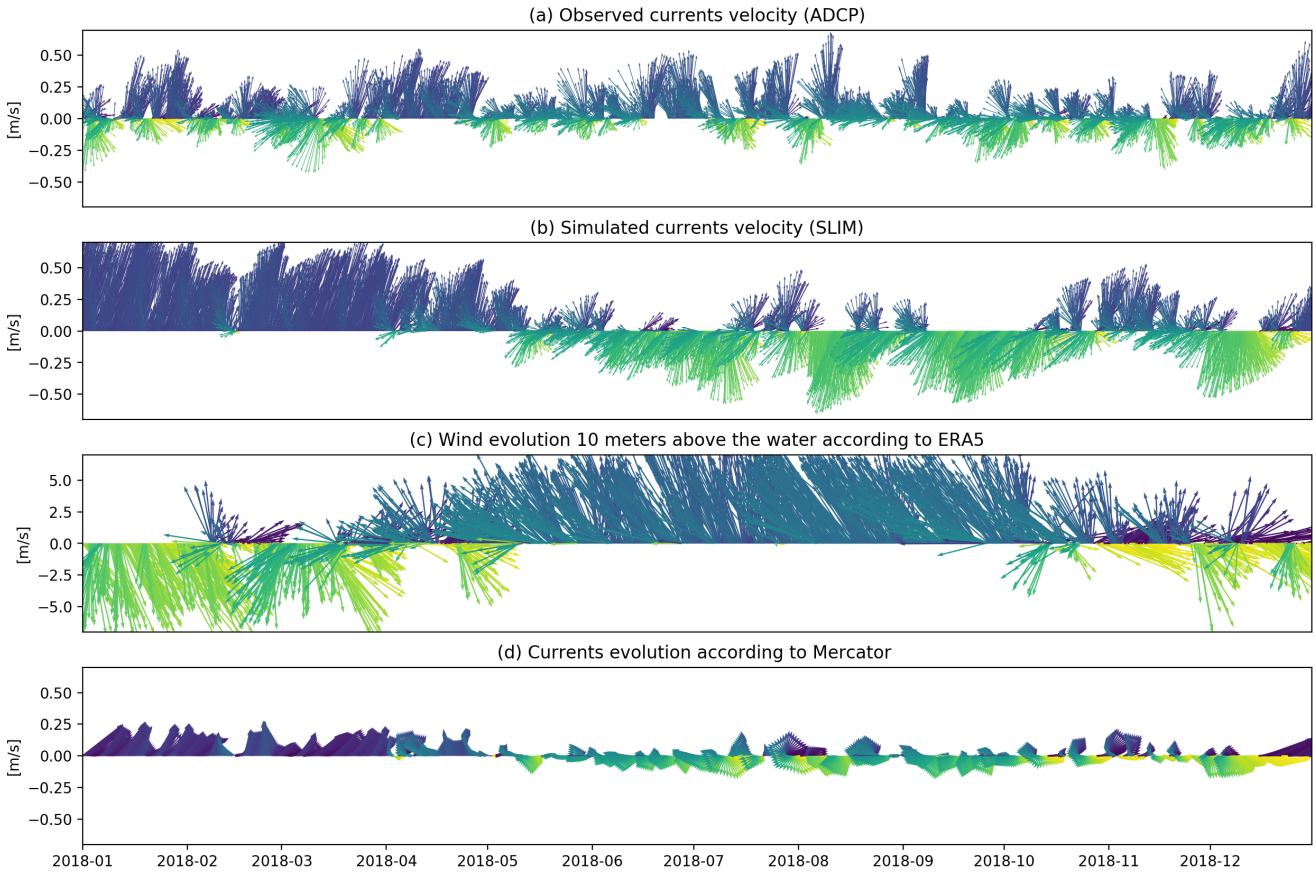

Figure 25: (a) and (b): comparison between observed and simulated current velocity with SLIM; (c) wind velocity at the same location and (d) simulated current velocity with NEMO

To ensure that the 2D modelling is adequate for the Mahé plateau, it must be ensured that the velocity profile is constant over depth. Fig. 26 shows the velocity profile at the eastern observation point of Mahé (SLOMO). The current magnitude appears to be constant over the first 30 metres. Considering that the shelf is only 50m deep on average, the use of 2D seems to be justified.

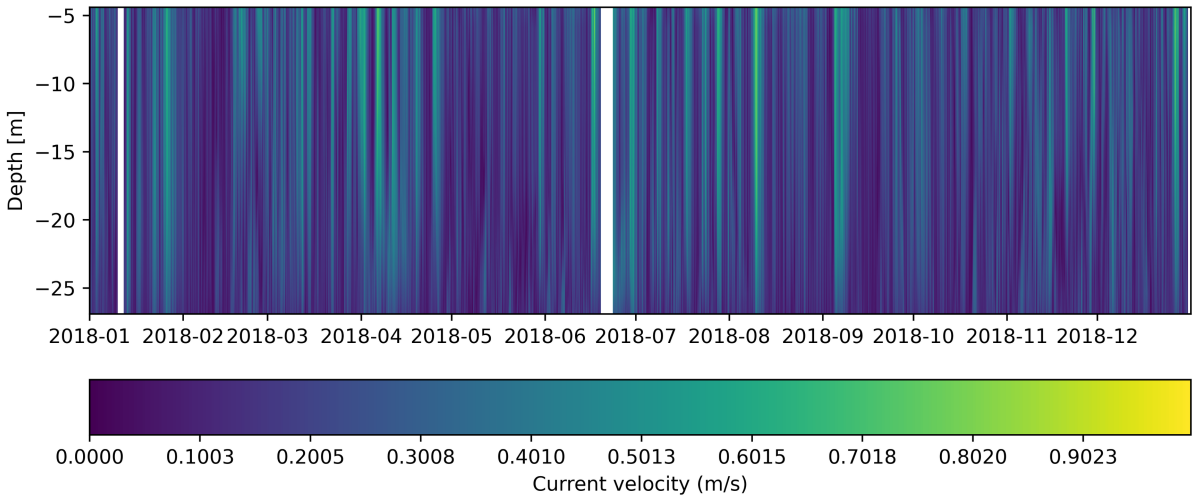

Figure 26: Currents velocity profile (SLOMO East of Mahé observations) for the year 2018

3.1.2 Mercator forcing

Following the differences observed between the observed and simulated Mercator velocities (cfr. Fig. 25), the use of these data could be discussed. To evaluate the impact of these data, used as deep ocean boundary conditions, a 3-month simulation was performed without using the Mercator data (Fig. 27).

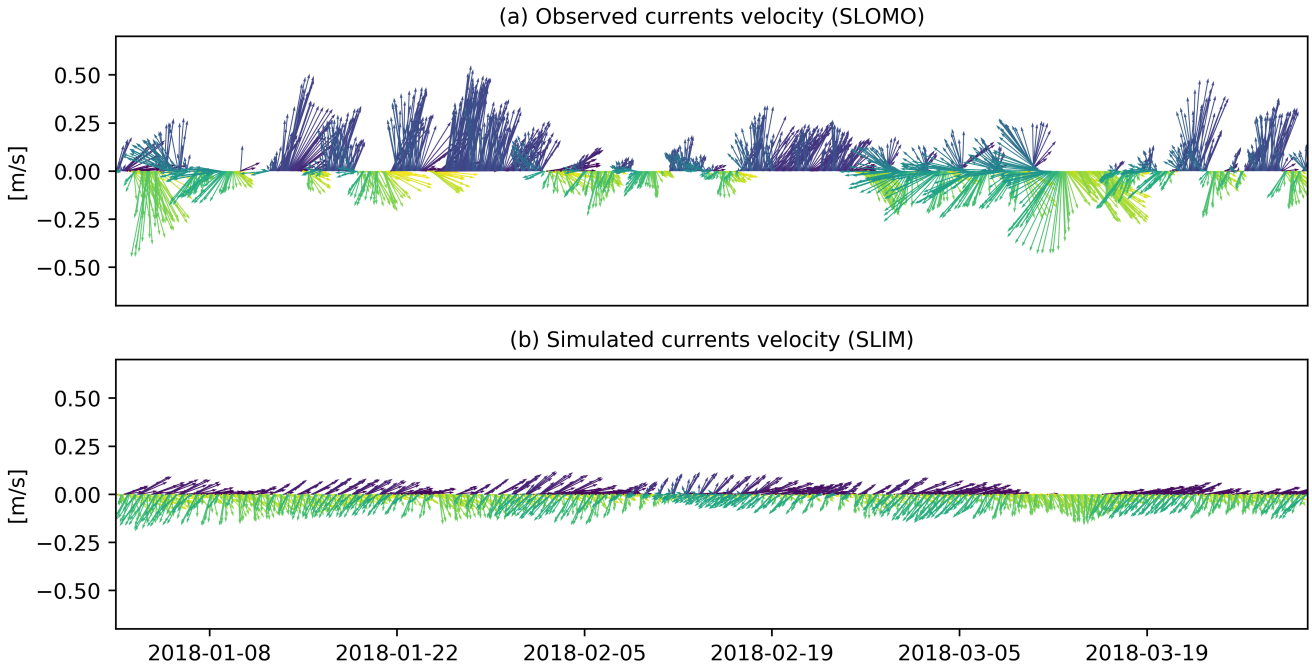

Figure 27: Quiver plots for the East observations point for a 3-month simulation without taking Mercator as forcing

Fig. 28 shows the histograms of direction and amplitudes comparison between SLIM simulation and observations.

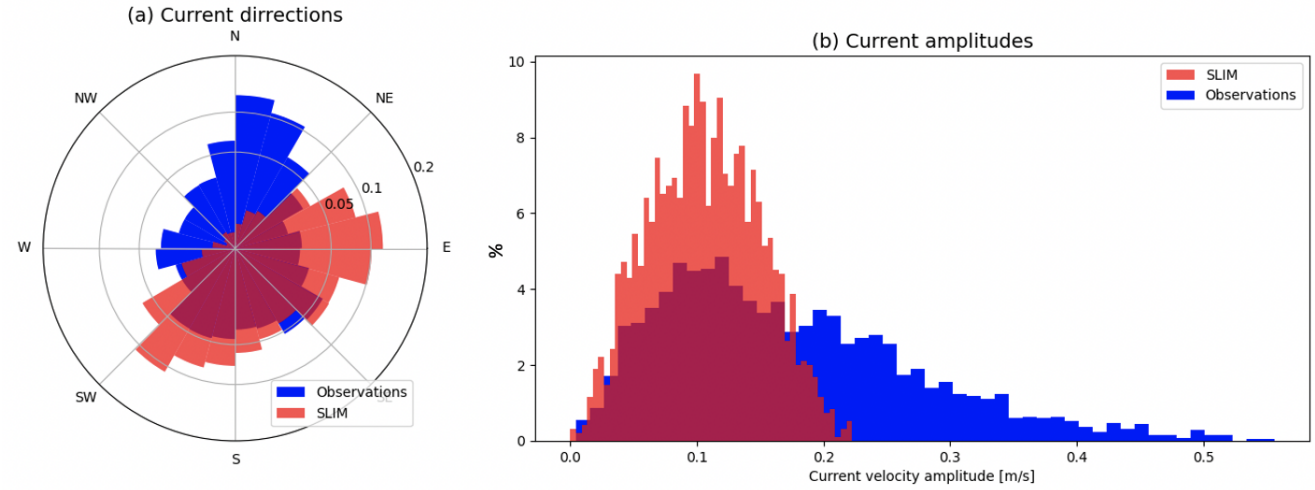

Figure 28: Histograms of (a) the direction and (b) amplitudes of the currents comparing SLIM without Mercator and SLOMO observations for the 3-month period (East point of Mahé)

RMSE_{mean} = 0.13 m/s | RMSE_{u} = 0.13 m/s | RMSE_{v} = 0.19 m/s

The simulated currents are very weak compared to the observed currents, there is a large underestimation (Fig. 28). In addition, the directions are much less reliable with random directions that are not in agreement with the observations. There is no observed seasonal variation in the simulated currents. Due to this underestimation, the RMSE takes smaller values (averaged on the 3-month period) and are highlighted by the current directions and amplitudes comparison with observations (Fig. 28).

Mercator have therefore a huge impact on the simulations. It allows the simulations to show marked seasonal variations as well as higher current magnitudes, thus approaching natural values.

3.2 Seasonality of the atmospheric and oceanic circulation

The results of the hydrodynamic simulations will drive the dispersion of seagrass propagules. The currents on the Seychelles plateau are influenced by two monsoon seasons: a northwest (NW) monsoon and a southeast (SE) monsoon [91]. These two seasons usually last a little less than 6 months with inter-seasonal months. The wind will follow an opposite trend and will also be detailed.

3.2.1 Southeast monsoon

The SE monsoon occurs during the austral winter from May to October [91]. The global currents for this period are shown in Fig. 29, according to the Marine Spatial Plan [54]. Focusing on the Mahé plateau, the currents are globally oriented towards the East with however some particular cases at the East and West ends of the plateau.

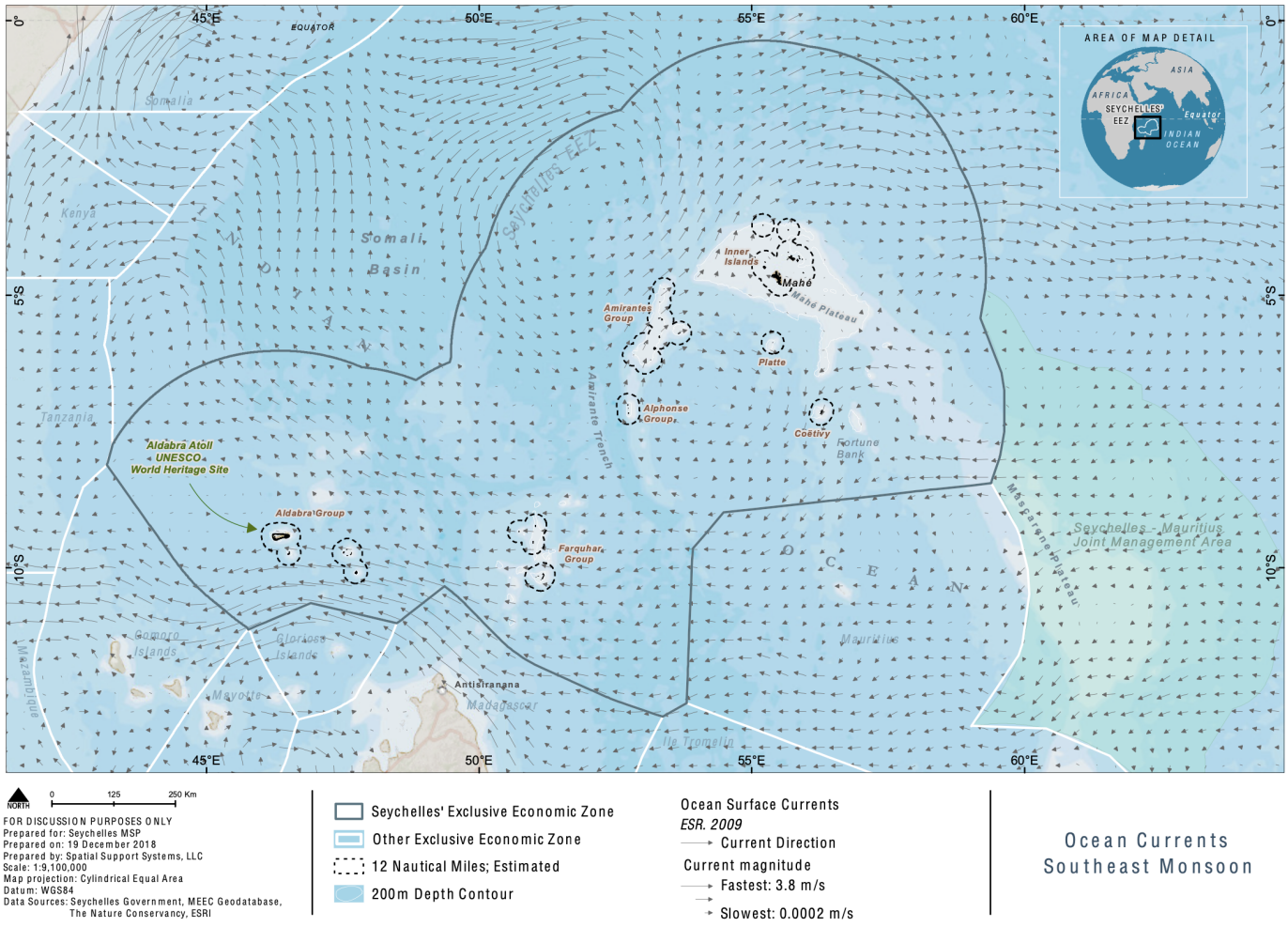

Figure 29: Seychelles ocean currents during the southeast monsoon [54]

The simulated currents on the plateau are shown in Fig. 30 and seem to reproduce this seasonal pattern quite well. May is a transition month between the two monsoons, the currents directions are quite variable. From June onwards, a tendency towards the west of the shelf is established with currents directed towards the south of the shelf. July and August are the months of the seasonal peak, with a clear trend towards higher current speeds at the extremities of the plateau. The trend continues in September and October. Overall the current speed is quite low, rarely exceeding 0.5 m/s.

The trend for wind forcing is much clearer due to its resolution of 30km. Fig. 31 shows it for the seasonal peak during the July-August period. The trend for these two months represents quite well the general wind trend observed during the entire SE monsoon. Winds are blowing to the northwest, to the opposite of the currents. Wind speed is in the range of 8-10 m/s, August being the month with the strongest wind velocity.

The wind will influence, by 1.5% of its speed, the particles transport. This represents roughly 0.15 m/s for this season. It's therefore important to know how and where it will influence virtual propagules. During this season the wind will reduce the particles speed as it's opposite from the currents direction.

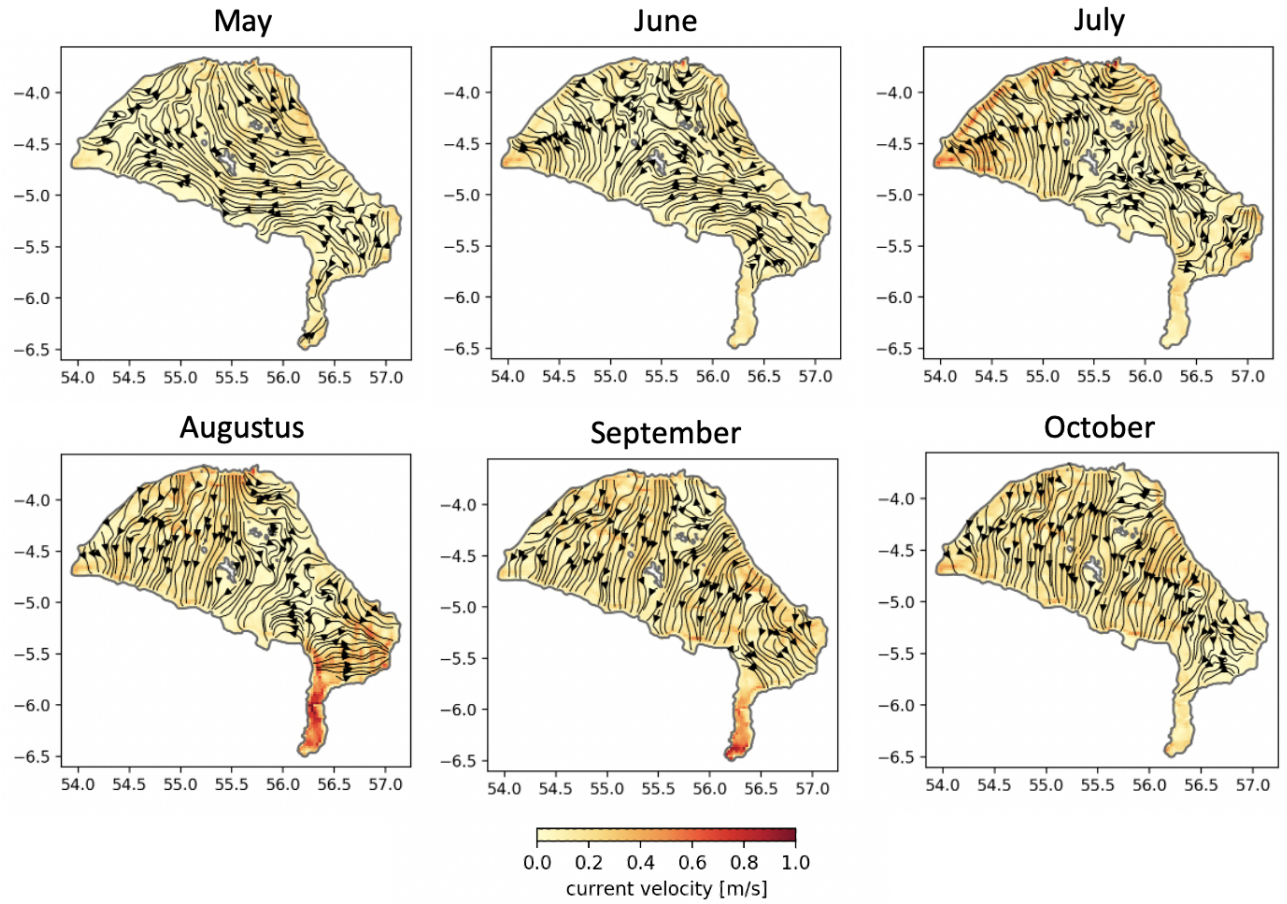

Figure 30: Residual circulation simulated on the Mahé plateau averaged on a three-year period (2018-2020) for the months of May to October

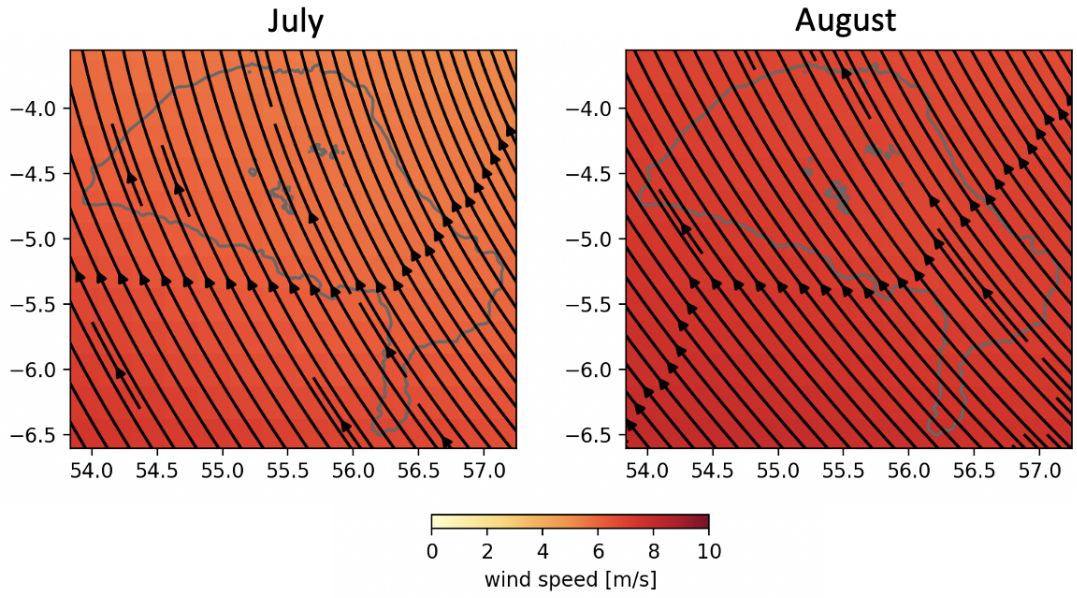

Figure 31: Mean wind speed over three-year period (2018-2020) during seasonal SE monsoon peak

3.2.2 Northwest monsoon

NW monsoon occurs during the austral summer, from November to April [91]. Again, the global scale currents dynamic of this period is showed in the Fig. 32.

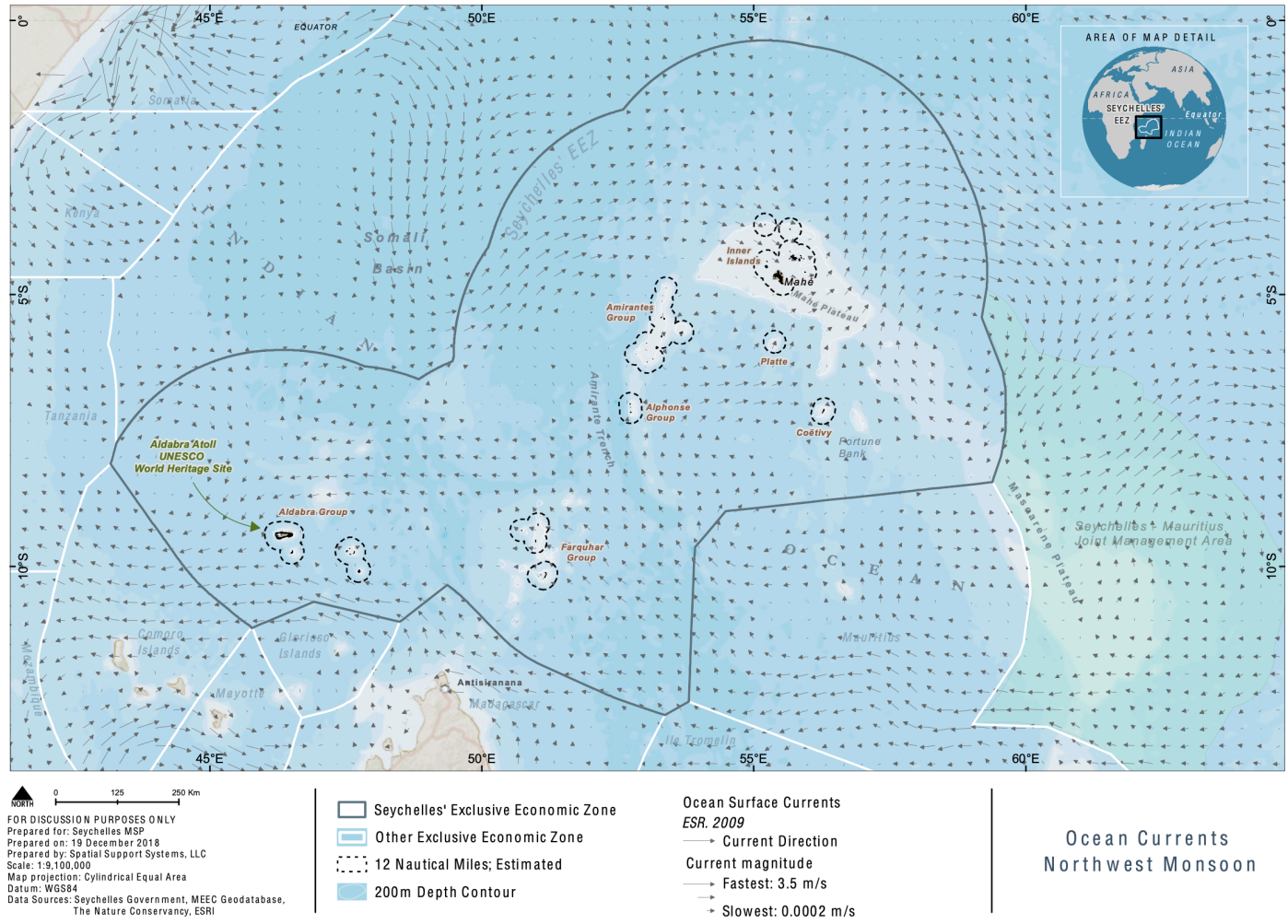

Figure 32: Seychelles ocean currents during the northwest monsoon [54]

The currents are quite different from the southeast monsoon. The ocean circulation of the plateau is mostly northeastward from December to April. During this period the currents will tend to leave the plateau from the north east (Fig. 32).

The simulated currents for this season represent quite well this trend (Fig. 33). The month of November is associated to a transition phase, the currents are very random, but the northeast tendency is beginning in December and follow it until April. Current speeds are higher than during the SE monsoon with currents of up to 0.6-0.8 m/s during the January-March period. These months being the seasonal peak.

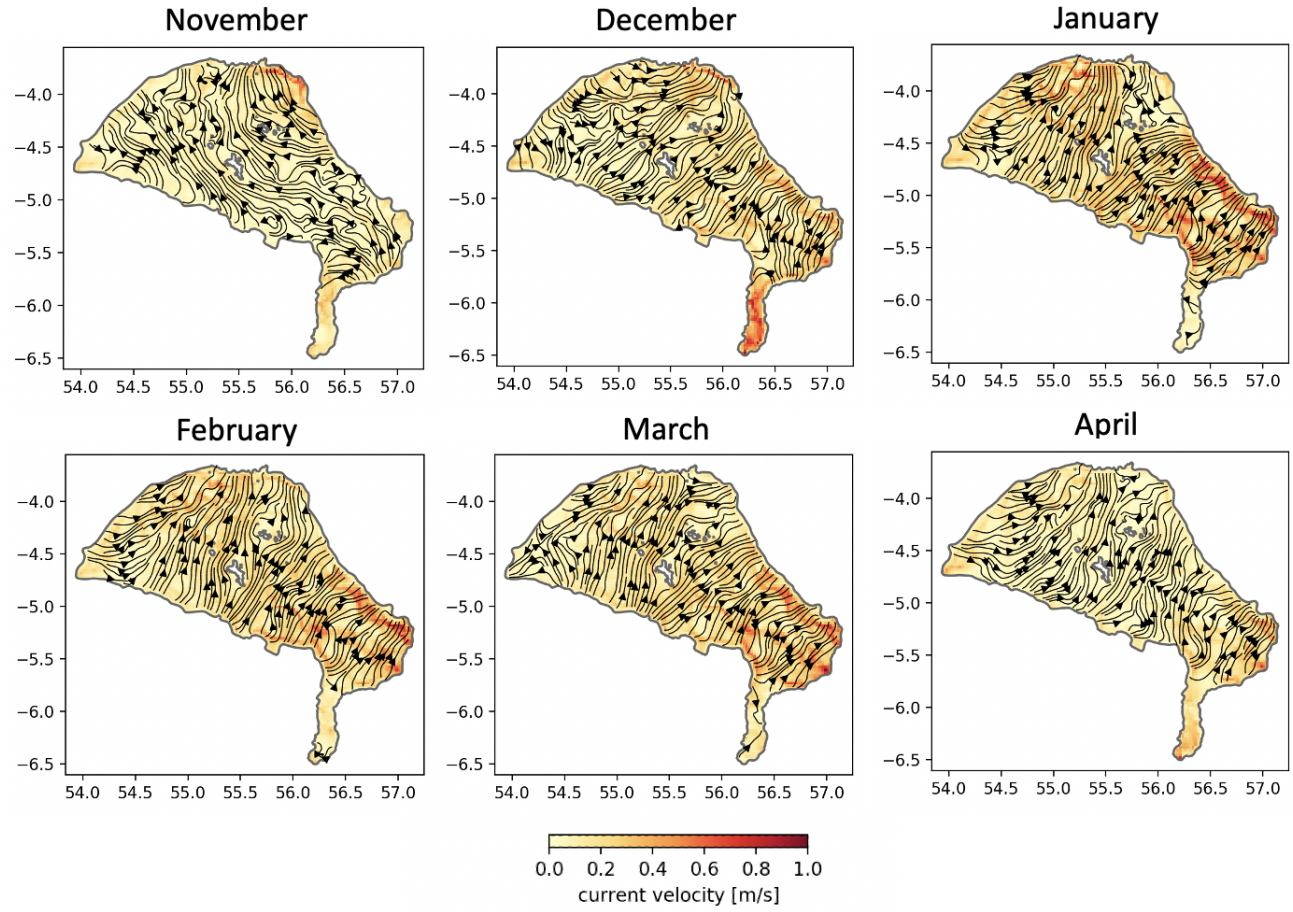

Figure 33: Residual circulation simulated on the Mahé plateau averaged on a three-year period (2018-2020) for the months of November to April

In terms of winds, they vary much more than in the SE monsoon where they had a constant direction. The winds tend to the same direction as the currents, and are oriented to the southeast during the peak seasonal months (Fig. 34). The months of November and April are subject to strong disturbances due to the change in the monsoon.

Winds will have a greater tendency to increase the speed of particles propagation during this season, as wind and current directions are oriented towards the east. But the wind is weaker than in the previous monsoon, here the maximum wind speed ranging until ∼5 m/s.

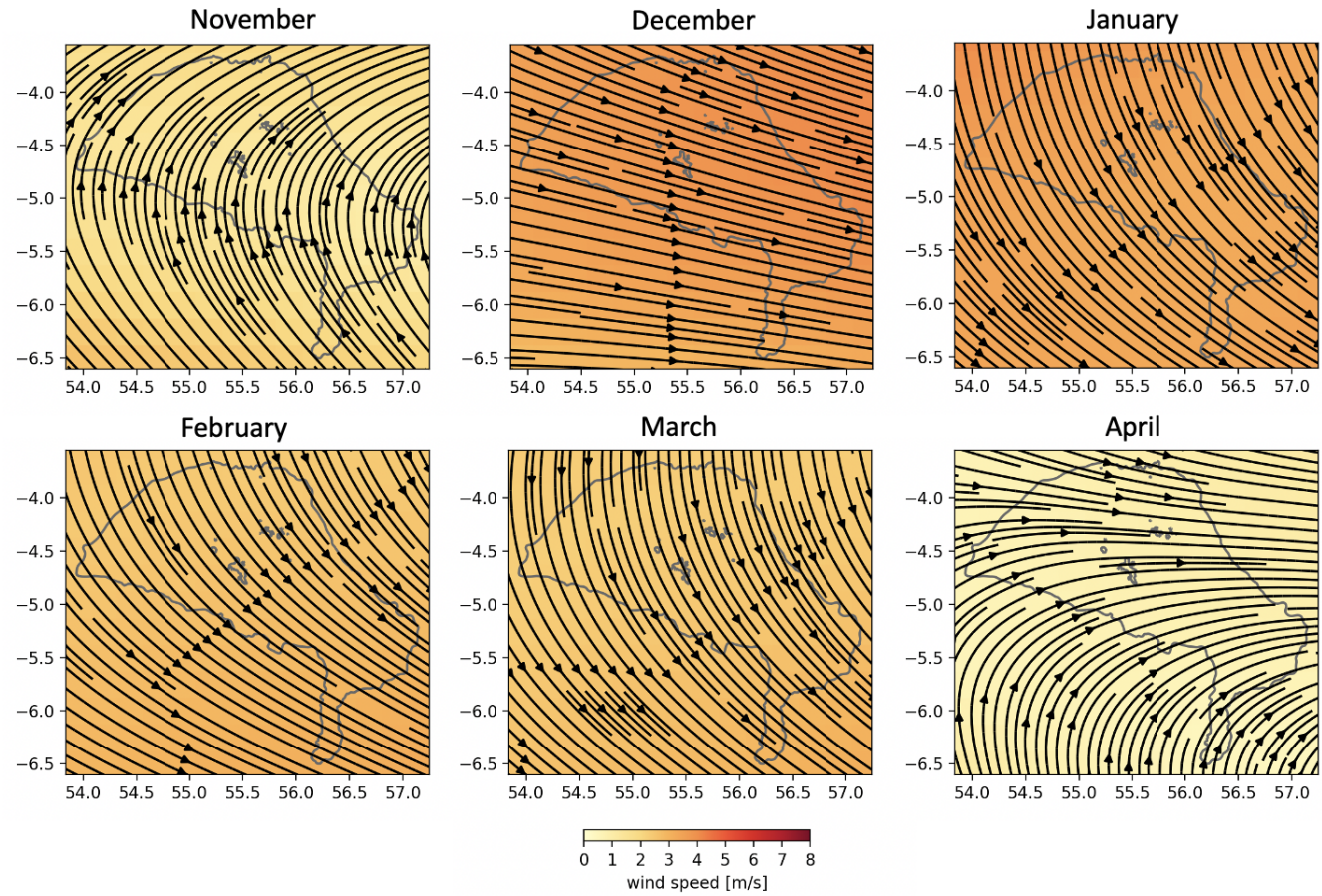

Figure 34: Mean wind speed over three-year period (2018-2020) during NW monsoon

3.3 Seagrass exports

This section will present the results obtained with the LPT model based on the hydrodynamic results obtained above (cfr. 3.2). The results for the virtual particles will be presented, it will be interesting to look at the seasonal variability of the particles arriving outside the plateau. Then a conversion will be performed and the rate of carbon exported monthly and annually over the 3 years will be established. In each step the results will be separated according to the areas studied (observed patches, 20m isobath and total area).

3.3.1 LPT simulations

As said before the virtual particles are released every 3 hours with a density of 50 per km^2. This means that every month about 5.10^6 virtual propagules are released in total in the studied area (this number varies with the number of days in the month). The variability is in the number of particles that leave the plateau, this is expressed as the percentage of particles reaching outside.

Fig. 35 show the three-year average percentage particles leaving shelf evolution for the studied areas during months. The chances of a particle leaving the plateau are quite high, ranging from 80 to 97%. The difference between values from the 20m isobath and from the observed patches is high, this is explained by the difference in localisation in the plateau. Indeed, 20m isobath areas are located near the shelf boundaries, hence reducing the distance between the habitat and the deep ocean. The observed patches are located near the islands of Mahé, Praslin and La Digue in the centre of the

plateau, increasing the distance until the deep ocean compared to the hypothetical areas. Rates for isobath areas are also higher on average. This is again due to the location of these habitats.

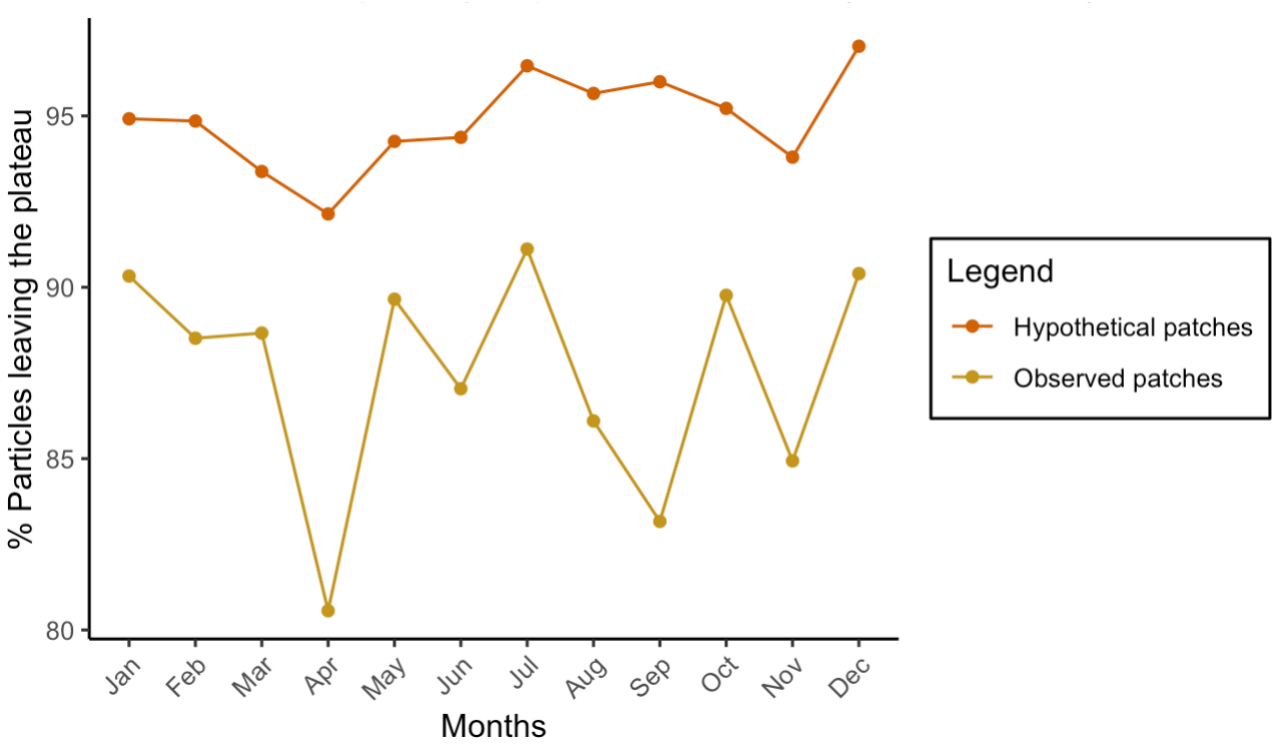

Figure 35: Evolution of the export rate outside the plateau averaged for three-year period compared for two habitats

In addition to these differences between habitats, it is interesting to see a seasonal variability that seems to be common to the different habitats. Figure 35 shows that the largest values for the isobath areas are also the largest values for the observed patches. July and December are associated with a good export rate. The average rate for all habitats considered is very close to the rates observed for the 20m isobath. This average is influenced by the higher rate of particles leaving the shelf for the isobath as well as by the number of 20m isobath zones (59) compared to the number of zones for the observed patches (41) (cfr. section 2.2.1).

Given these averages over the three years, export rates will be more variable and interesting for observed patches. The evolution of these rates over the three years is shown in Fig. 36. The variability is higher with rates ranging from 70 to 95%. A seasonal pattern emerges, with some months exporting more than others and greater variability between months. For example, March and May have a variability very small over the 3 years. Conversely, there are great down peaks for the months of April 2019 and June 2018. But overall, the trends are roughly the same for all three years: when the export rate goes down, it goes down for each year and when it goes up, it goes up for all. This seasonality is important and will influence the carbon conversion for each month.

In order to look at the results from another angle, a colormap representing the export rates according to the location of the meadows was made (Fig. 37). Unsurprisingly, the most exporting meadows are those originating from the 20m isobath, as these areas are located quite close to the shelf boundary. Their export ratio was evaluated at 90-100% for most of them, with some exceptions in the range of 80-90%. This rate decreases as one approaches the centre of the shelf and the islands. The island of Mahé has a wide range of ratios, from 20% for its small areas, 70% for its coasts and 80% for an area further from the coast. The islands of Praslin and La Digue have a very good ratio ranging from 80 to 100%.

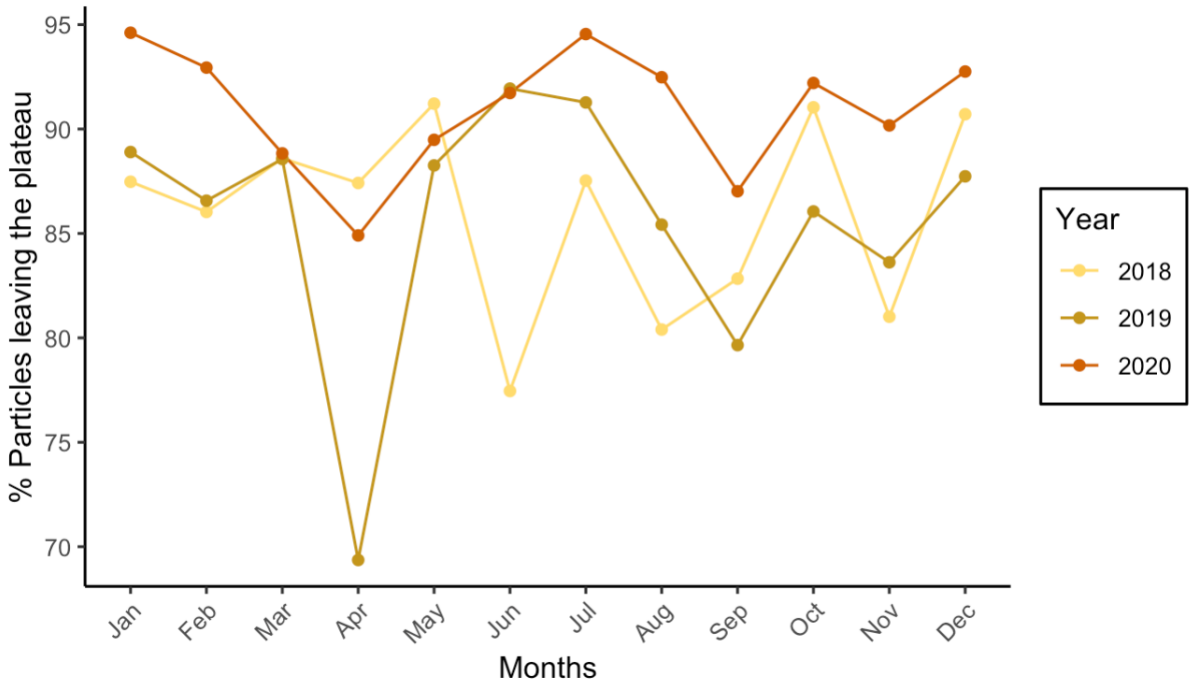

Figure 36: Evolution of the export rate outside the plateau for the observed patches

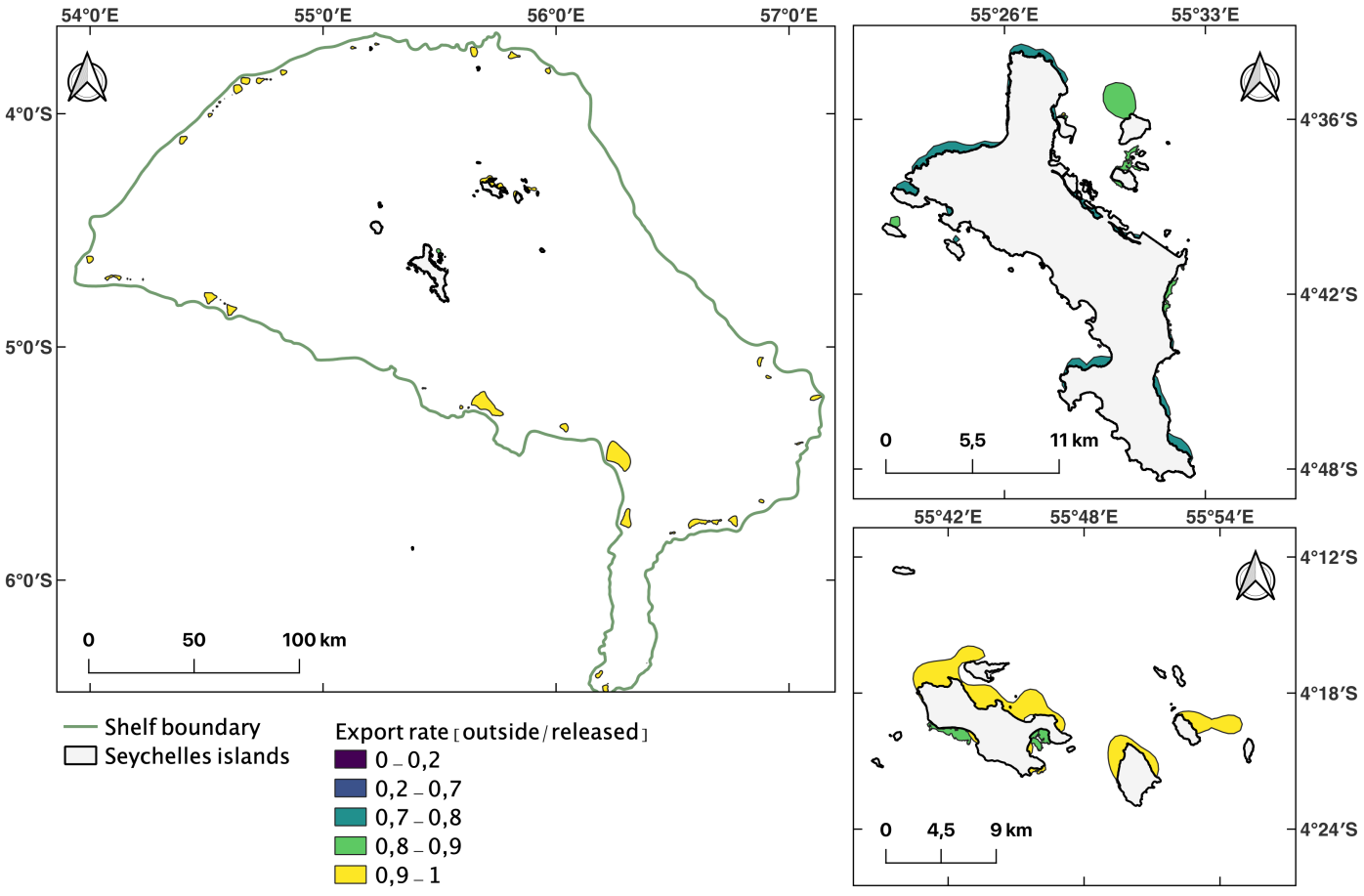

Figure 37: Georeferencing of export rates [particles outside/particles released] averaged over the 2018-20 period for seagrass meadows on the plateau

3.3.2 Carbon potential

The results of the simulations were converted into organic carbon quantities using equation 14. Fig. 38 shows the evolution of these quantities as a function of the months for the observed patches. Although there were interannual export variations during the LPT simulations, there are much less after conversion. Indeed, there is an almost straight line trend, which is mainly due to seasonal variations and to the linear interpolation performed on the leaf weight (cfr. Tab. 2).

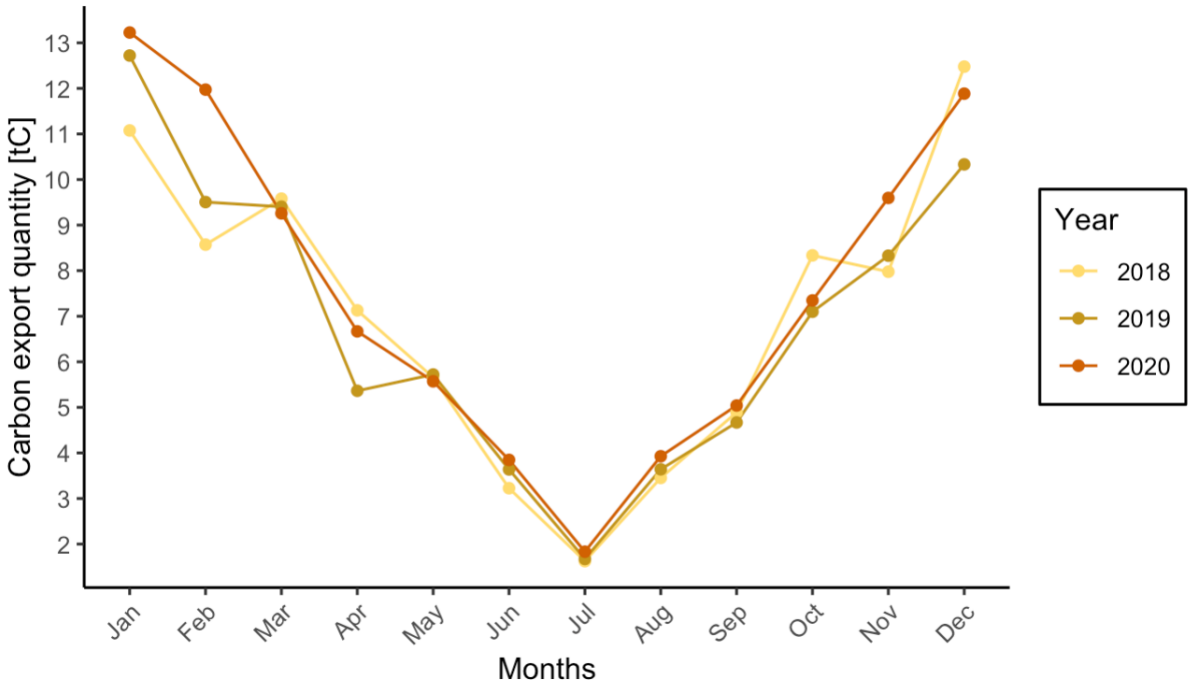

Figure 38: Evolution of carbon quantity export outside shelf for observed patches

In total, the seagrass meadows of the observed patches export 85,42 $tC.y^{-1}$ on average (cfr. Tab. 3). This amount of carbon is distributed differently from month to month with January contributing the most as it is the peak of meadows production. For the areas coming from the 20m isobath, meadows export 7.994,38 $tC.y^{-1}$. It's a huge difference compared to the observed patches, but it's mainly due to the difference in surface area of the two different habitats.

The NPP was estimated in order to have an additional comparison before checking the estimates made. On average over the 3 years, it reaches 1.353,89 tC and 128.285,24 tC for the observed patches and 20m isobath areas respectively (see Tab. 3). The fraction of carbon exported represents roughly 6% of this production.

/	Observed patches			Isobath 20m		
Month	**E [tC]**	**NPP [tC]**	**E/NPP**	**E [tC]**	**NPP [tC]**	**E/NPP**
January	12,34	205,01	0,0602	1.187,29	19.425,05	0,0611
February	10,02	158,32	0,0633	940,88	15.001,15	0,0627
March	9,41	145,04	0,0649	841,78	13.743,22	0,0613
April	6,39	111,60	0,0572	640,66	10.574,12	0,0606
May	5,65	85,59	0,0660	506,10	8.109,96	0,0624
June	3,57	53,57	0,0667	322,45	5.075,58	0,0635
July	1,71	25,63	0,0668	165,57	2.428,13	0,0682
August	3,67	55,35	0,0664	338,82	5.244,76	0,0646
September	4,87	82,83	0,0588	497,62	7.848,35	0,0634
October	7,59	115,32	0,0659	683,92	10.926,59	0,0626
November	8,63	140,36	0,0615	817,94	13.299,89	0,0615
December	11,56	175,28	0,0660	1.051,37	16.608,42	0,0633
TOTAL	85,42	1.353,89	/	7.994,38	128.285,24	/

Table 3: Quantities of carbon exported from the shelf averaged over the 3 years (E), NPP and ratio of export rate to NPP (E/NPP) for observed patches and 20m isobath areas

4 Discussion

The results of the study show that seagrass meadows on the Seychelles plateau contribute to 6% of their NPP to marine carbone sequestration. This represents $8{,}1.10^3$ tC.y^{-1} on average for the 3-year simulation for all habitats. However, this exported quantity is subject to variations due to changes in the oceanic and atmospheric circulation but also to the location of the meadows. The majority of meadows have a ratio of exported particles outside of the plateau to released particles above 80% but this number varies according to the location of the meadows, which may be more or less favourable to the currents. Another important factor contributing to the variability of exports is seasonality. The Seychelles is subject to two monsoons which are characterised by two seasonal peaks (in july and in january). Seagrass exports vary between these two extremes. Smaller variations are observed between the same months over the 3 years as well as between months within the same year.

The export rate is often expressed as a percentage of the primary production of marine ecosystems in the literature. This study suggests that the Seychelles seagrasses export 6% of their NPP. Duarte et al. (2017) [92], based on worldwide observations, have estimated that seagrasses export 24,3% of their NPP. There seems to be a big difference between the two but it should be kept in mind that for this study an export means that the seagrass propagule has left its original location. In the context of this work, the amount exported represents the fraction of particles that leaves the plateau and hence reaches the deep ocean. There is thus a difference in distance between the observations in the literature and the estimate made in this work. The particles simulated by the LPT model have to travel approximately 50-190km from Mahé island to leave the shelf and reach the deep ocean. If the Seychelles seagrass meadows export 24,3% of their NPP out of their original position, this means that about a quarter (6% of the 24,3%) of these exports goes directly to the deep ocean. This is quite promising.

Focusing on the georeferencing of the seagrass meadows in the plateau, results show a large heterogeneity between their respective export rate (Fig. 37). The export rate here is defined as the ratio of number of particles exported off the shelf to the total number particles released. It can range from 6% for small areas near islands to 80% for the majority meadows we considered. This large difference is due to the meadows location and oceanic circulation at those locations. This spatial variability is much less marked for the 20m isobath areas due to the much smaller distance from the shelf boundary. In addition to it, there is also a temporal variability played by oceanic and atmospheric circulations. Again, this heterogeneity is less distinct for the 20m isobath habitat (Fig. 35). For the observed patches, there is a clear trend with some months of the year during which exports are systematically larger during the 3-year period (Fig. 36).

Converted into carbon quantities, our results suggest that Seychelles seagrass meadows export $8{,}1.10^3$ tC.y^{-1} (Tab. 3). When we distinguish the observed meadows and those that are hypothetical, we obtain 85,42 tC.y^{-1} for the observed patches and $7{,}99.10^3$ tC.y^{-1} for the 20m isobath areas. This difference is explained mainly by the distance to the deep ocean and the surface areas covered. Converting the observations of Duarte (2017) [93] for the same surface area, carbon export quantities of seagrasses range from $1{,}1.10^4$ to $5{,}14.10^4$ tC.y^{-1}. The estimation of this study seems slightly under the Duarte estimation but it remains very close to it. It's again important to remember that the Duarte estimation focus on seagrass fragments that leave the place and not the plateau. To put these values in perspective, Duarte also estimated the export rate of mangroves, an other BC ecosystem. The latter covers 29 km^2 in Seychelles [94]. The corresponding export quantity is evaluate to range between $2{,}96.10^3$ and $9{,}31.10^3$ tC.y^{-1}. There appear to be no salt marshes on the Seychelles plateau according to UNEP [95], making mangroves and seagrasses the two main BC ecosystems in the region. Based on exports, the seagrasses of the plateau would then have a greater potential than the mangroves, contributing to 47-73% of the total carbon exported from BC ecosystems, only considering seagrass meadows on the plateau. Always bearing in mind that the mangroves cover a

smaller area in the region.

In other words, considering that all the carbon exported is sequestered in the deep ocean, the carbon sequestration from all the seagrass meadows on the plateau could offset the CO_{2e} emissions of 1505 Seychellois, i.e. representing 1,6% of the total Seychelles emissions. The mean annual emissions per capita is set to 5,38 tCO_{2e} in this region [96] and the population of the Seychelles is 96.762 [96]. This may not seem like much, but the Seychelles plateau represents only 3% of its EEZ (cfr. section 1.5). On the international carbon market, a tonne of carbon can be sold for €82,35 in Europe, $35,25 in Australia or $11,50 in South Korea [97]. These amounts vary greatly and depend strongly on local policies. Currently, the Seychelles have not yet entered the Emission Trading System (ETS) [98], but if they decide to do so, their seagrass exports could contribute to a cheque for €405.000 if we take into account an average of €50 per tonne of carbon considering the above-mentioned amounts. On this scale it already looks much more interesting and could be very promising in the context of the Blue Economy objective named *"Securing healthy, resilient and productive oceans through the valuation of the coastal and marine ecosystems; oceans, climate resilience and adaptation"* [96]. This results demonstrate the potential of BC ecosystems and especially seagrass meadows. It can be applied everywhere where there are seagrasses, i.e. in all continents except Antartica and Blue Economy can therefore be a huge lever of action against climate change. Countries with large EEZs such as France, the United States or Australia could have a real impact on this environmental crisis.

The results exposed in this study have limitations. First, an important assumption, for the hydrodynamic part, was that the current velocities were constant along the entire water column. This resulted in the use of 2D SLIM. To discuss it, a velocity profile has been established for an observation point in the plateau (Fig. 26). A second point to clarify is the use of the forcing between the outer shelf and deep areas and the inner shelf where 2D was used. This transition was made using Mercator data and this impact was presented in the Fig. 27 and 28. In order to improve the results, the use of Mercator data could be changed and different boundary conditions could be found. If the results represent the global dynamics well, each of the simulations carried out overestimates or underestimates the speed of the currents. However, the directions are better represented with Mercator. Despite the fact that Mercator data are regularly updated, there is no data verification for the Seychelles region. It has also been shown that the model is more often wrong at mid-latitudes and at the equator [99], location of the studied area. Nevertheless, the SLIM2D model represents quite well the dynamics of the ocean circulation on the Mahé Plateau compared to observations. With more accurate data this model could be maybe more efficient but constitute a good basis for further studies.

The virtual particles simulations were performed with a Lagrangian particle transport model. These simulations were carried out for every month of the year during 3 years, i.e. 36 simulations. The number of simulations ensures the robustness of the results, however only one year (2018) was validated with hydrodynamic observations. Taking into account a longer period of time could provide greater representativeness of the variability of currents. It could be interesting to look at the export rate for a year disturbed by an extreme event such as a tropical cyclone or a more extreme monsoon. The temporality of the parameters could also be subject to more robustness. Indeed, the lifetime parameter used in the transport model is defined on the basis of an average between several species and set at 70 days. On the one hand, this lifetime should be subject to variability and on the other hand, as the simulations are performed every month ($\sim$30 days), the simulations never reach 70 days. The lifetime effect is therefore not represented in this model. In future work, it would be interesting to define a species-specific lifetime or a lifetime subject to more variability in order to obtain a representation closer to reality by including both inter-monthly variations and a more relevant lifetime.

For the seagrass propagules modelling, the first assumption that has been made is the selection of parameters. For this work, no particular seagrass species was selected. The buoyancy parameters

were observed for the species *Zostera muelleri*; the leaf life time was estimated based on an average of several seagrass species; the dry weight parameters were defined on the species *Zostera marina* and finally the daily export rates were based on the species *Syringodium*. These data were also used due to the lack of data on the Seychelles plateau. In the Western Indian Ocean (WIO), there are four main seagrass genera: *Hydrocharytaceae* (5 species), *Zosteraceae* (1 species), *Cymodoceaceae* (5 species) and *Ruppiaceae* (1 species) [100]. The biological traits of seagrass species are quite variable [101] and therefore impact the results. In order to improve the results, species-specific parameters could be defined. The model could also be improved. Currently the model only disperses particles that appear at a defined time step. A more specific development could also calculate the number of particles that leave their original patch in order to have a better comparison with the literature or include a fraction of particles that settle directly at the foot of the seagrass meadows in order to have an estimate of the carbon burial. The latter being a fraction of carbon storage that is not negligible depending on the species and region. But to establish this more specific model, more precise local biological and physical characteristics are required.

As this master thesis is one of the first modelling studies about seagrass meadows in the plateau, there is no clear estimation for the marine carbon sequestration. The only resource is the other studies, sometimes in very different places. One of the limitations is the spatial variability of seagrass meadows and the large differences between two estimates due to uncertainties about the area covered by seagrass in the world. Indeed, the surface area used in seagrass studies can range from $0{,}15.10^6$ [102], defined as lower limit, to $4{,}32.10^6$ km^2 [103], upper limit. The estimates of NPP and productivity are based on areas that can vary by a factor of 10, so it is difficult to compare the results calculated. There is therefore large opportunities to improve this estimation by future studies as the lack of data is the most important limitation in this calculus. But with new studies and observations available, the non-specificity of the results by not selecting a particular species could be resolved. Focusing on one or more species could have a more significant impact on this calculation, especially for local species. The knowledge of seagrass species in detail could allow the consideration of new parameters such as carbon burial amounts or physical characteristics such as habitat depths or more precise soil criteria. Here, only depth was taken into account to define the areas of hypothetical seagrass presence. However, it would be interesting to compare the results of this work with future estimates for local species in order to have more distance and robustness towards the latter.

For future perspectives and in order to improve these results, it would be interesting to make a more precise habitat map by surveying the species present on the Seychelles plateau. A project is currently underway and it will be interesting to re-estimate the fraction of carbon exported by taking into account the new habitats identified. In this work only 4 km^2 have been considered and these are close to the islands, so easily identifiable, but the potential for further confirmed areas is enormous given all the suitable areas on the shelf ($\sim$466 km^2).

5 Conclusion

In recent years, there has been a great deal of work assessing the current environmental crisis. Among all these reports, a new concept has emerged: Blue Carbon. Indeed, scientific and technological progress has made it increasingly clear that marine ecosystems can be used as a lever to mitigate climate change. Seagrass meadows are one of these ecosystems that effectively act as a carbon sink, either locally through burial or further away through fragments export to the deep ocean. It's therefore important to quantify these different carbon sinks. This study tried to improve this knowledge by focusing on the seagrass meadows of the Seychelles plateau, with as goal to estimate the fraction of seagrass propagules that leave the shelf for the deep ocean where they can settle down to more than 1000m depth where their carbon will be sequestrated for hundreds of years.

The first step to estimate the dispersal of the seagrass fragments is to simulate oceanic circulation on the plateau. SLIM2D model has been used to do this during a 3-year period (2018-20). The 2D modelling was chosen because of the shallow depth of the plateau ($\sim$50m). Simulations are based on an unstructured mesh which allows local mesh refinements in areas of interest while keeping a coarser resolution where the dynamics is smoother. A LPT model was then used based on the hydrodynamic outputs of SLIM to simulate the dispersion of propagules. This model was implemented in such a way that it takes into account an average life span for seagrass fragments and the evolution of their buoyancy in the water column. These parameters were defined on the basis of observations. LPT simulations were carried out for each month for 3 years (2018-20) in order to represent the seasonal variability and to have robust results. The outputs of the LPT simulations have been used to calculate the number of virtual particles that have leaved the shelf as well as the number of total particles that have been released. In order to express the results in terms of a mass of carbon, a conversion has been made based on Duarte conversion factor which allows to convert DW into carbon content. Based on literature, an estimation of the NPP of the different habitats was calculated to compare exports to seagrass production.

This modelling approach allows to give an answer to the research question exposed in the beginning of this study:

How much do seagrass meadows could contribute to marine carbon sequestration in the Seychelles?

Results suggest that seagrass meadows of the Seychelles plateau contribute by roughly 6% of their NPP to marine carbon sequestration. This value represents the rate of seagrass fragments that end up off the shelf on average each month. This means that 6% of the seagrass NPP can potentially contribute to this sequestration. There is no difference in this aspect between the observed patches and the areas of hypothetical seagrass presence.

The main difference between the different habitats is the ratio of the number of particles exported to the number of particles released by the meadow in question. This ratio can vary from $\sim$0.06 for some very small meadows close to the islands where export seems difficult to achieve to $\sim$0.99 for large hypothetical areas at the edge of the shelf. However, the majority of meadows have a ratio above 0.8 with differences depending on their location.

These ratio highlight the seagrass power and geographical variations. But seasonality has also an impact on the export flux. Indeed, wind and currents drive the seagrass propagules transport and therefore generate a temporal heterogeneity. Considering the ratio number of particles outside shelf versus total particles released, as exposed in the previous paragraph, this ratio range from 0.7 for April 2019 to 0.95 for January 2020 only taking into account the observed patches. These monthly variations are much less pronounced for the hypothetical areas.

Converting these ratios into carbon quantities, with the data used, seagrass would export 8,1.10^3 tC.y^{-1} on average for the 3 years and habitats combined. This amount is distributed between the observed patches and the hypothetical areas at 85,42 and 7.994,38 tC.y^{-1} respectively. But as explained in the discussion, many assumptions and approximations have been made and it will be more interesting to retain that 6% of the NPP of the Seychelles plateau seagrasses can contribute to marine carbon sequestration. This ratio can more easily be confronted with future studies that could take place with more data available such as a map of seagrass habitats or specific biological and physical characteristics.

Seychelles seagrasses have a great potential to sequester carbon. There are few studies that provide data on these ecosystems for the Seychelles. However, these results are quite promising in the perspective of the Blue Economy developed by the Seychelles government.

References

[1] Will Steffen, Paul J. Crutzen, and John R. McNeill. The anthropocene: Are humans now overwhelming the great forces of nature. *Ambio*, 36:614–621, 2007. DOI: https://doi.org/10.1579/0044-7447(2007)36[614:TAAHNO]2.0.CO;2.

[2] Waters C. N., Zalasiewicz J., Summerhayes C., Barnosky A. D., Poirier C., Ga uszka A., Cearreta A., Edgeworth M., Ellis E. C., Ellis M., Jeandel C., Leinfelder R., McNeill J. R., Richter D. d., Steffen W., Syvitski J., Vidas D., Wagreich M., Williams M., Zhisheng A., Grinevald J., Odada E., Oreskes N., and Wolfe A. P. The anthropocene is functionally and stratigraphically distinct from the holocene. *Science*, 351 (6269), 2016. doi:10.1126/science.aad2622.

[3] Hanqin Tian, Guangsheng Chen, Chaoqun Lu, Xiaofeng Xu, Wei Ren, Bowen Zhang, Kamaljit Banger, Bo Tao, Shufen Pan, Mingliang Liu, Chi Zhang, Lori Bruhwiler, and Steven Wofsy. Global methane and nitrous oxide emissions from terrestrial ecosystems due to multiple environmental changes. *Ecosystem Health and Sustainability*, 1(1):1–20, 2015. doi: 10.1890/EHS14-0015.1.

[4] A. Ito and M. Inatomi. Use of a process-based model for assessing the methane budgets of global terrestrial ecosystems and evaluation of uncertainty. *Biogeosciences*, (9):759–773, 2012. https://doi.org/10.5194/bg-9-759-2012 [Accessed 21/05/2022].

[5] Susan Solomon. Stratospheric ozone depletion: A review of concepts and history. *Reviews of Geophysics*, 37(3):275–316, 1999. https://doi.org/10.1029/1999RG900008 [Accessed 21/05/2022].

[6] S F Rowland. Stratospheric ozone depletion. *Annual Review of Physical Chemistry*, 42(1):731–768, 1991. https://doi.org/10.1146/annurev.pc.42.100191.003503[Accessed 21/05/2022].

[7] Cliff S. Law, James J. Bell, Helen C. Bostock, Chris E. Cornwall, Vonda J. Cummings, Kim Currie, Simon K. Davy, Malindi Gammon, Christopher D. Hepburn, Catriona L. Hurd, Miles Lamare, Sara E. Mikaloff-Fletcher, Wendy A. Nelson, Darren M. Parsons, Norman L. C. Ragg, Mary A. Sewell, Abigail M. Smith, and Dianne M. Tracey. Ocean acidification in new zealand waters: trends and impacts. *New Zealand Journal of Marine and Freshwater Research*, 52(2):155–195, 2018. https://doi.org/10.1080/00288330.2017.1374983 [Accessed 21/05/2022].

[8] Robert W. Howarth. Coastal nitrogen pollution: A review of sources and trends globally and regionally. *Harmful Algae*, 8(1):14–20, 2008. https://doi.org/10.1016/j.hal.2008.08.015 [Accessed 21/05/2022].

[9] Rosamond L. Naylor, Rebecca J. Goldburg, Jurgenne H. Primavera, Nils Kautsky, Malcolm C. M. Beveridge, Jason Clay, Carl Folke, Jane Lubchenco, Harold Mooney, and Max Troell. Effect of aquaculture on world fish supplies. *Nature*, (405):1017–1024, 2000. https://doi.org/10.1038/35016500 [Accessed 21/05/2022].

[10] Steffen W., Broadgate W., Deutsch L., Gaffney O., and Ludwig C. The trajectory of the anthropocene: The great acceleration. *The Anthropocene Review*, 2:81–98, 2015.

[11] Johan Rockström, Will Steffen, Kevin Noone, Åsa Persson, F. Stuart Chapin, Eric F. Lambin, Timothy M. Lenton, Marten Scheffer, Carl Folke, Hans Joachim Schellnhuber, Björn Nykvist, Cynthia A. de Wit, Terry Hughes, Sander van der Leeuw, Henning Rodhe, Sverker Sörlin,

Peter K. Snyder, Robert Costanza, Uno Svedin, Malin Falkenmark, Louise Karlberg, Robert W. Corell, Victoria J. Fabry, James Hansen, Brian Walker, Diana Liverman, Katherine Richardson, Paul Crutzen, and Jonathan A. Foley. A safe operating space for humanity. *Nature*, 461:472–475, 2009.

[12] Surajit Das and Neelam Mangwani. Ocean acidification and marine microorganisms: responses and consequences. *Oceanologia*, 57(4):349–361, 2015. https://doi.org/10.1016/j.oceano.2015.07.003.

[13] K. E. Carpenter, M. Abrar, G. Aeby, R. B. Aronson, S. Banks, A. Bruckner, A. Chiriboga, J. Cortes, J. C. Delbeek, and L. DeVantier. One-third of reef-building corals face elevated extinction risk from climate change and local impacts. *Science*, 321(5888):560–563, 2008. doi:10.1126/science.1159196.

[14] Nancy Knowlton. The future of coral reefs. *PNAS*, 98(10):5419–5425, 2001. www.pnas.org/cgi/doi/10.1073/pnas.091092998.

[15] Masson-Delmotte V., P. Zhai, A. Pirani, S.L. Connors, C. Péan, S. Berger, N. Caud, Y. Chen, L. Goldfarb, M.I. Gomis, M. Huang, K. Leitzell, E. Lonnoy, J.B.R. Matthews, T.K. Maycock, T. Waterfield, O. Yelekçi, R. Yu;, and B. Zhou (eds.). Climate change 2021: The physical science basis. contribution of working group i to the sixth assessment report of the intergovernmental panel on climate change. *IPCC, 2021: Summary for Policymakers*, 2021.

[16] Pamela Chasek. Stockholm et la naissance de la diplomatie environnementale. *International Institute for Sustainable Development*, 2020. https://www.iisd.org/system/files/2021-04/still-one-earth-stockholm-FR.pdf [Accessed on the 08/02/2022].

[17] United Nations Environment Programme. Emissions gap report 2021: The heat is on – a world of climate promises not yet delivered. 2021. ISBN: 978-92-807-3890-2.

[18] R.K. Dixon and D.P. Turner. The global carbon cycle and climate change: Responses and feedbacks from below-ground systems. *Environmental Pollution*, 73(3-4):245–262, 1991. doi:10.1016/0269-7491(91)90052-x.

[19] Goosse H. *Climate system dynamics and modelling*. Cambridge University Press, 2015.

[20] Pierre Friedlingstein, Laurent Bopp, Philippe Ciais, Jean-Louis Dufresne, Laurent Fairhead, Hervé LeTreut, Patrick Monfray, and James Orr. Positive feedback between future climate change and the carbon cycle. *Geophysical Research Letters*, 28(8):1543–1546, 2001. https://doi.org/10.1029/2000GL012015.

[21] Nellemann C., Corcoran E., Duarte C. M., Valdés L., De Young C., Fonseca L., and Grimsditch G. *Blue Carbon. A Rapid Response Assessment*. United Nations Environment Programme, 2009. ISBN: 978-82-7701-060-1.

[22] Tyler Volk and Martin I. Hoffert. *Ocean carbon pumps: Analysis of relative strengths and efficiencies in ocean-driven atmospheric CO2 changes*, volume 32 of *Geophysical Monograph Series: 99-110*. 1985. doi:10.1029/gm032p0099.

[23] D. M. Sigman and M. P. Hain. The biological productivity of the ocean: Section 3. *Nature Education Knowledge*, 3(10):19, 2012.

[24] P. Ciais, C. Sabine, G. Bala, L. Bopp, V. Brovkin, J. Canadell, A. Chhabra, R. DeFries, J. Galloway, M. Heimann, C. Jones, C. Le Quéré, R.B. Myneni, S. Piao, and P. Thornton. Carbon and other biogeochemical cycles. in: Climate change 2013: The physical science basis. contribution of working group i to the fifth assessment report of the intergovernmental panel on climate change. *IPCC*, 2013.

[25] J. A. Raven and P. G. Falkowski. Oceanic sinks for atmospheric co2. *Plant, Cell and Environment*, 22(6):741–755, 1999. https://doi.org/10.1046/j.1365-3040.1999.00419.x.

[26] Ittekkot Venugopalan. The abiotically driven biological pump in the ocean and short-term fluctuations in atmospheric co2 contents. *Global and Planetary Change*, 8(1-2):17–25, 1993. doi:10.1016/0921-8181(93)90060-2.

[27] Andrew J. Watson, Ute Schuster, Jamie D. Shutler, Thomas Holding, Ian G. C. Ashton, Peter Landschützer, David K. Woolf, and Lonneke Goddijn-Murphy. Revised estimates of ocean-atmosphere co2 flux are consistent with ocean carbon inventory. *Nature Communications*, 11(4422), 2020. https://doi.org/10.1038/s41467-020-18203-3.

[28] Ove Hoegh-Guldberg, Ken Caldeira, Thierry Chopin, Steve Gaines, Peter Haugan, Mark Hemer, Jennifer Howard, Manaswita Konar, Dorte Krause-Jensen, Elizabeth Lindstad, Catherine E. Lovelock, Mark Michelin, Finn Gunnar Nielsen, Eliza Northrop, Robert Parker, Joyashree Roy, Tristan Smith, Shreya Some, and Peter Tyedmers. The ocean as a solution to climate change: Five opportunities for action. *Washington, DC: World Resources Institute*, 2019. Available online at http://www.oceanpanel.org/climate [Accessed 12/02/2022].

[29] Martin R. Stuchtey, Adrien Vincent, Andreas Merkl, Maximilian Bucher, Peter M. Haugan, Jane Lubchenco, and Mari Elka Pangestu. Ocean solutions that benefit people, nature and the economy. *Washington, DC: World Resources Institute*, 2020. http://www.oceanpanel.org/ocean-solutions.

[30] Oscar Serrano, Jeffrey J. Kelleway, Catherine Lovelock, and Paul S. Lavery. Chapter 28 - conservation of blue carbon ecosystems for climate change mitigation and adaptation. In Gerardo M.E. Perillo, Eric Wolanski, Donald R. Cahoon, and Charles S. Hopkinson, editors, *Coastal Wetlands*, pages 965–996. Elsevier, 2019. https://doi.org/10.1016/B978-0-444-63893-9.00028-9.

[31] Len J McKenzie, Lina M Nordlund, Benjamin L Jones, Leanne C Cullen-Unsworth, Chris Roelfsema, and Richard K F Unsworth. The global distribution of seagrass meadows. *Environmental Research Letters*, 15(7):074041, jul 2020. doi: 10.1088/1748-9326/ab7d06.

[32] Y. Pan, R. A. Birdsey, J. Fang, R. Houghton, P. E. Kauppi, W. A. Kurz, O. L. Phillips, A. Shvidenko, S. L. Lewis, J. G. Canadell, P. Ciais, R. B. Jackson, S. W. Pacala, A. D. McGuire, S. Piao, A. Rautiainen, S. Sitch, and D. Hayes. A large and persistent carbon sink in the world's forests. *Science*, 333(6045):988–993, 2011. doi:10.1126/science.1201609.

[33] James W. Fourqurean, Carlos M. Duarte, Hilary Kennedy, Núria Marbà, Marianne Holmer, Miguel Angel Mateo, Eugenia T. Apostolaki, Gary A. Kendrick, Dorte Krause-Jensen, Karen J. McGlathery, and Oscar Serrano. Seagrass ecosystems as a globally significant carbon stock. *Nature Geoscience*, 5(7):505–509, 2012. doi: 10.1038/ngeo1477.

[34] Lesley Hughes. Biological consequences of global warming: is the signal already apparent? *Trends in Ecology and Evolution*, 15(2):56–61, 2000. https://doi.org/10.1016/S0169-5347(99)01764-4.

[35] Lijing Cheng, John Abraham, Kevin E. Trenberth, John Fasullo, Tim Boyer, Michael E. Mann, Jiang Zhu, Fan Wang, Ricardo Locarnini, Yuanlong Li, Bin Zhang, Zhetao Tan, Fujiang Yu, Liying Wan, Xingrong Chen, Xiangzhou Song, Yulong Liu, Franco Reseghetti, Simona Simoncelli, Viktor Gouretski, Gengxin Chen, Alexey Mishonov, and Jim Reagan. Another record: Ocean warming continues through 2021 despite la niña conditions. *Advances in Atmospheric Sciences*, 39(3):373–385, 2022. https://doi.org/10.1007/s00376-022-1461-3.

[36] Gattuso; Jean-Pierre, Magnan; Alexandre K., Bopp; Laurent, Cheung; William W. L., Duarte; Carlos M., Hinkel; Jochen, Mcleod; Elizabeth, Micheli; Fiorenza, Oschlies; Andreas, Williamson; Phillip, Billé; Raphaël, Chalastani; Vasiliki I., Gates; Ruth D., Irisson; Jean-Olivier, Middelburg; Jack J., Pörtner; Hans-Otto, and Rau; Greg H. Ocean solutions to address climate change and its effects on marine ecosystems. *Frontiers in Marine Science*, 5(337), 2018. doi:10.3389/fmars.2018.00337.

[37] Lovelock C.E. and Duarte C.M. Dimensions of blue carbon and emerging perspectives. *Biology Letters*, 15(3), 2019. http://dx.doi.org/10.1098/rsbl.2018.0781.

[38] Juha Siikamäki, James N. Sanchirico, Sunny Jardine, David McLaughlin, and Daniel Morris. Blue carbon: Coastal ecosystems, their carbon storage, and potential for reducing emissions. *Environment: Science and Policy for Sustainable Development*, 55(6):14–29, 2013. DOI: 10.1080/00139157.2013.843981.

[39] Peter I. Macreadie, Andrea Anton, John A. Raven, Nicola Beaumont, Rod M. Connolly, Daniel A. Friess, Jeffrey J. Kelleway, Hilary Kennedy, Tomohiro Kuwae, Paul S. Lavery, Catherine E. Lovelock, Dan A. Smale, Eugenia T. Apostolaki, Trisha B. Atwood, Jeff Baldock, Thomas S. Bianchi, Gail L. Chmura, Bradley D. Eyre, James W. Fourqurean, Jason M. Hall-Spencer, Mark Huxham, Iris E. Hendriks, Dorte Krause-Jensen, Dan Laffoley, Tiziana Luisetti, Núria Marbà, Pere Masque, Karen J. McGlathery, J. Patrick Megonigal, Daniel Murdiyarso, Bayden D. Russell, Rui Santos, Oscar Serrano, Brian R. Silliman, Kenta Watanabe, and Carlos M. Duarte. The future of blue carbon science. *Nature Communications*, 10(3998), 2019. https://doi.org/10.1038/s41467-019-11693-w.

[40] Leanne Cullen-Unsworth and Richard Unsworth. Seagrass meadows, ecosystem services, and sustainability. *Environment: Science and Policy for Sustainable Development*, 55(3):14–28, 2013. DOI: 10.1080/00139157.2013.785864.

[41] Kenneth L. Heck Jr., Tim J. B. Carruthers, Carlos M. Duarte, A. Randall Hughes, Gary Kendrick, Robert J. Orth, , and Susan W. Williams. Trophic transfers from seagrass meadows subsidize diverse marine and terrestrial consumers. *Ecosystems*, 11:1198–1210, 2008. DOI: 10.1007/s10021-008-9155-y.

[42] G. Rowe, M. Sibuet, J. Deming, A. Khripounoff, J. Tietjen, S. Macko, and R. Theroux. Total' sediment biomass and preliminary estimates of organic carbon residence time in deep-sea benthos. *Marine Ecology Progress Series*, 79(1/2):99–114, 1991. https://www.jstor.org/stable/44634790.

[43] M.A. Hemminga, N. Marbà, and J. Stapel. Leaf nutrient resorption, leaf lifespan and the retention of nutrients in seagrass systems. *Aquatic Botany*, 65(1):141–158, 1999. https://doi.org/10.1016/S0304-3770(99)00037-6.

[44] Suchanek Thomas H., Williams Susan L., John C. Ogden, Hubbard Dennis K., and Gill Ivan P. Utilization of shallow-water seagrass detritus by carribbean deep-sea macrofauna: δ^{13}c evidence. *Deep Sea Research Part A. Oceanographic Research Papers*, 32(2):201–214, 1985. doi:10.1016/0198-0149(85)90028-7.

[45] Toshihiro Miyajima, Masakazu Hori, Masami Hamaguchi, Hiromori Shimabukuro, Hiroshi Adachi, Hiroya Yamano, and Masahiro Nakaoka. Geographic variability in organic carbon stockand accumulation rate in sediments of eastand southeast asian seagrass meadows. *Global Biogeochemical Cycles*, 29(4):397–415, 2015. https://doi.org/10.1002/2014GB004979.

[46] I. Mazarrasa, N. Marbà, C. E. Lovelock, O. Serrano, P. S. Lavery, J. W. Fourqurean, H. Kennedy, M. A. Mateo, D. Krause-Jensen, A. D. L. Steven, and C. M. Duarte. Seagrass meadows as a globally significant carbonate reservoir. *Biogeosciences*, 12(16):4993–5003, 2015. doi:10.5194/bg-12-4993-2015.

[47] Biedinger N. and Fleischmann K. *Seychelles. in: Ecological Studies (Analysis and Synthesis)*, volume 46. Springer, Berlin, Heidelberg, 2000. https://doi.org/10.1007/978-3-642-59773-2_14.

[48] John Lablache and Sharon Uranie. Seychelles taking steps to protect more marine areas of its oceanic zone. *Seychelles News Agency*, 2014. http://www.seychellesnewsagency.com/articles/702/Seychelles+taking+steps+to+protect+more+marine+areas+of+its+oceanic+zone#:~:text=(Seychelles%20News%20Agency)%20%2D%20The,size%20of%20the%20United%20Kingdom. [Accessed 22/05/2022].

[49] Seychelles Fishing Authority. Mahé plateau trap and line fishery co-management plan. 2019. https://sfa.sc/images/2021/06/18/Mahe_Plateau_Trap_and_Line_Fishery_Co-Mangement_Plan_-_March_2019.pdf [Accessed 22/05/2022].

[50] John Nevill, Jacques Prescott, Nirmal Jivan Shah, and Marie-May Jeremie. Seychelles biodiversity strategy and action plan 2015-2020. 2014. https://chm.cbd.int/api/v2013/documents/4E62B15F-2926-5F4D-5D3C-D9597D60A0A9/attachments/204620/Seychelles%20NBSAP.pdf [Accessed 16/02/2022].

[51] Mathieu Laurence F., Langford Ian H., and Kenyon Wendy. Valuing marine parks in a developing country: a case study of the seychelles. *Environment and Development Economics*, 8(2):373–390, 2003. doi:10.1017/S1355770X0300196.

[52] Kemper Karin. The seychelles blue bond: Good for business and the planet. *Revue Analyse Financière*, (70), 2019. https://ssrn.com/abstract=3805926 [Accessed 16/02/2022].

[53] World Bank. Sovereign blue bond issuance: Frequently asked questions, 2018. https://www.worldbank.org/en/news/feature/2018/10/29/sovereign-blue-bond-issuance-frequently-asked-questions [Accessed 16/02/2022].

[54] Smith J.L., R.Tingey, and H.E. Sims. Seychelles marine spatial plan atlas. *Developed by The Nature Conservancy for the Seychelles MSP Initiative*, 2021. Unpublished maps accessed at www.seymsp.com [Accessed 05/04/2022].

[55] SeyCCAT. Seychelles' conservation and climate adaptation trust (seyccat): Achieving conservation through innovative finance and creative collaborations. https://seyccat.org [Accessed 16/02/2022].

[56] Roland Duval. Seagrass meadows awareness to highlight seyccat's involvement at cop 26. *Seychelles Nation*, 2021. https://nation.sc/articles/10638/seagrass-meadows-awareness-to-highlight-seyccats-involvement-at-cop-26-.

[57] SeyCCAT. A promising future for seychelles' seagrass. https://seyccat.org/a-promising-future-for-seychelles-seagrass/ [Accessed 16/02/2022].

[58] Christine Bertram, Martin Quaas, Thorsten B. H. Reusch, Athanasios T. Vafeidis, Claudia Wolff, and Wilfried Rickels. The blue carbon wealth of nations. *Nature Climate Change*, 11:704–709, 2021. https://doi.org/10.1038/s41558-021-01089-4 [Accessed 23/05/2022].

[59] Lifen Jiang, Junyi Liang, Xingjie Lu, Enqing Hou, Forrest M. Hoffman, and Yiqi Luo. Country-level land carbon sink and its causing components by the middle of the twenty-first century. *Ecological Processes*, 10(61), 2021. https://doi.org/10.1186/s13717-021-00328-y [Accessed 23/05/2022].

[60] Palacios MM, Waryszak P, Costa MDP, Wartman M, Ebrahim A, and Macreadie PI. Literature review: Blue carbon research in the tropical western indian ocean wio. a report submitted to the seychelles conservation climate adaptation trust (seyccat). *Deakin University, Australia*, 2021. https://seyccat.org/wp-content/uploads/2020/01/BlueCarbonLab_LitReport_Seychelles_20210301_final.pdf.

[61] Short FT UNEP-WCMC. Global distribution of seagrasses (version 7.1). seventh update to the data layer used in green and short (2003). *Cambridge (UK): UN Environment Programme World Conservation Monitoring Centre*, 2021. Data DOI: https://doi.org/10.34892/x6r3-d211.

[62] GEBCO Compilation Group. Gebco 2021 grid, 2021. doi:10.5285/c6612cbe-50b3-0cff-e053-6c86abc09f8f.

[63] NOAA National Geophysical Data Center. Etopo1 1 arc-minute global relief model, 2009. https://www.ngdc.noaa.gov/mgg/global/global.html [Accessed 07/04/2022].

[64] NOAA; NCEI. Gebco-2021 basemap (noaa ncei visualization). A color shaded relief visualization of the General Bathymetric Chart of the Oceans (GEBCO) GEBCO-2021 global land and seafloor elevation dataset; https://www.ncei.noaa.gov/maps/iho_dcdb/ [Accessed 08/04/2022].

[65] Benjamin de Brye, Anouk de Brauwere, Olivier Gourgue, Tuomas Kärnä, Jonathan Lambrechts, Richard Comblen, and Eric Deleersnijder. A finite-element, multi-scale model of the scheldt tributaries, river, estuary and rofi. *Coastal Engineering*, 57(9):850–863, 2010. doi: https://doi.org/10.1016/j.coastaleng.2010.04.001.

[66] Cushman-Roisin B. and Beckers J-M. *Introduction to Geophysical Fluid Dynamics: Physical and Numerical Aspects*, volume 101. 2006. ISBN: 978-0-12-088759-0.

[67] S. D. Smith and E. G. Banke. Variation of the sea surface drag coefficient with wind speed. *Quartely Journal of the Royal Meteorological Society*, 101(429):665–673, 1975. doi:10.1002/qj.49710142920.

[68] G.L. Geernaert. On the importance of the drag coefficient in air-sea interactions. *Dynamics of Atmospheres and Oceans*, 11(1):19–38, 1987. doi: https://doi.org/10.1016/0377-0265(87)90012-1.

[69] J. Smagorinsky. General circulation experiments with the primitive equations. 1963. https://doi.org/10.1175/1520-0493(1963)091%3C0099:GCEWTP%3E2.3.CO;2.

[70] Jonathan Lambrechts, Emmanuel Hanert, Eric Deleersnijder, Paul-Emile Bernard, Vincent Legat, Jean-François Remacle, and Eric Wolanski. A multi-scale model of the hydrodynamics of the whole great barrier reef. *Estuarine, Coastal and Shelf Science*, 79(1):143–151, 2008. https://doi.org/10.1016/j.ecss.2008.03.016.

[71] Short FT UNEP-WCMC. Global distribution of seagrasses (version 7.1). seventh update to the data layer used in green and short (2003). *Cambridge (UK): UN Environment World Conservation Monitoring Centre*, 2021. Data DOI: https://doi.org/10.34892/x6r3-d211.

[72] K.Nadia Dimou and E.Eric Adams. A random-walk, particle tracking model for well-mixed estuaries and coastal waters. *Estuarine, Coastal and Shelf Science*, 37(1):99–110, 1993. https://doi.org/10.1006/ecss.1993.1044.

[73] Christopher Thomas. Modelling marine connectivity in the great barrier reef and exploring its ecological implications. *Doctoral dissertation, UCL (unpublished doctoral dissertation)*, 2015.

[74] Simon Spagnol, Eric Wolanski, Eric Deleersnijder, Richard Brinkman, Felicity Mcallister, Benoit Cushman-Roisin, and Emmanuel Hanert. An error frequently made in the evaluation of advective transport in two-dimensional lagrangian models of advection-diffusion in coral reef waters. *Marine Ecology Progress Series*, 235:–, 01 2002.

[75] B. de Brye, S. Schellen, M.G. Sassi, B. Vermeulen, T. Karna, E. Deleersnijder, and A.J.F. Hoitink. Preliminary results of a finite-element, multi-scale model of the mahakam delta (indonesia). *Ocean Dynamics*, 61(8):1107–1120, 2011. doi:10.1007/s10236-011-0410-y.

[76] Akira Okubo. Oceanic diffusion diagrams. *Deep Sea Research and Oceanographic Abstracts*, 18(8):789–802, 1971. https://doi.org/10.1016/0011-7471(71)90046-5.

[77] Fernando P. Andutta, Peter V. Ridd, and Eric Wolanski. Dynamics of hypersaline coastal waters in the great barrier reef. *Estuarine, Coastal and Shelf Science*, 94(4):299–305, 2011. https://doi.org/10.1016/j.ecss.2011.06.009.

[78] R.E. Stafford-Bell, A.A. Chariton, and R.W. Robinson. Prolonged buoyancy and viability of zostera muelleri irmisch ex asch. vegetative fragments indicate a strong dispersal potential. *Journal of Experimental Marine Biology and Ecology*, 464:52–57, 2015. https://doi.org/10.1016/j.jembe.2014.12.014.

[79] Carlos M. Duarte. Seagrass nutrient content. *Marine Ecology Progress Series*, 67:201–207, 1990. https://www.int-res.com/articles/meps/67/m067p201.pdf [Accessed 07/05/2022].

[80] 030012 AIP Conference Proceedings 2120. 2019. https://doi.org/10.1063/1.5115616 [Accessed 07/05/2022].

[81] Birgit Olesen and K Sand-Jensen. Biomass-density patterns in the temperate seagrass zostera marina. *Marine Ecology-progress Series - MAR ECOL-PROGR SER*, 109:283–291, 1994. doi:10.3354/meps109283.

[82] Nuria Marba, Carlos Duarte, Ana Alexandre, and Susana Cabaço. *How do seagrasses grow and spread*, pages 11–18. 2004. ISBN:8789143213.

[83] A.W.D. Larkum, L.C. Collett, and R.J. Williams. The standing stock, growth and shoot production of zostera capricorni aschers. in botany bay, new south wales, australia. *Aquatic Botany*, 19(3):307–327, 1984. https://doi.org/10.1016/0304-3770(84)90046-9.

[84] S. J. Turner. Growth and productivity of intertidal zostera capricorni in new zealand estuaries. *New Zealand Journal of Marine and Freshwater Research*, 41(1):77–90, 2007. https://doi.org/10.1080/00288330709509897.

[85] Brian Fry and Robert W. Virnstein. Leaf production and export of the seagrass syringodium filiforme kütz. in indian river lagoon, florida. *Aquatic Botany*, 30(3):261–266, 1988. https://doi.org/10.1016/0304-3770(88)90057-5.

[86] National Weather Service. Duration of summer season in south florida. https://www.weather.gov/mfl/summer_season [Accessed 16/05/2022].

[87] Carlos M. Duarte and Just Cebrián. The fate of marine autotrophic production. *Limnology and oceanography*, 41(8):1758–1766, 1996. https://doi.org/10.4319/lo.1996.41.8.1758.

[88] Heidi Dierssen, Richard Zimmerman, Lisa Drake, and David Burdige. Benthic ecology from space: Optics and net primary production in seagrass and benthic algae across the great bahama bank. *Marine Ecology-progress Series - MAR ECOL-PROGR SER*, 411:16, 2010. doi: 10.3354/meps08665.

[89] Shih-Han Chiu, Yen-Hsun Huang, and Hsing-Juh Lin. Carbon budget of leaves of the tropical intertidal seagrass thalassia hemprichii. *Estuarine, Coastal and Shelf Science*, 125:27–35, 2013. doi: 10.1016/j.ecss.2013.03.026.

[90] Madec Gurvan, Romain Bourdallé-Badie, Pierre-Antoine Bouttier, Clément Bricaud, Diego Bruciaferri, Daley Calvert, Jérôme Chanut, Emanuela Clementi, Andrew Coward, Damiano Delrosso, Christian Ethé, Simona Flavoni, Tim Graham, James Harle, Doroteaciro Iovino, Dan Lea, Claire Lévy, Tomas Lovato, Nicolas Martin, Sébastien Masson, Silvia Mocavero, Julien Paul, Clément Rousset, Dave Storkey, Andrea Storto, and Martin Vancoppenolle. Nemo ocean engine, 2017. Fix broken cross-references, still revision 8625 from SVN repository. https://doi.org/10.5281/zenodo.3248739 [Accessed 16/05/2022].

[91] Aurélie V. Duhec, Richard F. Jeanne, Nikolai Maximenko, and Jan Hafner. Composition and potential origin of marine debris stranded in the western indian ocean on remote alphonse island, seychelles. *Marine Pollution Bulletin*, 96(1):76–86, 2015. https://doi.org/10.1016/j.marpolbul.2015.05.042 [Accessed 23/05/2022].

[92] Carlos M. Duarte and Dorte Krause-Jensen. Export from seagrass meadows contributes to marine carbon sequestration. *Frontiers in Marine Science*, 4, 2017. https://www.frontiersin.org/article/10.3389/fmars.2017.00013 [Accessed 11/06/2022].

[93] C. M. Duarte. Reviews and syntheses: Hidden forests, the role of vegetated coastal habitats in the ocean carbon budget. *Biogeosciences*, 14(2):301–310, 2017. https://doi.org/10.5194/bg-14-301-2017 [Accessed 22/05/2022].

[94] The World Bank. International bank for reconstruction and development project appraisal document on a proposed loan in the amount of us$5 million a proposed guarantee in the amount of up to eur5 million (or us$ equivalent) a proposed grant from the global environment facility trust fund in the amount of us$5.29 million and a proposed loan from the global environment facility trust fund in the amount of us$5 million to the republic of seychelles for a third south west indian ocean fisheries governance and shared growth project. *Environment and Natural Resources Global Practice*, 2017. https://documents1.worldbank.org/curated/en/394051505478217219/pdf/SEYCHELLES-PAD-09122017.pdf [Accessed 11/06/2022].

[95] Mcowen C., Weatherdon LV., Bochove J., Sullivan E., Blyth S., Zockler C., Stanwell-Smith D., Kingston N., Martin CS., Spalding M., and Fletcher S. A global map of saltmarshes (v6.1). *Biodiversity Data Journal 5: e11764*, 2017. Paper DOI: https://doi.org/10.3897/BDJ.5.e11764; Data DOI: https://doi.org/10.34892/07vk-ws51 [Accessed 12/06/2022].

[96] Government of Seychelles. Seychelles' national climate change policy, ministry of environment, energy and climate change, seychelles. 2020. http://www.meecc.gov.sc/wp-content/uploads/2019/10/seychelles-national-climate-change-policy-may-2020.pdf [Accessed 12/06/2022].

[97] Carbon Credits. Live carbon prices today. https://carboncredits.com/carbon-prices-today/ [Accessed 13/06/2022].

[98] World Bank. Carbon pricing dashboard. https://carbonpricingdashboard.worldbank.org [Accessed 13/06/2022].

[99] J.-M. Lellouche, E. Greiner, O. Le Galloudec, G. Garric, C. Regnier, M. Drevillon, M. Benkiran, C.-E. Testut, R. Bourdalle-Badie, F. Gasparin, O. Hernandez, B. Levier, Y. Drillet, E. Remy, P.-Y. Le Traon, and P.-Y. Le Traon. Recent updates to the copernicus marine service global ocean monitoring and forecasting real-time 1/12° high-resolution system. *Ocean science*, 14:1093 – 1126, 2018. https://doi.org/10.5194/os-14-1093-2018 [Accessed 07/06/2022].

[100] Martin Gullström, Maricela de la Torre Castro, Salomão O. Bandeira, Mats Björk, Mattis Dahlberg, Nils Kautsky, Patrik Rönnbäck, and Marcus C. Öhman. Seagrass ecosystems in the western indian ocean. *Ambio*, 31(7/8):588–596, 2002. http://www.jstor.org/stable/4315313 [Accessed 03/06/2022].

[101] Carlos M Duarte and Carina L Chiscano. Seagrass biomass and production: a reassessment. *Aquatic Botany*, 65(1):159–174, 1999. doi: https://doi.org/10.1016/S0304-3770(99)00038-8.

[102] E. P. Green and F. T. Short. World atlas of seagrasses. *Berkeley, CA, California University Press*, 2003. https://www.researchgate.net/publication/269988511_World_Atlas_of_Seagrasses [Accessed 12/06/2022].

[103] J.-P. Gattuso, B. Gentili, C. M. Duarte, J. A. Kleypas, J. J. Middelburg, and D. Antoine. Light availability in the coastal ocean: impact on the distribution of benthic photosynthetic organisms and their contribution to primary production. *Biogeosciences*, 3(4):489–513, 2006. https://bg.copernicus.org/articles/3/489/2006/ [Accessed 12/06/2022].

Appendices

A Hydrodynamic model validation (North point of Mahé, January to April 2018)

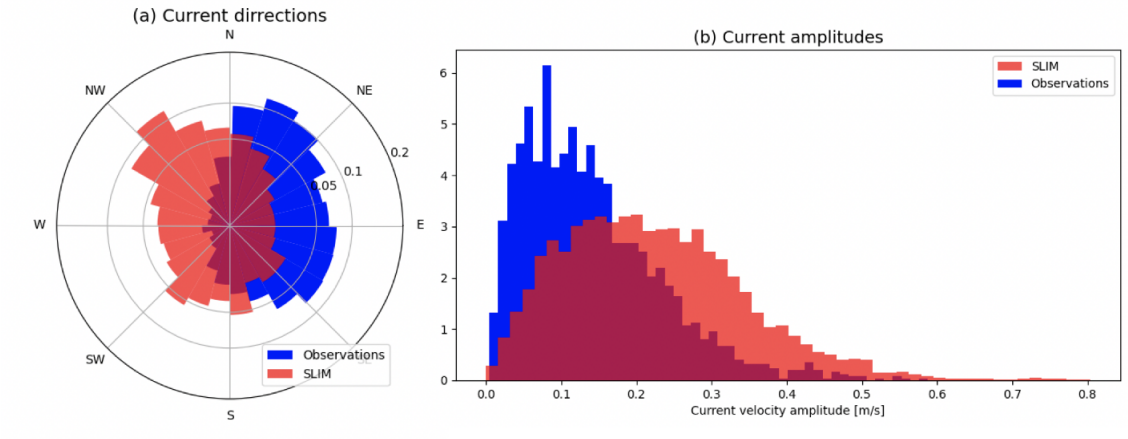

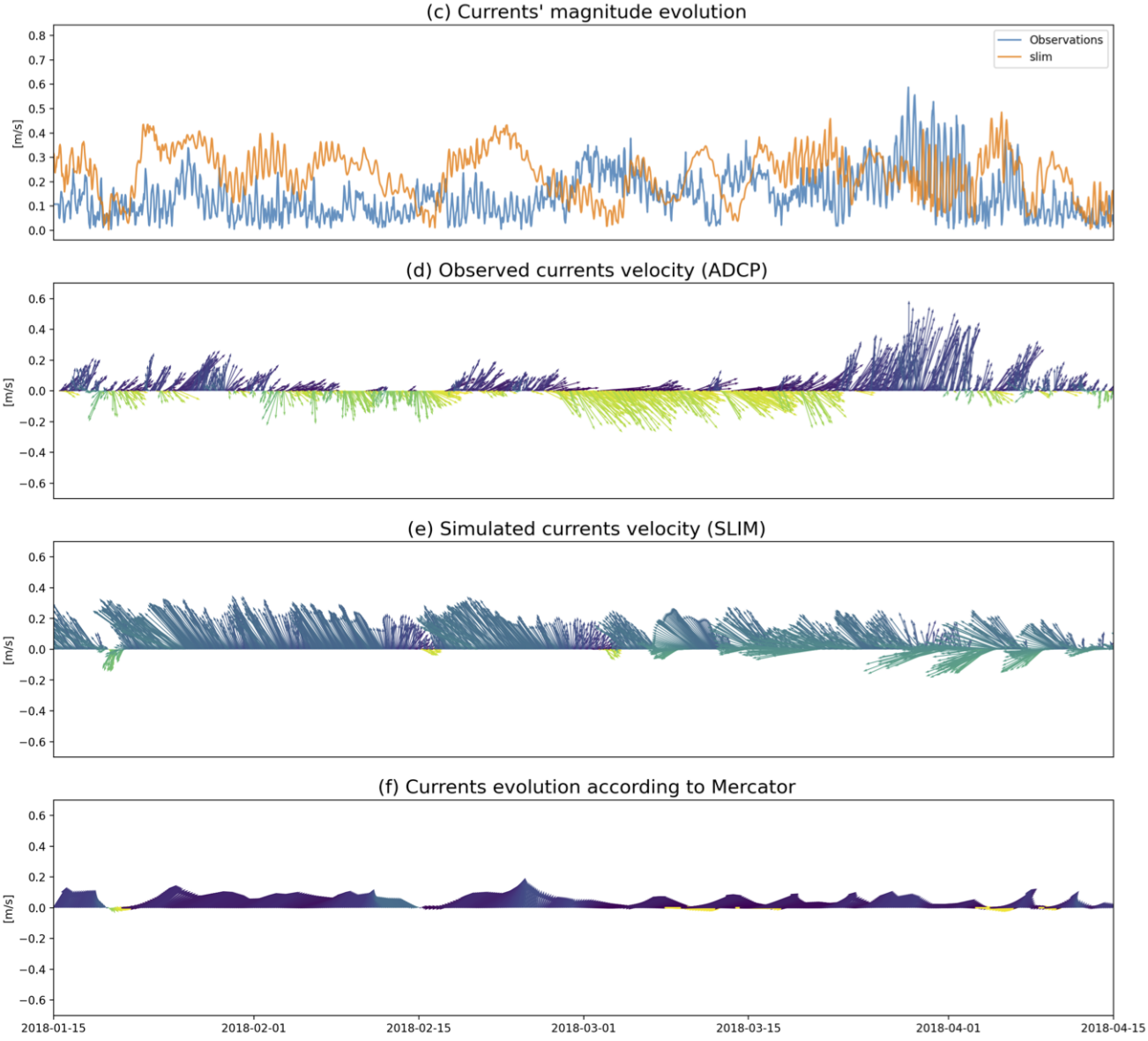

Investigating the contribution of Seychelles' seagrass meadows to marine carbon sequestration

Douchan Hanuise

The oceans are a key component of the climate system. They cover about 72% of the Earth's surface and have already absorbed about 40% of the carbon that was emitted by human activities since the 19th century. Coastal ecosystems, such as seagrass meadows and mangroves, play a particular role in this blue carbon budget. They have the potential to capture carbon and to store it in deep reservoirs where it will remain for hundreds of years. This carbon sequestration potential remains however poorly understood and unquantified for most coastal ecosystems in the World. Here, we try to estimate the carbon sequestration potential of seagrass meadows on the Seychelles plateau. Seychelles has been developing extensively its blue economy and is keen to estimate the carbon offsetting capacity of its marine ecosystem. We develop a high-resolution ocean circulation model of Seychelles plateau and simulate ocean currents over 3-year period (2018-2020). These currents are then used to simulate the transport of virtual seagrass fragments from the different confirmed and potential meadows present on the plateau. Our results suggest that most of the seagrass meadows export a large fraction (>80%) of their fragments outside of the plateau, where the carbon contained in the fragments can settle to >1000m depth. We estimate that ~6% of Seychelles seagrass meadows net primary production could be sequestrated in the deep ocean. This corresponds to ~85 tC/yr for confirmed meadows and ~7994 tC/yr for potential meadows. These estimates should help Seychelles quantify its global contribution toward net-zero emissions, as envisaged by the Paris Agreement on climate change.

UNIVERSITÉ CATHOLIQUE DE LOUVAIN
Faculté des bioingénieurs
Croix du Sud, 2 bte L7.05.01, 1348 Louvain-la-Neuve, Belgique | **www.uclouvain.be/agro**